International Scientific-Technical and Production Journal

The Paton WELDING JOURNAL

December
2004
12

English translation of the monthly «Avtomaticheskaya Svarka» (Automatic Welding) journal published in Russian since 1948

Founders: *E.O. Paton Electric Welding Institute of the NAS of Ukraine*
International Association «Welding»

Publisher: *International Association «Welding»*

Address:
E.O. Paton Electric Welding Institute,
International Association «Welding»,
11, Bozhenko str., 03680, Kyiv, Ukraine
Tel.: (38044) 227 67 57
Fax: (38044) 268 04 86
E-mail: journal@paton.kiev.ua
http://www.nas.gov.ua/pwj

State Registration Certificate
KV 4790 of 09.01.2001

Subscriptions:
$460, 12 issues per year,
postage and packaging included.
Back issues available.

CONTENTS

ROLE OF SEGREGATION OF OXYGEN IN WELDING OF INVAR TYPE ALLOYS

K.A. YUSHCHENKO, V.S. SAVCHENKO and **T.M. STARUSHCHENKO**
E.O. Paton Electric Welding Institute, NASU, Kiev, Ukraine

It has been found that cracks in welding of Fe–36 % Ni alloy are formed primarily at temperatures that are much lower than solidus temperature, i.e. within the ductility-dip temperature range. Conditions causing enrichment of weld metal with oxygen are formed in a joint during the welding process. Subsequent cooling leads to enrichment of high-angle grain boundaries with oxygen due to thermal-deformation processes occurring in metal, which leads to decrease in ductility and embrittlement. Investigations by the Varestraint test method have shown existence of quantitative relationship between the effect of oxygen and ductility dip in the weld metal.

Keywords: *Invar type alloy, ductility, segregation, enrichment with oxygen, brittle fracture, solidus, hot cracks, grain boundaries, welded joint, Auger spectroscopy*

Peculiar thermal-physical properties of Fe–Ni alloys of the Invar type (Fe–36 % Ni) combined with high ductility and toughness, including at low temperatures, provided their wide application in machine building and instrument making industries.

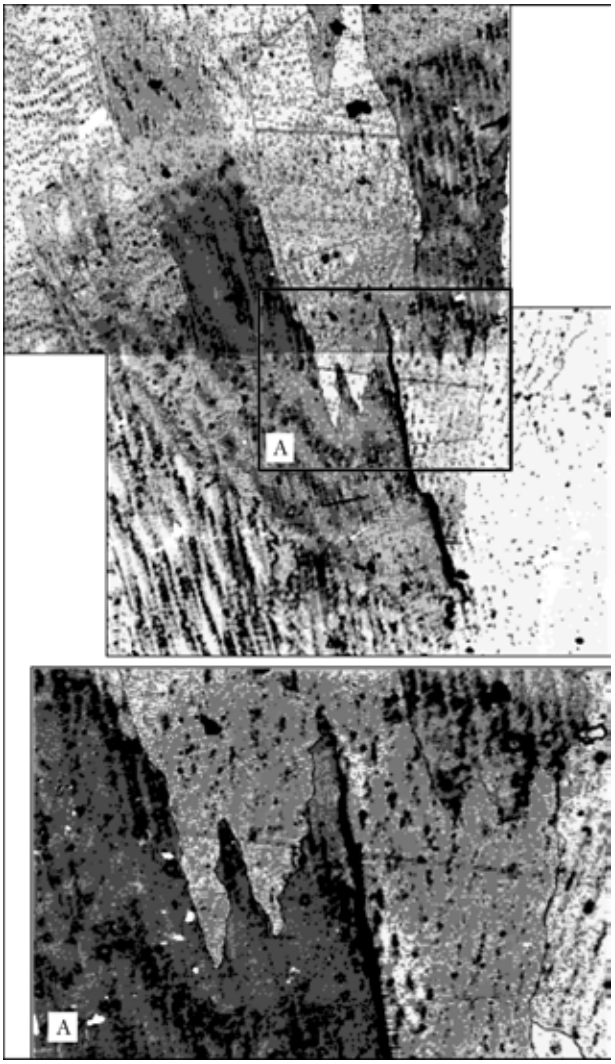

Figure 1. Microstructure of weld metal with underbead hot crack in multi-layer welding of alloy 36NKh (×200; A ––– ×400)

Alloy of the Invar type has the following chemical composition, wt.%: 0.05C, 0.10Si, 0.35Mn, 35.6Ni, 0.45Cr, 0.004S, 0.006P, 0.002[O], 0.00015[H].

Investigations show that welds in this alloy are very sensitive to hot cracking. As found in study [1], the cracks are initiated in two temperature ranges, including at temperatures below 1100 °C (i.e. below solidus temperature T_S), propagate along the grain boundaries and are formed during the process of cooling of the weld metal (Figure 1). Low content of sulphur and phosphorus fails to prevent hot cracking in welding of the Invar type alloys. It is reported [1, 2] that oxygen can initiate hot cracks of the above type.

Study of high-temperature ductility of the Invar type alloy and welds indicated (Figure 2) that loss (dip) of ductility of metal occurs at a plastic deformation rate of 0.043 s^{-1} within the 600–1100 °C temperature range. Besides, the higher the oxygen content of a material investigated, the higher the loss.

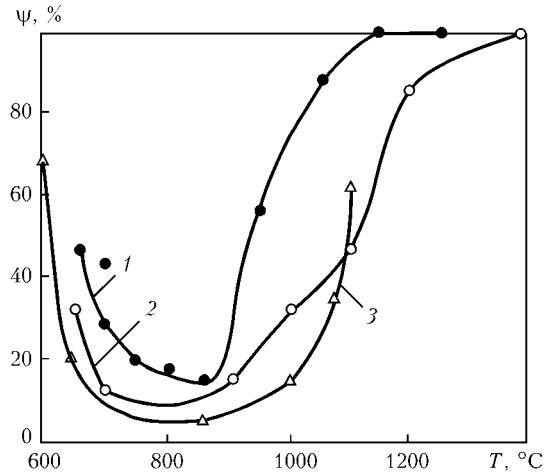

Figure 2. Temperature dependence of ductility ψ of base (*1*) and weld metals (*2*, *3*): *1–3* — oxygen content 0.002, 0.028 and 0.052 wt.%, respectively

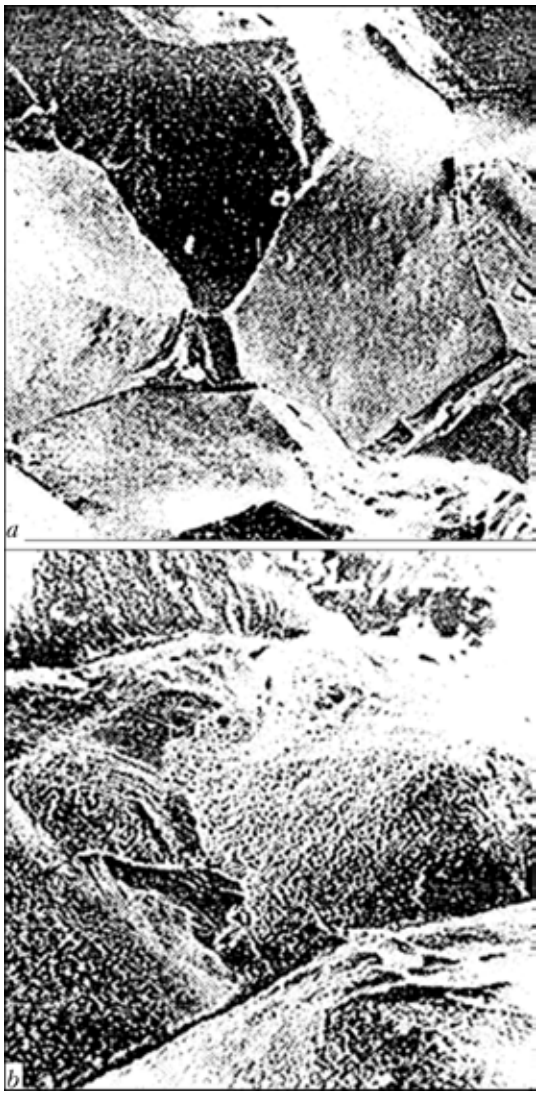

Figure 3. Fractographs of fracture surfaces of 36NKh alloy specimens at a temperature of 725 °C: *a* — ×150; *b* — ×450

Fractographs of fracture surface of specimens of alloy 36NKh at a temperature of 725 °C (Figure 3) show the presence of mostly brittle intergranular fracture with traces of micro plastic deformation. In this connection, it is suggested that the probable cause of

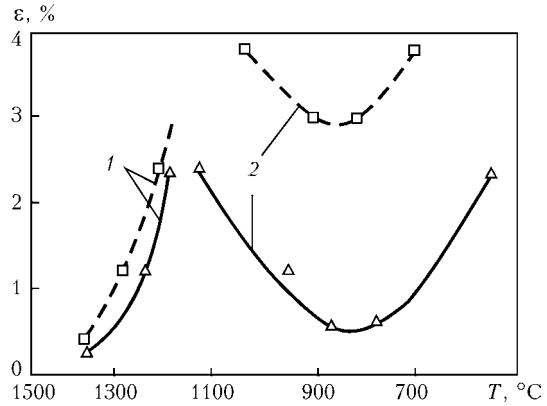

Figure 4. Effect of oxygen on brittle temperature range of alloy Fe--36 % Ni: *1* — BTR; *2* — DTR; solid curves — oxygen content 0.047 wt.%; dashed curves — 0.0016 wt.%; ε — plastic deformation

hot cracking in the ductility-dip temperature range (DTR) is non-equilibrium diffusion of atoms of impurity elements (e.g. oxygen) present in solid solution at the grain boundaries. In this case the decisive factor that determines the rate of diffusion is a high-temperature plastic strain, which is always present in the weld metal and HAZ during welding. Sensitivity of the weld metal to cracking during welding was quantitatively estimated by dynamic loading of test plates $4 \times 150 \times 150$ mm in size using the Varestraint test machine [3]. Welding was performed by the TIG method under the chosen conditions (I_w = 120 A, U_a = 12 V, v_w = 10 m / h) at a constant value of deformation (1.25 %) of surface layers of the test plates.

The test methods initiating formation of cracks provided for making one- and two-pass welds: the first was made on base metal to estimate crack resistance of the one-pass weld, and the second was made in two passes on base metal. The second pass provided overlapping of approximately 60 % of the first pass (to model properties of multi-layer cladding).

Results of the tests of a series of specimens with different oxygen content are shown in Figure 4, and appearance of the welds after the tests is shown in Figure 5. Analysis of the results indicates that the

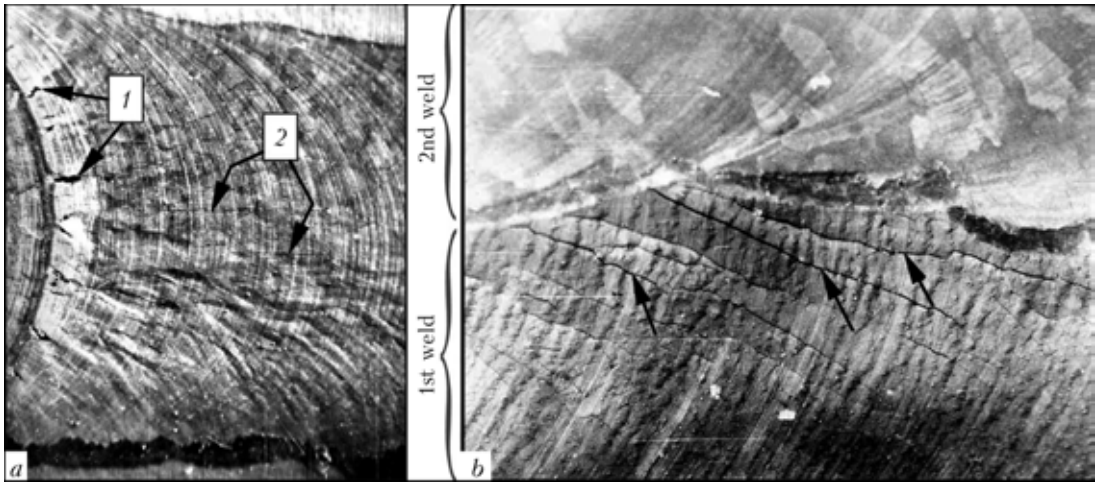

Figure 5. Appearance of one- (*a*) and two-pass (*b*) welds in alloy 36NKh after tests: *1, 2* — cracks in BTR and DTR, respectively (cracks in the first weld were formed under the effect of deformation experienced in making the second weld)

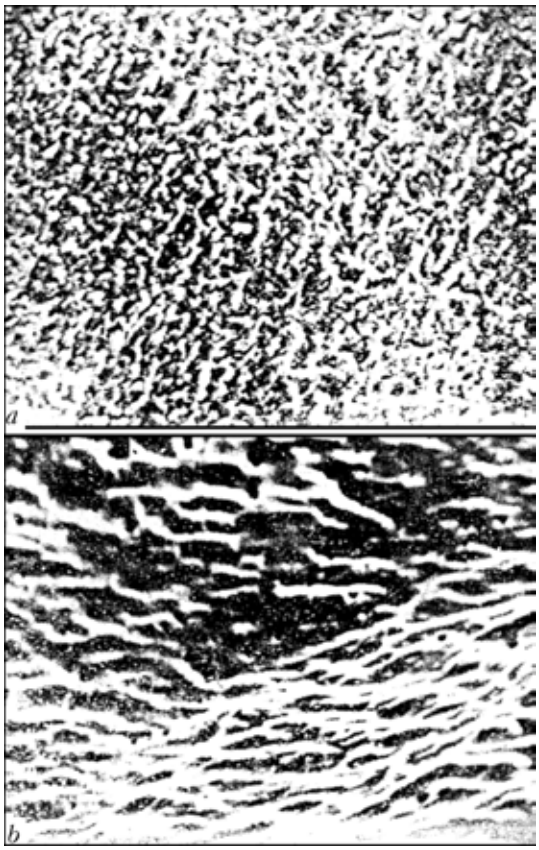

Figure 6. Fractographs of DTR crack surface: *a* — ×1100; *b* — ×3650

weld metal with an alloying system of the Invar type is characterised by the presence of two types of the ductility-dip ranges ---- DTR and high-temperature ductility-dip range BTR (Figure 4), oxygen affecting ductility characteristics mainly in DTR. It should be noted that sensitivity to formation of the underbead type cracks in this case is higher than in the weld made during the testing process (Figure 5, *b*). It is likely that this is the case of the total effect of oxygen on sensitivity to embrittlement of the first weld both during the process of its making outside the Varestraint test machine and during repeated heating and simultaneous forced dynamic deformation using the above testing machine.

Fractographs of the DTR crack surfaces shown in Figure 6 and character of crack propagation (see Figure 5, *b*) are indicative of the presence of brittle intergranular fracture with traces of micro plastic deformation. Characteristics of the crack surface can be estimated as type *R* [4]. Elemental composition of the DTR crack surface and surface of the intact cast metal as a reference was examined using the LAS-2000 model unit for 3D analysis by the Auger spectroscopy method. Distribution of elements through metal thickness (from the fracture surface) was examined by layer-by-layer etching with argon ions. Working vacuum during the measurement process was $1.6 \cdot 10^{-8}$ Pa, which allowed keeping a clean surface for 16 h after removal of adsorbed substances and contaminants (formed in etching for 1 min).

Profile records of distribution and variation of the content of main and impurity elements during the etching process are shown in Figure 7. It follows from the data given that chemical composition of metal near the fracture surface remains unchanged in etching for 4–5 min (Figure 7, *a*). Chemical composition of matrix of the weld metal is revealed after etching for

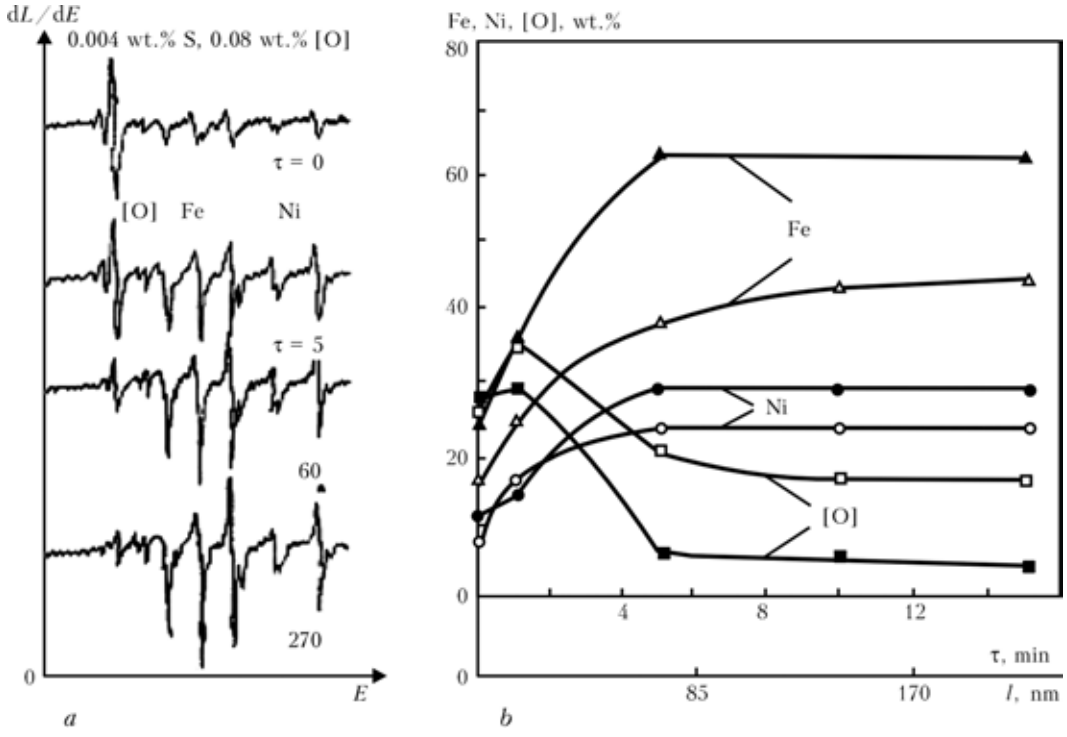

Figure 7. Variation in intensity of iron, nickel and oxygen lines on fracture surface of a specimen (*a*) and content of the above elements in surface layer (*b*) depending upon etching time τ: solid curves ---- intact weld metal; dashed curves ---- crack surface; *I* — intensity of secondary characteristic measurement; *E* — kinetic energy; *l* ---- distance from grain boundary

5 min (Figure 7, *b*), whereas near the fracture surface it cannot be revealed even after 230 min of continuous etching.

It should be noted that the major part of carbon as an interstitial impurity is removed from the surface after etching for 30 s. The content of carbon in deeper metal layers becomes lower than the sensitivity limit of Auger spectroscopy. Similar picture is observed also in etching of a hot crack surface. Sulphur is removed after etching for 15 s. Nitrogen is not detected in the spectrum. Hydrogen cannot be revealed by the Auger spectroscopy method either. However, at increased temperatures (more than 400 °C) its mobility is known to be so high that it exerts no effect on formation and growth of hot cracks in the weld metal, although the hydrogen content of the weld metal is a bit higher than in the base metal. In both cases the oxygen peak is seen for a much longer time: for 90 min of etching in the base metal, and for more than 230 min of etching on the fracture surface. Therefore, it can be suggested that the base metal surface is covered by an oxide film about 1.30 μm thick, and the hot crack surface is covered by an oxide film more than 3.45 μm thick.

To check the probability of mass transfer of oxygen from depth of the weld to its fracture surface, the intensities of peaks of individual elements on crack surfaces of specimens were compared in the as-welded condition and after holding in super high vacuum ($1 \cdot 10^{-8}$ Pa) for 1.8 and 20 days. It was done on the basis that deposition of adsorbed substances occurs uniformly and with the same intensity both on the fracture surface and on the surface of the intact weld.

As proved by the experiments, sorption of oxygen is most intensive during the first hours and days after etching of the metal surface. Then the rates of adsorption and desorption of oxygen become approximately equal. The chemosorbed layer is left on the surface, and the intensity of mass transfer of this impurity from the bulk of the base metal to its surface remains almost unchanged for 20 days. Therefore, despite the fact that reactivity of oxygen is high and its diffusion coefficient in metal at room temperature is very low (about $1 \cdot 10^{-16}$ cm^2 / s), the surface layer of the crack has an increased content of oxygen, which is caused by its transfer from the bulk of metal.

Experimental results suggest that redistribution of oxygen takes place in metal investigated. Hence, segregation of this impurity increases, thus leading to oxygen enrichment of grain boundaries and oxygen depletion of a grain body.

It should be expected that peculiarities of the mechanism of internal deformation in alloy Fe–36 % Ni may play a decisive role in increasing its resistance to underbead crack formation.

According to the generally accepted notion, the process of realisation of internal deformation occurs with participation of either dislocation (translation) [5] or turning (rotation) mechanism, depending upon the external factors and type of the deformed metal. Characteristic regularities of the latter mechanism show up most often under complex thermal-deformation conditions. It can be suggested that differences between the above mechanisms have a substantial effect on resistance to plastic deformation and, as a consequence, on underbead crack formation.

In this connection, it would be expedient to specify peculiarities of deformation (including the intragranular one) of the weld metals with a different sensitivity to underbead crack formation.

The fine structure determining characteristic features of variations in the dislocation structure of metal during the plastic deformation process and its resistance to high-temperature deformation was examined by an example of two alloying systems of the weld metal (Table) with high and low sensitivity to cracking.

Comparative evaluation of variations in the fine structure was performed on specimens with a gauge part diameter of 4 mm, made from metal of the upper bead of the multi-pass welds in the as-welded condition and after extra deformation (to 10 %) at a temperature of 700 °C and rate of $5.66 \cdot 10^{-2}$ s^{-1}, which corresponded to behaviour of metal within DTR.

In the weld metal with alloying system I (see the Table) an increase of 10 % in the deformation degree leads to formation in internal volumes of intensive banded structures (deformation bands), i.e. mechanical twins, and bands related to collective forms of movement of the crystalline lattice defects propagating in the bulk of grain (Figure 8, *a*). Low-angle grain boundaries do not exert a retardation effect on movement of the deformation bands, whereas high-angle grain boundaries block further displacement of the slip bands into neighbouring grains (Figure 8, *b*).

Initiation of banded structures occurs in certain regions in a chaotic dislocation ensemble characterised by a high density of the lattice defects ($\rho \approx 1 \cdot 10^{11}$–$1 \cdot 10^{12}$ cm^{-2}).

Chemical composition and sensitivity of weld metal to underbead crack formation

Alloying system	*Material*	*Content of elements, wt.%*							*Sensitivity to underbead crack formation*
		C	*Mn*	*Si*	*Cr*	*Ni*	*Mo*	*Other*	
I	36NKh	0.05	0.35	0.1	0.45	35.6	–	0.004S, 0.006P, 0.002[O], 0.0015[H]	High
II	03Kh18N19G10AM3 (Fe–Cr–Ni–Mn–N)	0.03	11.2	0.5	0.5	13.5	2.6	0.004S	Low

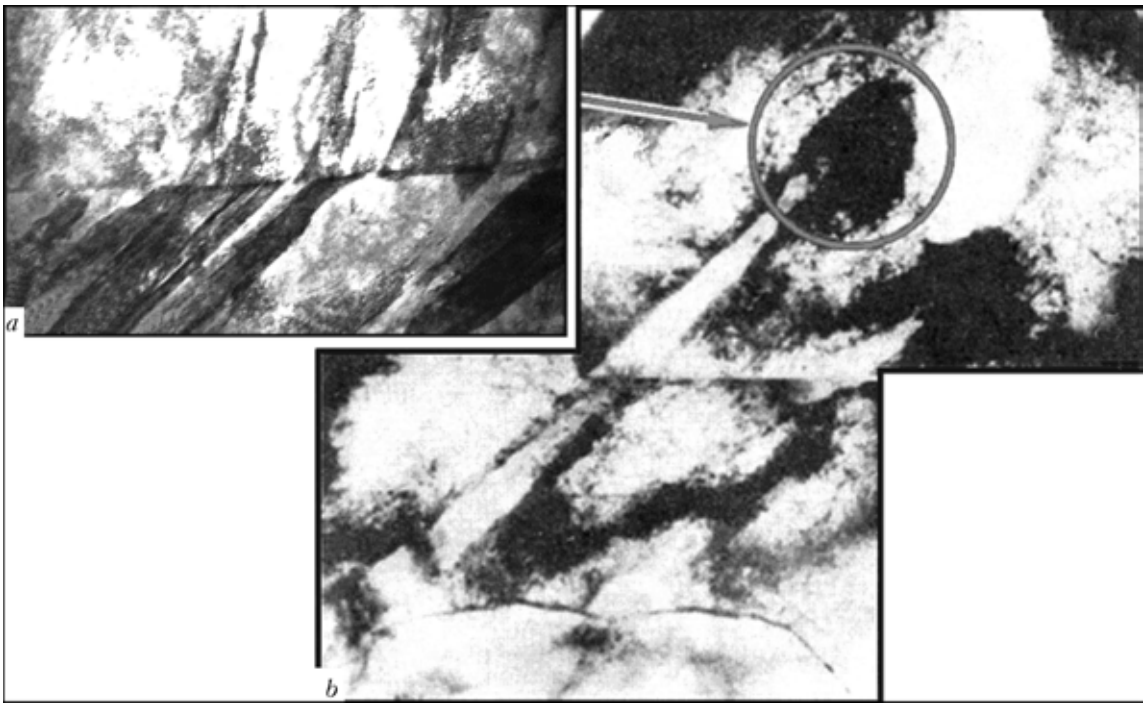

Figure 8. Fine structure of weld metal of alloying system I after forced deformation at 700 °C: *a* — intragranular; *b* — interface zone (arrow shows region of initiation of banded species) (×1000)

Presence of individual dislocations in the investigated structure of the weld metal of alloying system I along the crystallographic slip systems in the bulk of grain in the case of absence of forced deformation and formation of extended banded species in grains with growth of external loading are indicative of the fact that intragranular plastic deformation is caused by the classical dislocation (translation) mechanisms [5]. The «intensity» (length) of shears (translations) and a high degree of mobility of lattice defects in the field of stresses are caused in many respects by a high energy of stacking faults in metal of the Fe–Ni alloying system, on the one hand, and, reportedly, by an insignificant obstacle for the deformation movement, on the other hand. It should be emphasised that intensive collective movements of lattice defects in the bulk of grains, directed to the boundaries, are accompanied by «transportation» of impurity elements and their concentration in a region of grain boundaries, which was seen in dark field structural and micro diffraction images. It is likely that the specific character of movement of lattice defects in the plastic deformation process determines the presence of segregation clusters and new phases along the grain boundaries and their absence in the bulk of grains.

Therefore, detailed analysis of structural elements, distribution of phases and peculiarities of the mechanism of plastic deformation indicates that a highly heterogeneous structure is formed in the weld metal with the Fe–Ni alloying system, caused by realisation of the translation mechanism of plastic deformation. This heterogeneous structure has a substantial gradient between the grain body and high-angle grain boundaries in dislocation density and presence of phase precipitates and segregations.

Structure of the weld metal with alloying system II (Fe–Cr–Ni–Mn–N) and high crack resistance is characterised, first of all, by the presence of phase precipitates (PP), which have a high degree of dispersion ($d_{PP} \approx 0.04$–0.21 μm) and are heterogeneously distributed in the entire volume of the weld metal (particle spacing $l_p \approx 0.25$–0.30 μm).

As the deformation degree grows, the dislocation density and hindered shears in the crystallographic slip planes increase uniformly in the bulk of grain. Split dislocations are sometimes formed, which is indicative of a general decrease in stacking fault (SF) energy γ_{SF} of metal in transition from alloying system I to alloying system II.

It is likely that hindered translations of individual dislocations within the slip systems are a consequence of a general decrease in γ_{SF} as a result of alloying. Naturally, this hampers plastic deformation by the classical dislocation mechanism, which is characterised by a transverse dislocation slip.

In this case, transition of a dislocation to other slip plane for metal with a low value of γ_{SF} is possible only on the condition of joining (transformation of partial dislocation into the full one). The wider the stacking fault (i.e. the lower the value of γ_{SF}), which is characteristic of the weld metal of alloying system II, the higher the energy intensity of this process.

Complex dislocation restructuring of any type and interaction of dislocations of different slip systems are thought to lead to formation of a mesh structure [5] (Figure 9).

Result of changing of the deformation mechanism is that dispersed fragments about 0.25–0.30 μm in size, bordered with zones with a high dislocation density, are formed on the base of the mesh structure

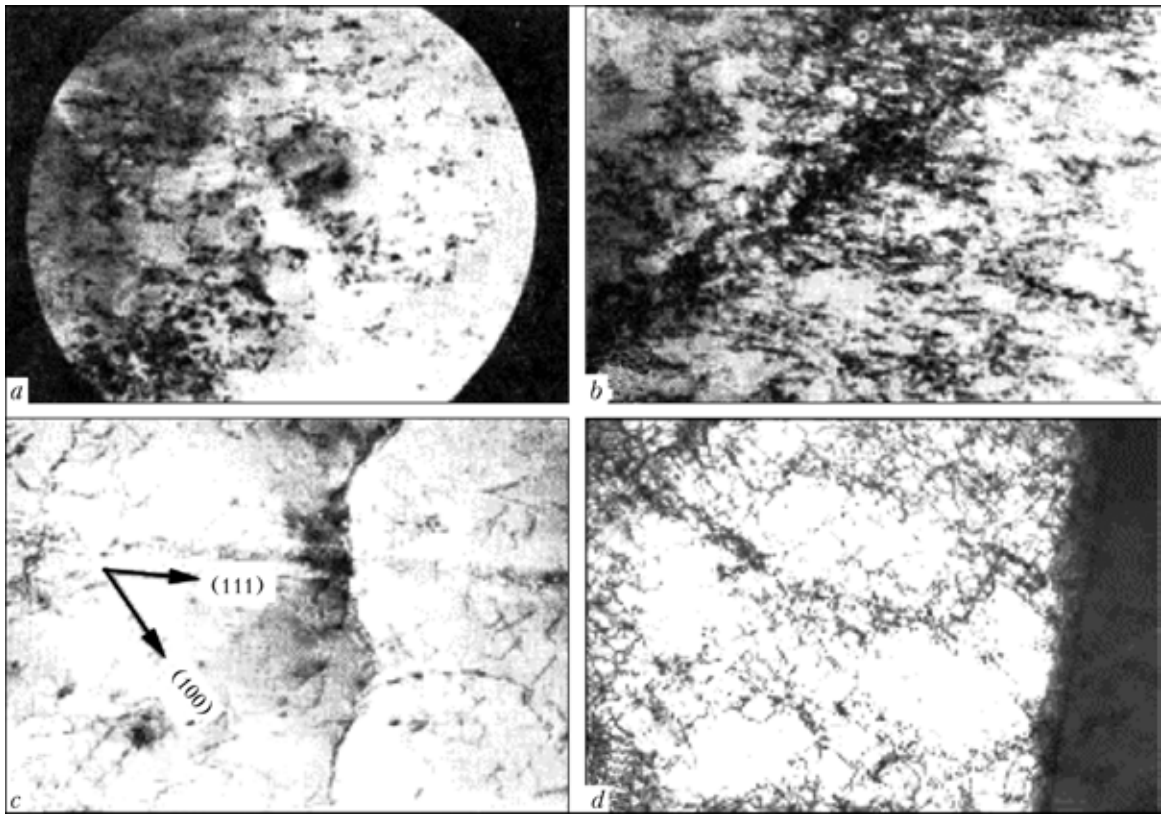

Figure 9. Fine structure of weld metal of alloying system II: *a* — dispersed precipitates of redundant phases in the bulk of grains; *b* — dislocation structure of boundary region; *c* — split dislocations in weld structure; *d* — fragmentation of metal structure after forced deformation at 700 °C (×20,000)

(Figure 9, *d*). Hence, the neighbouring micro volumes turn to finite angles. In such cases relaxation of internal stresses occurs through plastic turns (rotations).

Therefore, the experiments showed that structures greatly differing in presence and distribution of impurities, morphology of phase precipitates, grain sizes, sizes of sub-structural elements and character of movement of the crystalline lattice defects in the field of

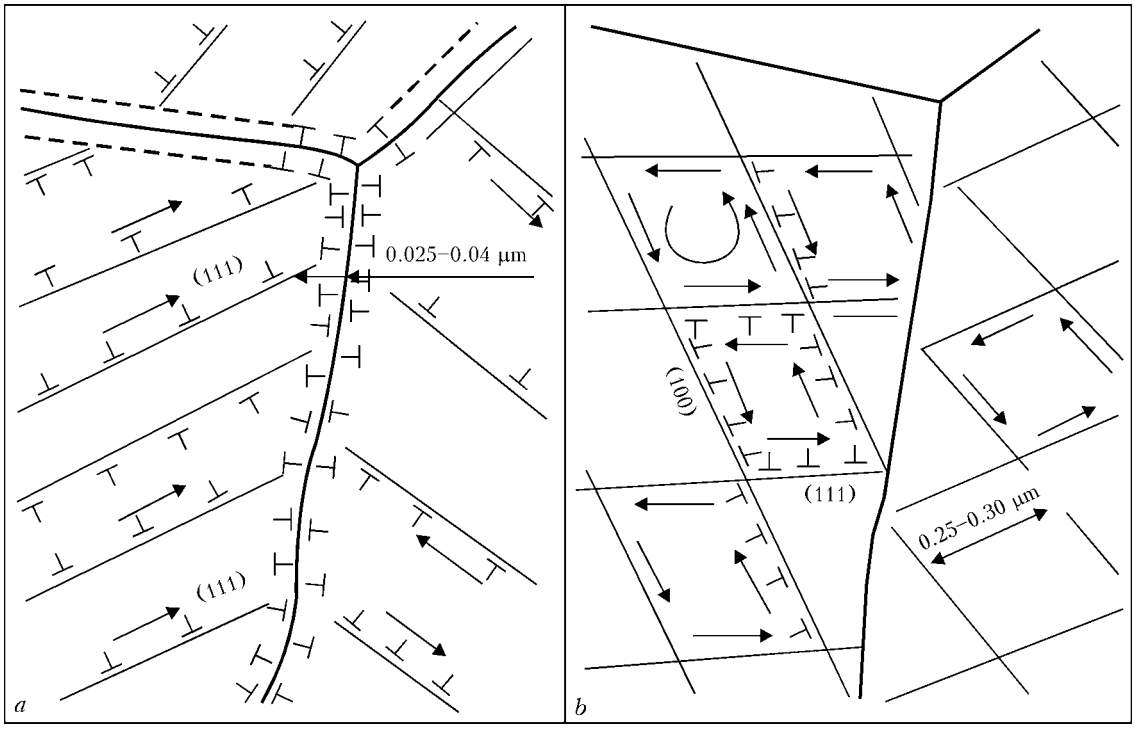

Figure 10. Schematic of formation of structures in deformed metal of alloying systems I (*a*) and II (*b*) (arrows indicate directions of rotation of weld metal fragments)

effective stresses are formed under similar thermal-deformation conditions in weld metals of different alloying systems. The character of movement of the crystalline lattice defects in the field of effective stresses indicates that the mechanism of plastic deformation in certain micro volumes of the weld metal with different alloying systems is also different: the dislocation mechanism of plastic deformation is realised primarily with alloying system I, and the rotation mechanism occurs with alloying system II (Figures 8 and 9).

It can be suggested that changing of the plastic deformation mechanism has a decisive effect on the processes of mass transfer of impurity elements that cause embrittlement along the grain boundaries. In the first case, with the translation mechanism taking place (Figure 8, *a*), the intensive intragranular slip to a distance comparable with grain size (where dislocations move from the bulk of grain to grain boundaries) favours the dislocation transfer of these elements to the grain boundaries. In the second case (Figure 10), with involvement of the rotation mechanism, there is no distinct trend to movement of dislocations oriented to the grain boundaries, despite the equal deformation of metal; oriented macro deformation of a specimen at a micro level occurs mostly through rotational movement of the intragranular structure elements. As applied to the Invar alloy, the above specific character of the mechanism of intragranular plastic deformation favours, eventually, enrichment of grain boundaries with oxygen, which causes formation of underbead cracks in multi-layer welds.

CONCLUSIONS

1. Hot underbead cracks in multi-layer welds with the Invar type alloying are formed along the grain boundaries.

2. Increased content of impurity elements, and first of all oxygen, is fixed on the surface of underbead cracks in multi-layer welds with the Invar type alloying.

3. Enrichment of grain boundaries with oxygen during the welding process, leading to formation of hot cracks in the welds, is controlled by the dislocation (translation) mechanism of plastic deformation.

1. Yushchenko, K.A., Starushchenko, T.M., Savchenko, V.S. (1983) Mechanism of formation of hot cracks induced by oxygen during welding of Invar alloy. *Avtomatich. Svarka*, **8**, 5--7.
2. Yushchenko, K.A., Starushchenko, T.M. (1981) Role of oxygen in crack formation during welding of Invar alloy. *Ibid*., **8**, 21–24.
3. Savage, W.F., Lundin, G.D. (1977) The Varestraint test. *Welding J*., 44(**10**), 433--442.
4. Matsuda, F., Nakagawa, H., Ogata, S. et al. (1978) Fractographic investigation on solidification crack in the Varestraint test of fully austenitic stainless steel — studies on fractography of welded zone (III). *Transact. of JWRI*, 7(**1**), 59–70.
5. Khirt, J., Lote, I. (1972) *Theory of dislocations*. Moscow: Atomizdat.

NUMERICAL SIMULATION OF THE SYSTEM OF POWER SOURCE–CONSUMABLE-ELECTRODE ARC

V.N. SIDORETS and **A.M. ZHERNOSEKOV**
E.O. Paton Electric Welding Institute, NASU, Kiev, Ukraine

A mathematical description of the power source–consumable-electrode arc system is proposed. Conditions of static existence of the system are studied, allowing for the thermophysical characteristics of the parameters and variation of electrode stick-out.

Keywords: *arc welding, consumable electrode, numerical simulation of the process, stationary arc length, object of regulation, static volt-ampere characteristics*

Development of new welding equipment for arc welding, namely power sources, automatic and semi-automatic machines, as well as systems of automatic regulation and stabilization of the process, requires comprehensive analysis of the power source–consumable-electrode arc system.

From this viewpoint, still urgent is the mathematical description of arc length variation in time as the controlled object, particularly in connection with appearance of advanced software, for instance MATLAB Simulink, allowing modeling of various electrical engineering systems. Important is the mathematical description of a static volt-ampere characteristic of a stable running of the welding process, which depends on various physical properties of electrode material.

Existing approaches do not quite clearly define the optimum criteria of the system of power source–consumable-electrode arc, as they differ by the conditions of conducting the experiments [1, 2], and do not take into account the features of volt-ampere characteristics of a stable running of arc welding process [3, 4].

In this study differential equations were derived, which were used to describe the system of power source–consumable-electrode arc and study the conditions of static existence of this system allowing for thermophysical characteristics of the parameters and variation of electrode stick-out.

Dynamics of electrode wire melting. We will consider the thermal processes in the consumable electrode with the following assumptions: stages of electrode stick-out heating and its melting are sufficiently separate and interact with each other so that the final heating conditions are the initial melting conditions; radiation from the electrode surface at the stage of electrode stick-out heating can be neglected; length of the melting zone is small compared to the stick-out; metal transfer is fine-drop (spray).

Thus, stick-out heating proceeds as a result of current flowing through it. Energy input through heat transfer from the meting zone at sufficiently high feed rates of electrode wire can be neglected.

Then, according to the law of energy conservation, all the power evolved from the current flowing through the stick-out, is used for increase of internal energy, i.e. heating:

$$mc\mathrm{d}T = Ri^2\mathrm{d}t, \qquad (1)$$

where m, R are the weight and electric resistance of an elementary section of the electrode, respectively; c is the specific heat content of the electrode metal; i is the instant value of welding current; dT, dt are the temperature and time increment, respectively.

Let us express the variables in expression (1) as specific characteristics

$$\gamma xSc\mathrm{d}T = \rho\frac{x}{S}i^2\mathrm{d}t,$$

where γ is the electrode metal density; x is the length of an elementary section of the electrode; S is the area of electrode cross-section; ρ is the specific electric resistance of electrode metal.

This yields the differential equation for the stick-out heating temperature

$$\frac{\mathrm{d}T}{\mathrm{d}t} = \frac{\rho i^2}{\gamma cS^2}. \qquad (2)$$

Considering that at the nozzle outlet the wire has temperature T_0, equation (2) can be integrated. As a result

$$T = T_0 + \frac{\rho i^2(l_w - l)}{\gamma cS^2 v},$$

where l_w is the distance between the nozzle and item; l is the arc length; v is the wire feed rate.

A different energy balance is found in the electrode melting zone. Energy comes from near-electrode region and is only consumed in metal melting:

$$U_{\mathrm{a}}i = \gamma Sv_{\mathrm{m}}\left[c(T_{\mathrm{m}} - T_0) + \lambda - \frac{\rho i^2(l_w - l)}{\gamma S^2 v_{\mathrm{m}}}\right], \qquad (3)$$

where U_{a} is the near-anode (or near-cathode, depending on welding current polarity) voltage drop, allowing for the potential of electron liberation from the

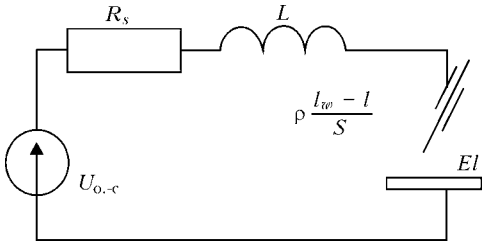

Figure 1. Electric circuit, modeling the process of consumable-electrode welding

metal; T_m is the metal melting temperature; λ is the specific heat of metal melting; v_m is the melting rate.

Equation (3) yields the stationary rate of electrode wire melting:

$$v_m = \frac{SU_a i + \rho(l_w - l)i^2}{\gamma S^2[c(T_m - T_0) + \lambda]}.$$

For a non-stationary case, arc length variation is given by the differential equation, where the right-hand part is exactly the difference between the rates of melting v_m and feed v of the wire

$$\frac{dl}{dt} = \frac{SU_a i + \rho(l_w - l)i^2}{\gamma S^2\,[c(T_m - T_0) + \lambda]} - v.$$

Dynamics of electric circuit with consumable-electrode arc. Electric circuit incorporating a consumable-electrode arc, can be represented by a schematic shown in Figure 1.

According to Kirchhoff's law, open-circuit voltage of the power source $U_{o.-c}$ is equal to the sum of voltage drops in circuit elements ---- ohmic resistance of the power source and current-carrying cables R_s, inductance of the power source and current-carrying cables L, ohmic resistance of the electrode wire section from the nozzle to the arc ---- and voltage drop in the arc gap:

$$U_{o.-c} = R_s i + L\frac{di}{dt} + \rho\frac{l_w - l}{S}i + El + U_{a-c},$$

where E is the electric field intensity in the arc column, independent on current; U_{a-c} is the sum of near-electrode voltage drops on the anode and the cathode (further on we will take $U_{o.-c} - U_{a-c}$ difference as the open-circuit voltage $U_{o.-c}$ of the power source to simplify the equations).

Allowing for the above, the system of differential equations which are used to describe the dynamic system of power source–consumable-electrode arc becomes

$$\begin{cases} \dfrac{dl}{dt} = \dfrac{SU_a i + \rho(l_w - l)i^2}{\gamma S^2 q} - v, \\ \dfrac{di}{dt} = \dfrac{1}{L}\left(U_{o.-c} - R_s i - \rho\dfrac{l_w - l}{S}i - El\right), \end{cases} \quad (4)$$

where $q = c(T_m - T_0) + \lambda$ is the constant determining the thermophysical properties of electrode wire metal.

This system of differential equations will be the further object of study. It is obvious that its main property is non-linearity. Therefore, let us successively apply all the steps of studying such systems, the first of which is study of special points (or equilibrium points).

Static condition of the system of power source–consumable-electrode arc. In order to study the special points, let us put the right-hand parts of equation (4) to zero to obtain a non-linear system of equations

$$\begin{cases} \dfrac{SU_a I_0 + \rho(l_w - l_0)I_0^2}{\gamma S^2 q} - v = 0, \\ U_{o.-c} - R_s I_0 - \rho\dfrac{l_w - l_0}{S}I_0 - El_0 = 0 \end{cases} \quad (5)$$

relative to coordinates of special point I_0 and l_0.

Dependence of l_0 on I_0 can be found from the first equation of system (5):

$$l_0 = \frac{\rho l_w I_0^2 + SU_a I_0 - q v \gamma S}{\rho I_0^2}. \quad (6)$$

Substituting this formula into the second equation of system (5), we can find expressions, which determine dependence of I_0 and l_0 on the parameters of the welding process and electric circuit:

$$\rho R_s I_0^3 - (U_{o.-c} + U_a - El_w)I_0^2 + S(EU_a + qv\gamma\rho)I_0 - qv\gamma ES^2 = 0, \quad (7)$$

$$\begin{aligned} &\rho E^2 l_0^3 + \rho(qv\gamma\rho - E(2U_{o.-c} + U_a + El_w))l_0^2 + \ldots + \\ &+ [\rho U_{o.-c}(U_{o.-c} + U_a + 2El_w) + \\ &+ (R_s S + \rho l_w)(EU_a - 2qv\gamma\rho)]l_0 + \ldots + \\ &+ qv\gamma(R_s S + \rho l_w)^2 - U_{o.-c}U_a(R_s S + \rho l_w) - \\ &- \rho U_{o.-c}^2 l_w = 0. \end{aligned} \quad (8)$$

Both these equations are cubic and it can be shown that (7) has one positive root, whereas expression (8) can have both positive and negative roots. Let us study the issue.

In physical terms the stationary arc length has the following constraints: arc length should be positive and cannot be greater than the distance between the nozzle and item:

$$0 < l < l_w. \quad (9)$$

Expression (9) can be called the condition of existence of the consumable-electrode welding process. Substituting the limit values of arc length from (9) into (7), (8) we obtain the constraints on parameters corresponding to this condition of existence:

$$qv\gamma(SR_s + \rho l_w)^2 - U_{o.-c}U_a(SR_s + \rho l_w) - \rho U_{o.-c}^2 l_w = 0,$$
$$qv\gamma SR_s - U_{o.-c}U_a + U_a El_w = 0.$$

Conditions of existence for electrode wire feed rate are as follows:

$$U_{o.-c}\frac{SR_s U_a + \rho l_w(U_{o.-c} + U_a)}{q\gamma SR_s} > v > U_a\frac{U_{o.-c} - El_w}{q\gamma SR_s}. \quad (10)$$

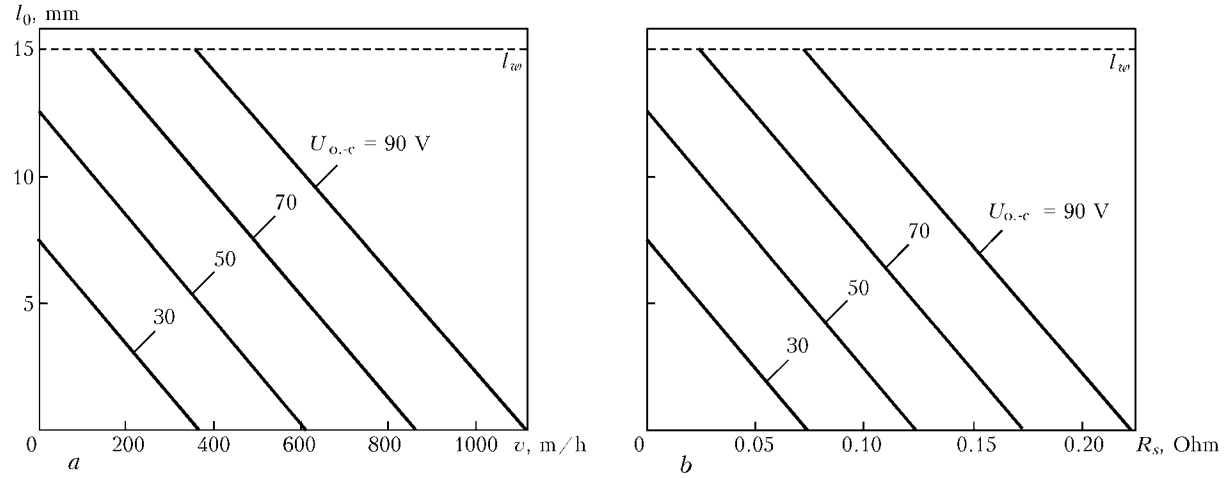

Figure 2. Dependence of a stationary arc length l_0 on rate v of electrode wire feed (*a*) and resistance R_s (*b*)

If the maximum feed rate (left-hand part of the expression), at which the wire rests against the item, is always achievable, the minimum feed rate (right-hand part of the expression), at which the electrode melts up to the nozzle, is possible either at sufficiently high values of open-circuit voltage of the power source $U_{o.-c} > El_w$, or at sufficiently small distances from the nozzle to the item $l_w < U_{o.-c} / E$.

Direction of inequality in (10) and further on is marked so as to ensure the correspondence with (9). Here and further on the numerical examples and figures are made for electrode wire of Sv-08G2S type of 1.6 mm diameter.

Figure 2, *a* shows the constraints on electrode wire feed rate expressed by inequalities (10).

For welding process parameter the distance from the nozzle to the item l_w and conditions of existence can be represented as

$$l_{w\,\max} > l_w > \frac{U_{o.-c}U_{a} - qv\gamma SR_s}{EU_{a}}, \qquad (11)$$

where $l_{w\,\max}$ is the maximum distance from the nozzle to the item, at which the welding process is possible. This value can be determined by solving the quadratic equation

$$qv\gamma\rho^2 l_w^2 - \rho[U_{o.-c}(U_{o.-c} + U_{a}) - 2qv\gamma SR_s]l_w + \\ + SR_s(qv\gamma SR_s - U_{o.-c}U_{a}) = 0. \qquad (12)$$

Physical sense of such a constraint is clear. Welding current is limited at large electrode stick-outs, thus preventing melting. Maximum distance from the nozzle to the item will be in place either at a large enough open-circuit voltage

$$U_{o.-c} > \frac{qv\gamma SR_s}{U_{a}} \qquad (13)$$

or at a small enough rate of electrode wire feed

$$v < \frac{U_{o.-c}U_{a}}{qv\gamma SR_s}.$$

If condition (13) is not satisfied, the constraint imposed by the right-hand part of condition (11), is invalid. In this case valid is a constraint, which is applied by the left-hand part of this expression, taking the form of $l_{w\,\min} < l_w < l_{w\,\max}$, where $l_{w\,\min}$ and $l_{w\,\max}$ are the values which are the roots of the quadratic equation (12).

It is also obvious that at sufficiently small open-circuit voltages

$$U_{o.-c} < 2\sqrt{qv\gamma SR_s} - U_{a}$$

the welding process is impossible.

Let us analyze the influence of resistance R_s, which determines the slope of the external characteristic of the power source. Resistance constrains are

$$R_{s\,\max} > R_s > U_{a}\frac{U_{o.-c} - El_w}{qv\gamma S},$$

where $R_{s\,\max}$ is the value, which can be calculated as the root of the following equation:

$$qv\gamma S^2 R_s^2 + S(2qv\gamma\rho l_w - U_{o.-c}U_{a})R_s + \\ + \rho l_w(qv\gamma\rho l_w - U_{o.-c}(U_{o.-c} - U_{a})) = 0.$$

Figure 2, *b* shows the constraints imposed on resistance R_s. They consist in that at sufficiently large values of open-circuit voltage of the power source ($U_{o.-c} > El_w$) it is necessary to ensure a certain slope of the external characteristic of the source by introducing a minimum R_s. The process cannot be implemented under other conditions. In the case of very «stringent» volt-ampere characteristics of the power source, the electrode wire will melt up to the nozzle.

Open-circuit voltage is another parameter, characterizing the power source. Constraints imposed on it have the form of

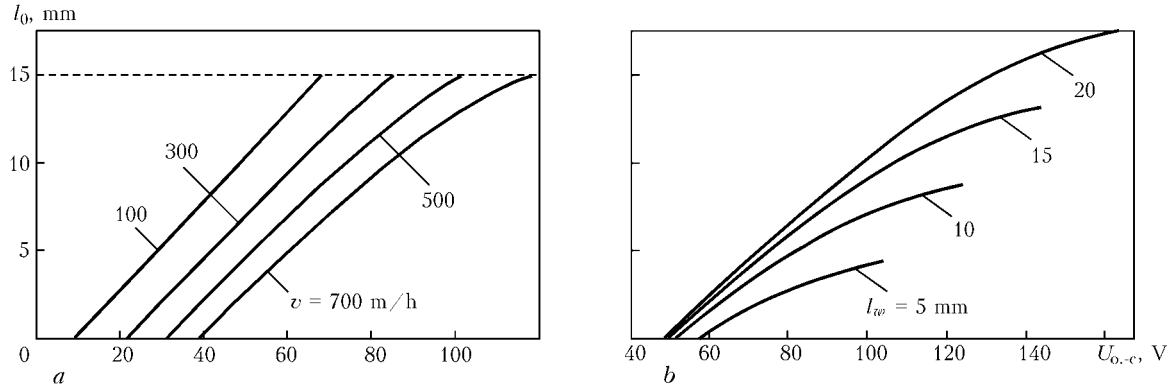

Figure 3. Dependence of stationary arc length l_0 on open-circuit voltage $U_{o.-c}$ of a source at different rates v of electrode wire feed (*a*) and distance l_w between the nozzle and item (*b*)

$$U_{o.-c\ min} < U_{o.-c} < \frac{qv\gamma SR_s + U_a El_w}{U_a},$$

where $U_{o.-c\ min}$ is the minimum value of open-circuit voltage found from the following equation:

$$\rho l_w U_{o.-c}^2 + U_a(SR_s + \rho l_w)U_{o.-c} - qv\gamma(SR_s + \rho l_w)^2 = 0.$$

Figure 3 shows the constraints, which are imposed on the open-circuit voltage of the source at different welding process parameters. Figure 3, *b* shows that the constraints are becoming more «stringent» with smaller distance between the nozzle and item.

Static volt-ampere characteristic of a consumable-electrode arc. Stationary value of arc length studied above, is important in determination of the static volt-ampere characteristic of the arc. This is attributable to the fact that it is easier to experimentally measure this characteristic, i.e. voltage dependence on current. With our assumptions the arc column voltage is related to its length by ratio $U_0 = El_0$.

Allowing for stationary arc length determined by formula (6), the expression for the static volt-ampere characteristic becomes

$$U_0 = E\,\frac{\rho l_w I_0^2 + SU_a I_0 - qv\gamma S}{\rho I_0^2}. \qquad (14)$$

As is seen from (14), the static volt-ampere characteristic is determined by the parameters of the arc (E, U_a), electrode wire (S, ρ, γ, q) and parameters of the welding process (v, l_w), but is not determined by the electric circuit parameters ($U_{o.-c}$, R_s, L).

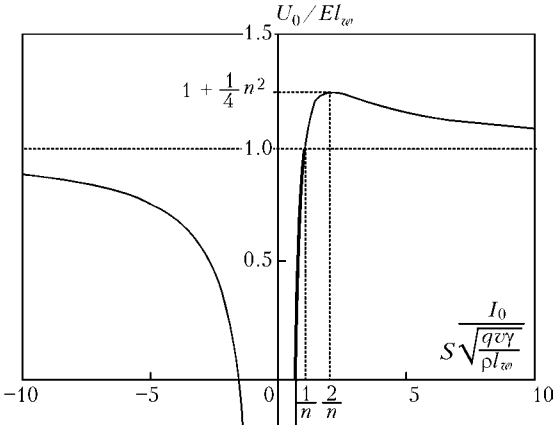

Figure 4. General view of function u'

For the analysis to be comprehensive, let us dwell in greater detail on studying the general properties of function (14).

At selection of scale of voltage El_w and current $S\sqrt{(qv\gamma)/\rho l_w)}$, expression (14) can be presented as a one-parameter function:

$$u' = 1 + \frac{n}{i'} - \frac{1}{i'^2},$$

where u' and i' are the scaled values of voltage and current, respectively; $n = U_a/\sqrt{qv\gamma\rho l_w}$ is the sole parameter, which combines the parameters of the arc, electrode wire and the welding process.

It should noted that the form of this function does not essentially depend on parameter n. The maximum always lies higher than and to the right of the point of the function crossing the unity level, i.e. does not enter the region of existence, which in Figure 4 is shown by a heavy line, with any parameter values.

Thus, the static volt-ampere characteristic of the consumable-electrode arc is always a rising characteristic without extremums, and exists only in a certain range of currents.

Figure 5 shows a family of volt-ampere characteristics. From the Figure it is seen that the conditions of existence (9) imposed on the arc length, also affect the static condition current of the considered system.

For a consumable-electrode arc it may vary in the following limits:

$$I_{0\ min} < I_0 < \frac{qv\gamma S}{U_a}, \qquad (15)$$

where $I_{0\ min}$ is the minimum current of the consumable-electrode arc, where the value can be easily determined by solving the following quadratic equation:

$$\rho l_w I_0^2 + SU_a\, I_0 - qv\gamma S^2 = 0. \qquad (16)$$

It is obvious that expressions (15) and (16) can be used at selection of welding current by electrode wire and welding process parameters.

Figure 6 shows the influence of the slope of the external characteristic of the power source on the

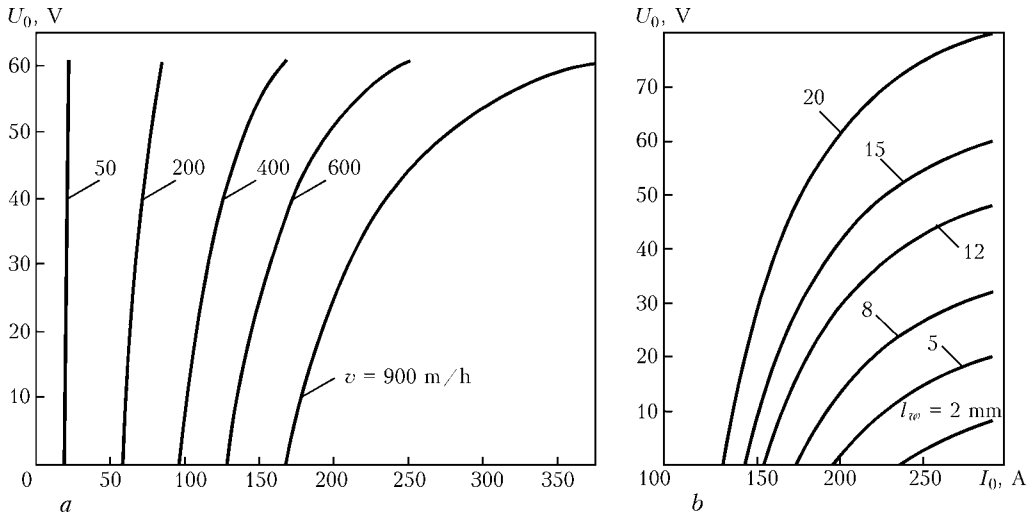

Figure 5. Static volt-ampere characteristic U_0 of a consumable-electrode arc at different rates v of electrode wire feed (*a*) and distance l_w between the nozzle and item (*b*)

parameters of a stable welding process. The higher the open-circuit voltage, the greater the value of the minimum ballast resistance to satisfy the conditions of existence (9). At low values of open-circuit voltage, providing the full range of arc current variation (15) requires special power sources with rising external characteristics [1].

In the case of application of the traditional power sources the range of arc current variation is reduced: $I_{0\,\min} < I_0 < I_{0\,\max}$, where $I_{0\,\max}$ iis the maximum current of the consumable-electrode arc, where the value can be determined by solving the following quadratic equation:

$$\rho(U_{o.-c} + U_{à} - El_w)I_0^2 - S(qv\gamma\rho + EU_{à})I_0 + qv\gamma ES^2 = 0.$$

In Figure 6 this case corresponds to point curves. Maximum arc length, which corresponds to maximum current can be determined by solving the following equation:

$$E^2 l_0^2 + [qv\gamma\rho - E(2U_{o.-c} + U_{à})]l_0 + \\ + U_{o.-c}(U_{o.-c} + U_{à}) - qv\gamma\rho l_w = 0.$$

Studies [1, 2] give a sufficient number of experimental static volt-ampere characteristics of a consumable-electrode arc. They have diverse shapes, and are difficult to interpret or generalize (most probably, because of different experimental conditions). Let us illustrate it by several examples. A volt-ampere dependence can be measured by varying the current due to variation of the electrode wire feed rate. Such a technique is the most readily applicable for technologists. The static volt-ampere dependencies will have the shape, shown in Figure 7, *a*. They can be described using the following expression:

$$U_0 = E\,\frac{U_{o.-c}S - (R_sS + \rho l_w)I_0}{ES - \rho I_0}.$$

However, this is not the static volt-ampere characteristic of a consumable-electrode arc. This, essentially, is the external characteristic of the power source, allowing for the voltage drop on the electrode wire. Almost all the curves are of the same type, except for the case of low rates of electrode wire feed.

Figure 7, *b* shows the volt-ampere characteristics, which can be obtained by varying the arc current due to variation of the distance between the nozzle and item. The formula, describing these curves, has the following form:

$$U_0 = U_{o.-c} + U_{à} - R_sI_0 - \frac{qv\gamma S}{I_0}.$$

At large distances from the nozzle to the item, the characteristic can be manifested completely, at small distances ---- just partially, according to the conditions of existence. Quite often just part of the characteristic is determined in the experiment. This, probably, is what accounts for the scatter of experimental data [1, 2].

Transfer function of the consumable-electrode arc. The proposed model yields the transfer function of the consumable-electrode arc. As the arc as an element of the electric circuit is a bipole, the transfer function can be represented by resistance

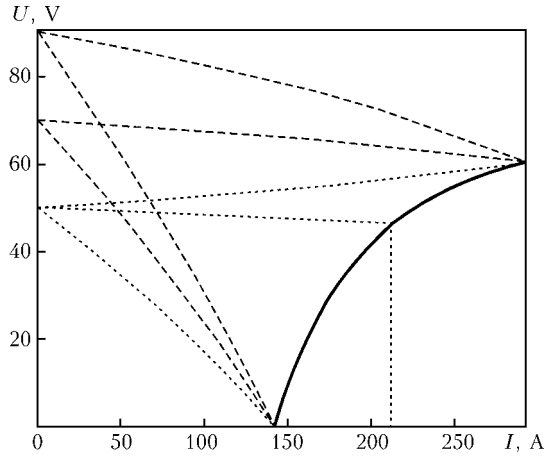

Figure 6. Static volt-ampere characteristic of a consumable-electrode arc (*solid lines*), and external characteristics of the power source (*dashed and point*)

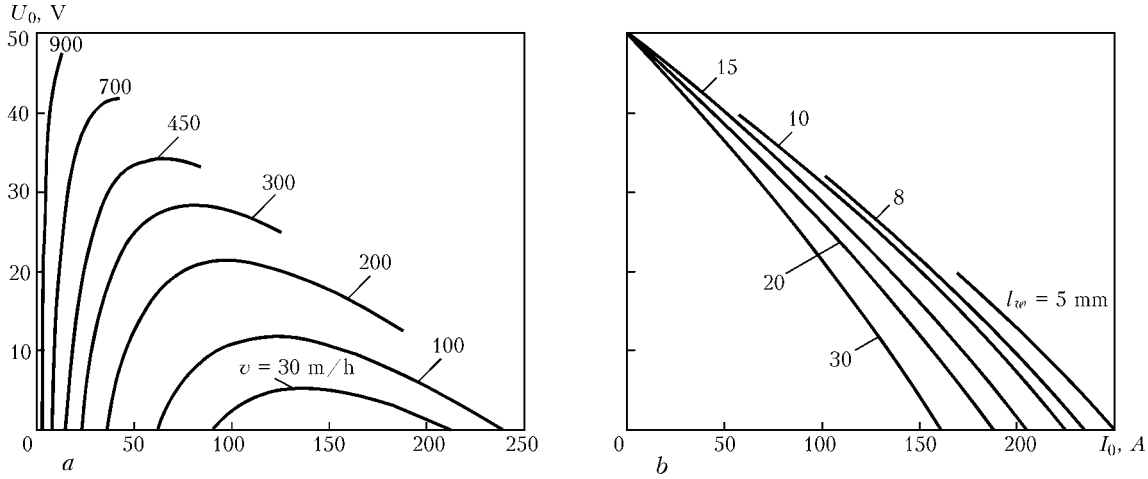

Figure 7. Volt-ampere characteristics obtained by variation of rate v of electrode wire feed (a) and distance l_w between the nozzle and item (b)

$$W(p) = \frac{\Delta u(p)}{\Delta i(p)},$$

where $\Delta u(p)$ and $\Delta i(p)$ are the Laplace maps for arc voltage and current increments. Allowing for $U_0 = El_0$, the voltage increment is proportional to arc length increment. In order to find the latter, let us use the first equation of system (4). As a result

$$W(p) = E\,\frac{SU_{\text{à}} + 2\rho(l_w - l_0)I_0}{\rho I_0^2}\,\frac{1}{\frac{q\gamma S^2}{\rho I_0^2}p + 1} = \frac{1}{\tau p + 1}.$$

This formula shows that in the case of a fine-drop transfer the consumable-electrode arc is an aperiodic link of the first order, where the gain is equal to

$$k = E\,\frac{SU_{\text{à}} + 2\rho(l_w - l_0)I_0}{\rho I_0^2},$$

and the characteristic time is

$$\tau = \frac{q\gamma S^2}{\rho I_0^2}.$$

At different parameter ratios, characteristic time τ can vary from tens of milliseconds to units of seconds.

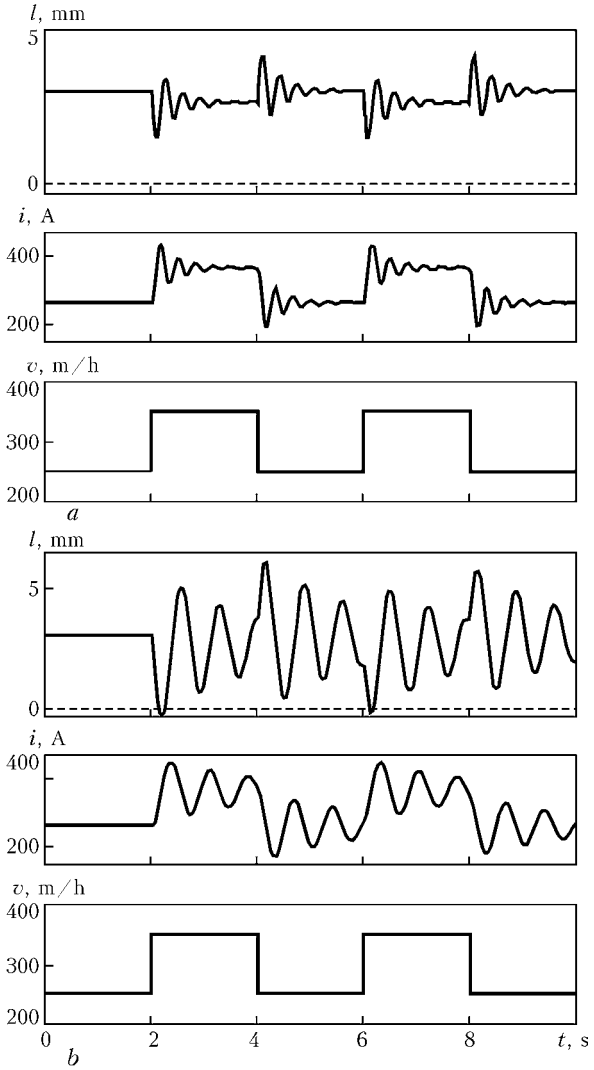

Figure 8. Oscillogram of reaction to disturbances by the rate of electrode wire feed of the system of power source–consumable-electrode arc at $U_{o.c}$ = 55 V, R_s = 0.05 Ohm, $L = 1\cdot10^{-2}$ (a) and $5\cdot10^{-2}$ (b) H

Stability of the system of power source–consumable-electrode arc. Investigations of the stability of this system can be divided into two stages, namely study of its static condition (described above) and its dynamic behaviour at small deviations from the static condition.

For this purpose let us find Jacobian matrix for the studied system (4)

$$J = \begin{bmatrix} \frac{\partial}{\partial i}\frac{di}{dt} & \frac{\partial}{\partial l}\frac{di}{dt} \\ \frac{\partial}{\partial i}\frac{dl}{dt} & \frac{\partial}{\partial l}\frac{dl}{dt} \end{bmatrix} =$$

$$= \begin{bmatrix} -\frac{1}{L}\left(R_s + \rho\,\frac{l_w - l_0}{S}\right) & \frac{1}{L}\left(\frac{\rho}{S}I_0 - E\right) \\ \frac{SU_{\text{à}} + 2\rho(l_w - l_0)I_0}{q\gamma S^2} & -\frac{\rho I_0^2}{q\gamma S^2} \end{bmatrix}$$

in the vicinity of the static condition. Then, characteristic equation is found from the condition $\det(J - \eta I) = 0$, and it has the form of (I is the unit matrix)

$$q\gamma LS^3\eta^2 + S[\rho LI_0^2 + q\gamma R_s S^2 + q\gamma\rho S(l_w - l_0)]\eta + \ldots +$$
$$+ EU_{\text{à}}S^2 + \rho SI_0[R_sI_0 - U_{\text{à}} - 2E(l_w - l_0)] -$$
$$- \rho^2 I_0^2(l_w - l_0) = 0,$$

where η are the proper values of the examined system.

Proceeding from the root values of the characteristic equation, it is possible to determine the nature of local stability of the dynamic system. The boundary condition, when the real part of proper values is zero, is similar to the condition, when the coefficient at η is zero, in our case:

$$\rho LI_0^2 + q\gamma S^2 R_s + q\gamma\rho S(l_w - l_0) = 0. \qquad (17)$$

As all the addends in formula (17) have positive values, the equality is not satisfied. Thus, the system is locally stable with all the parameter combinations and constraints remain only for the cases of (9) existence.

Numerical simulation and discussion of results. In order to study the dynamics and stability of the power source–consumable-electrode arc system, without limiting ourselves to the locality conditions, the proposed model (4) was transferred into the program software MATLAB Simulink environment. Time dependencies were derived for the transient processes. The case of system disturbance by the electrode wire feed rate is considered as the test case. Investigations confirmed the validity of the above conclusions on the local stability of the system. Although the consumable-electrode arc is an aperiodic link, it can have an oscillatory nature in the electric circuit, particularly, at large values of inductance L of the welding circuit choke and small values of ballast resistance R_s.

Figure 8 shows how the system of power source–consumable-electrode arc reacts to a disturbance by the electrode wire feed rate. It should be noted that at a stationary arc length the oscillatory process can lead to failure to satisfy the condition of existence of the arc (9) in the dynamics (see Figure 8, *b*), and this, in its turn, to shorting of the arc gap and disturbance of the welding process.

Period (up to 1 s) and amplitude (tens of amperes) of arc current oscillation in the transient process are quite large and may affect weld quality. This situation is difficult to influence. Choke inductance should be large enough so as to smooth the rectified current. Increase of resistance leads to deterioration of the energy characteristics of the welding process, as well as weight and dimensional characteristics of the power source.

One of the solutions in such a situation is to apply arc voltage and current feedbacks and replace the DC welding process by pulsed-arc welding.

CONCLUSIONS

1. The proposed model of the system of the power source–consumable-electrode arc allows determination of the welding process parameters and arc length, at which the welding process can be performed.

2. The static volt-ampere characteristic of the consumable-electrode arc has a rising shape and exists in a certain range of currents.

3. Obtained transfer function of the arc shows that in the case of fine-drop transfer the consumable-electrode arc can be regarded as the aperiodic link of the first order.

4. Local stability does not guarantee a normal reaction to disturbances arising in the system of the power source–consumable-electrode arc. Disturbance of the conditions of existence in the dynamics, i.e. transient process, is possible.

1. Zaruba, I.I., Kasatkin, B.S., Kakhovsky, N.I. et al. (1966) *CO_2 welding*. Kiev: Tekhnika.
2. Potapievsky, A.G. (1974) *Consumable electrode shielded-gas welding*. Moscow: Mashinostroenie.
3. Varukha, E.N., Doktorsky, R.Ya. (1991) Calculation of electrode fusion rate in mechanized welding. *Svarochn. Proizvodstvo*, **6**, 33–35.
4. Tsybulkin, G.A. (2002) Stability of GMAW. *The Paton Welding J.*, **5**, 14–16.

ANALYSIS OF THE MECHANISM OF JOINING AND FORMATION OF VISCOUS LAYER IN FRICTION STIR WELDING

R. CIRIC[1], **S. CANTRAK**[2] and **K. RAIC**[2]
[1]Higher Technical School, Cacak, Serbia and Monte Negro
[2]Beograd University, Beograd, Serbia and Monte Negro

Phenomena developing in the process of continuous friction stir welding of high-speed steel R6M5 to carbon steel 60 are considered. Mathematical expression to calculate radial displacements of metal directly up to the friction surface has been proposed and experimentally verified. Structure, phase composition and chemistry of a viscous layer, friction plane and neighbouring zones have been examined.

Keywords: *friction stir welding, high-speed steel, carbon steel, plastic deformation, calculation of displacements, viscous layer, joining mechanism, microstructure, phase composition*

The process of continuous friction stir welding (FSW) consists of five phases [1, 2]: initial friction (I), unstable friction (II), stable friction (III), the so-called quasi-stationary phase, deceleration (IV) and consolidation-forging (V). It has been found that phase III begins when the layer characterised by a high plasticity and low strength propagates over the entire friction plane [2–8]. It is thought that dynamic thermal equilibrium between the amounts of released heat and heat transferred to the base metal (BM) is established in this phase. Maximal temperatures and minimal friction coefficients are achieved in the friction plane, the started diffusion processes are accelerated, and conditions for formation of a metal layer in viscous state are created in this phase because of a high plastic deformation of thin contact layers of BM.

Unlike welding of similar metals, friction welding of materials with different thermal-physical properties provides the highest degree of deformation inside one of the materials joined, rather than at the end surfaces of BM [9–11]. This peculiarity is especially pronounced in friction welding of high-alloy high-speed steels (poly-phase materials with a carbide phase content of more than 20 %) to two-phase (pearlitic-ferritic) carbon steels.

Attempts have been made lately to describe certain phenomena taking place in the viscous layer in a phase of the so-called dynamic equilibrium in friction welding of similar materials [9, 12]. At the same time, neither qualitative nor quantitative description is available for the mechanism of flow of viscous fluid containing a large amount of solid phase in friction welding of dissimilar materials, e.g. high-speed to carbon steels.

Table 1. Comparative designations of steels used

Steel grade	*EN*	*DIN*	*W.Nr*	*AISI/AE*
R6M5*	HS 6-5-2	S 6-5-2	1.3343	611.M2
60	C-60	C-60	1.0601	–

*The used high-speed steel is manufactured as M-2 grade by «Comentrien», France.

The purpose of this study is to quantitatively measure parameters of plastic deformation in the immediate proximity to the friction plane, describe the mechanism of joining high-speed to carbon steels in the friction phase (primarily in phase III), and investigate physics of the process occurring in the viscous layer and neighbouring zones.

Materials and experimental procedure. The high-speed steel R6M5 and steel 60 samples (Table 1) with a diameter of 10 mm were used for welding. Chemical composition of these steels is given in Table 2. The materials were welded to each other by the continuous FSW method (Figure 1). Parameters of the process were as follows: friction pressure P_f = 80 MPa, friction time V_f, s (variable), and rotation frequency ω (in the experiment ω = const = 2850 min^{-1}). Parameters in the forging phase included pressure P_{for}, MPa, and time V_{for}, s. The R6M5 steel sample was rotated during the experiment.

Quantitative and qualitative analysis of layers in the friction plane zone, zone immediately adjoining the friction plane (high plasticity zone) and in the viscous layer was carried out on the experimental

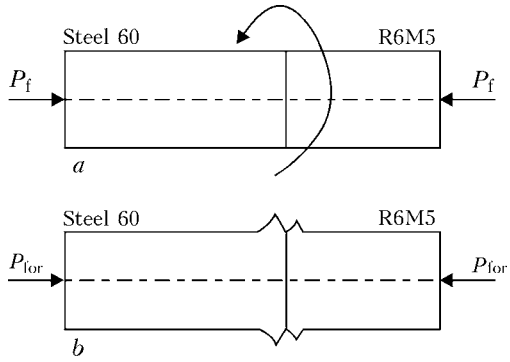

Figure 1. Flow diagram of continuous friction stir welding process in friction phase (*a*) and in consolidation-forging phase (*b*)

Table 2. Chemical composition and hardness of base materials

Steel	Content of elements, wt.%									Hardness HB
	C	Si	Mn	Cr	W	Mo	V	S	P	
R6M5*	0.86	N / D	N / D	4.07	6.03	4.75	1.82	0.0036	0.0137	260–272
60	0.63	0.194	0.82	0.0036	0.00273	–	–	N / D	N / D	N / D

*As-annealed.

samples. Measurements and calculations of shear of the base materials particles in the friction phase, as well as calculations of plastic deformation parameters were made to determine the character and degree of plastic deformation immediately near the friction plane. The mechanism of joining steel R6M5 to steel 60 in the friction phase, primarily in phase III of the process, was described on the basis of detailed metallography analysis and general studies.

Processes occurring in the viscous layer and neighbouring zones were investigated during experiments by the optical and quantitative optical microscopy, electron microscopy and energy-dispersion spectroscopy (EDS) analysis methods.

Effect of parameters of FSW of steel R6M5 to steel 60 on character of plastic deformation of layers immediately near the friction plane. The main purpose of the experiment was to measure the degree of plastic deformation of steel R6M5 within the friction plane zone in the friction phase using different FSW parameters. The experiment was conducted on samples with a diameter of 10 mm. Holes 0.7 mm in diameter were longitudinally drilled in the samples at different distances from the rotation axis, wherein copper conductors of the same diameter were inserted. The conductors were moved during the welding process together with the BM. Thin metal layers were removed from both base materials after welding. Then radial and tangential displacements of the holes (conductors) were measured, compared with a position before welding. This procedure was employed to evaluate shears at a distance of 0.5 mm and more from the joining line. However, it was impossible to measure shears in the zones located near the joining line because of a high deformation of the contact metal layers.

Rotation of a conductor between the neighbouring planes (transverse sections of a sample) spaced at 0.5 mm from each other was determined in a radial direction from diameter increment Δr, and in a tangential direction ---- from a change in arc length $\Delta s = r\Delta\alpha$, where $\Delta\alpha$ is the increment of the angle of rotation of a conductor along length $\Delta l = 0.5$ mm.

The total relative rotation (shear) is determined by the following relationship:

$$\gamma = \text{tg}\,\beta = \frac{\sqrt{(\Delta r)^2 + (\Delta s)^2}}{\Delta l}. \quad (1)$$

Elongation ε and deformation rate ε' can be determined from the following relationships [13]:

$$\varepsilon = (\gamma + \sqrt{1 + \gamma^2})^{1/(1-k)}, \quad (2)$$

$$\varepsilon' = \frac{\Delta\varepsilon}{V}, \quad (3)$$

where k is the shear deformation coefficient ($k = -1$); $\Delta\varepsilon$ is the increment of relative deformation along the length; V is the time of shortening of samples by the Δl value equal to $\Delta l / i$; and i is the rate of shortening of a test sample in the friction phase during welding, mm / s.

Figure 2 shows values of the degree of deformation (elongation) and rate of deformation of steel R6M5 in the friction phase, obtained on the basis of experimental results using equations (1) through (3). As seen from the measurement results, radial and tangential shears of metal at the measurement points grow with distance to the joining line and with increase of the initial distance of a hole (conductor) from the rotation axis, as well as with growth in P_f and V_f.

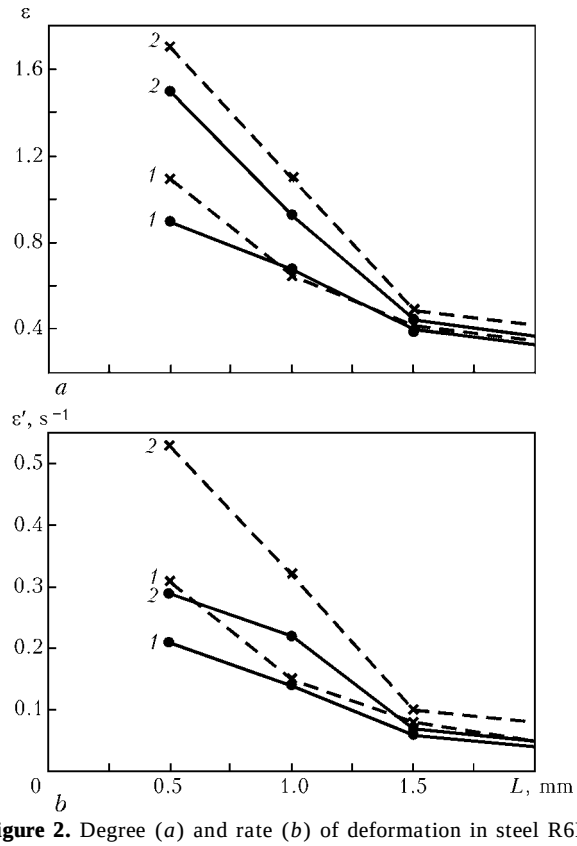

Figure 2. Degree (*a*) and rate (*b*) of deformation in steel R6M5 at different distance L from the friction surface at points initially located at 2.5 (curves *1*) and 4 mm (curves *2*) from the rotation axis at $V_f = 10$ (*solid curves*) and 12.5 s (*dashed curves*)

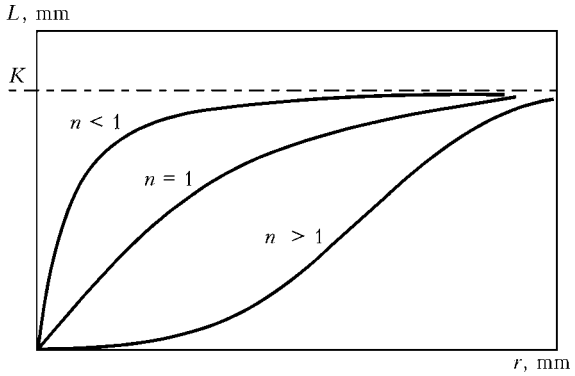

Figure 3. Plots of function (4) at different n values

Radial shears of the measurement points under the used FSW conditions are larger than tangential ones, the $\Delta r / \Delta s$ ratio growing with increase in distance from the rotation axis. Growth of radial displacements compared with tangential ones is attributable to consequences of FSW with a high rotation frequency, resulting in decrease in torsion of metal through depth. In this case the deformation takes place in a thinner metal layer. At the same time, it is easier for metal to flow in a radial direction because of a small diameter of BM (10 mm).

The degree and rate of deformation grow both with increase in V_f and initial distance of a measurement point from the rotation axis, and with decrease in distance to the joining line. A relatively high degree of plastic deformation of steel R6M5 ($\varepsilon = 0.45$–1.51) is provided at a distance of 0.5–1.0 mm from the joint.

Therefore, mainly the parameters of plastic deformation (Δr, Δs, γ, ε and ε') grow at a constant pressure and velocity of friction with increase in the friction time. At $V_f > 13.5$ s the process enters into the so-called quasi-stationary friction phase, in which the temperature-deformation conditions remain almost unchanged.

Measurement and calculation of displacements immediately near the friction plane in steel R6M5. The expression for calculation of displacements caused by thermal deformation in phase III of the FSW process immediately near the friction plane in steel R6M5 was derived during the studies. Measurement of a displacement was made in a region spaced at 0.4 mm from the friction plane. The latter is at a distance of 0.1 mm from the joining line between steel R6M5 and steel 60, and is located in steel R6M5. At the same time, the effect of other factors, such as position of a moveable rotation plane, presence of a viscous layer, mixing zone, dissolution of the carbide phase, high degree of alloying of the austenite phase, etc., makes it impossible to precisely measure the displacement in a region spaced at less than 0.2 mm from the joint (i.e. at 0.1 mm from the friction plane).

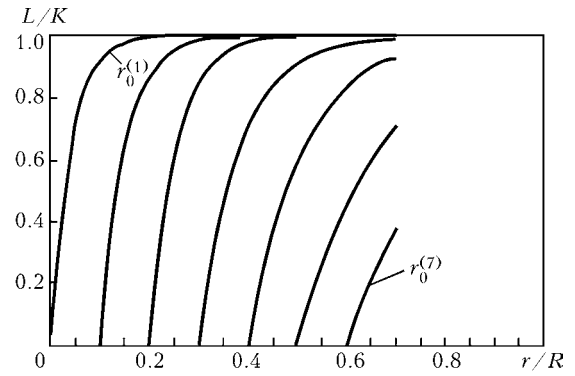

Figure 4. Radial displacements of carbide lines in steel R6M5 at different distances from the friction plane and initial distance from the rotation axis

The following general equation of the JMAK type [14–21], describing flow of a material, i.e. displacement of the carbide phase in the friction phase (Figure 3), has been derived on the basis of a detailed experimental analysis:

$$L = L(r, r_0, k, n) = K\left(1 - \exp\left[-\left(\frac{r - r_0}{k(r_0)}\right)^n\right]\right), \quad (4)$$

where L is the distance from the initial position of the plane, mm; r_0 is the initial distance of the carbide phase from the rotation axis at $L = 0$; $k(r_0)$ is the constant determining the slope of the curve (horizontal projection of a tangent line at intersection of axis r with asymptote (friction plane)); K is the initial distance of the measurement plane from the friction plane ($K = 0.4$ mm); n is the Avrami exponent [14–22]; $n \notin Q$, $n \notin R$ and $n > 0$.

Expression (4) does not allow for displacements in the tangential direction, which are much smaller than the radial ones, according to the measurement results given in [12].

According to studies [19–27], on the basis of numerous experimental values of dependence $\log R = f(\log \varepsilon')$ for high-speed steels [28] (where R is the strength), and on the basis of authors' investigation results, it is shown that at exponent $n \approx 1$ expression (4) has the following form:

$$L = L(r, r_0, k) = K\left(1 - \exp\left[\frac{r - r_0}{k(r_0)}\right]\right). \quad (5)$$

Accuracy of expression (5) was checked experimentally by analysis of rotation of carbide lines for samples made under different FSW conditions. Direct dependence of the slope of the curves upon the radial distance of a carbide line from the rotation axis, i.e. upon $k(r_0)$, was determined. The results obtained can be shown as a family of the curves with different (r_0) values (Figure 4).

The following preliminary conclusion can be made on the basis of analysis of experimental and calculation data:

- expression (5) makes it possible to calculate the family of the curves of radial displacements against distance from the friction plane and initial radial distance from the rotation axis (Figure 5);
- radial displacements Δr in the coaxial region of a sample grow with distance to the friction plane and with increase of the initial distance from rotation axis r_0, and asymptotically approach a finite value. Expression (5) holds for this region;

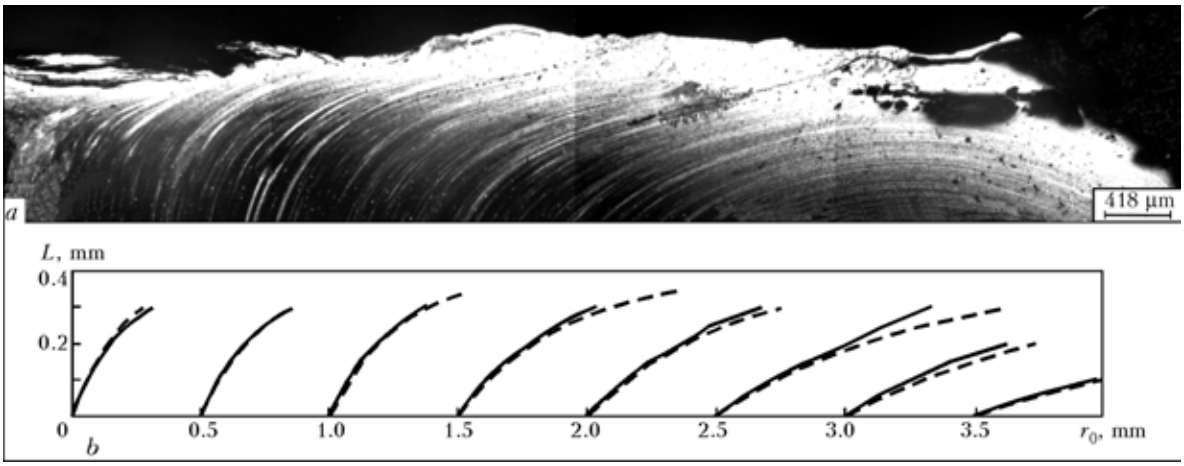

Figure 5. Microstructure of steel R6M5 in the friction plane region (*a*), and radial displacements ($\Delta r = r - r_0$) at a different distance from the friction plane, L, and different distance from the rotation axis, r_0 (*b*) (FSW without forging, V_f = 10 s): solid curve ---- experimental data; dashed curve — calculation data

• there is a «saddle-point» boundary in regions close to the external (cylindrical) surface of a sample. Here expression (5) holds directly up to the «saddle-point». Behind it the carbide lines continue moving in a radial direction, where they move from the friction plane;

• principles of displacement of a material in the coaxial region after asymptotic approach to the friction plane have not been analysed mathematically. It is thought that hard particles (carbides, non-metallic inclusions, etc.) in this zone enter into the viscous layer zone. Their further displacement follows the law of movement of hard particles in a viscous material. It is believed that non-metallic inclusions after entering into the viscous layer zone move very quickly in a tangential direction and are partially entrapped by the metal volumes, so that their forcing out from the friction zone (asymptotic plane) or their retention in it depends upon many factors. Investigation of the process of displacement of undesirable phase components (e.g. non-metallic inclusions) and their forcing out from the friction plane is of a high practical importance.

Mechanism of joining steel R6M5 to steel 60 in the friction phase. Physical model of the considered process of continuous FSW in the friction phase is based on friction of end surfaces of two cylinders, one of which (steel R6M5) is rotated at a high speed under high axial pressure and under conditions of a possible free outflow of the material in a radial direction. The process is characterised by a rapid increase in temperature and deformation in radial, tangential and axial directions, depending upon the assigned parameters of the process and peculiarities of BM [11, 29].

The beginning of phase I of continuous FSW is characterised by formation of the first bonds between steel R6M5 and steel 60, their disruption and transfer of particles of steel R6M5 to steel 60 [3, 7, 30]. Because of a relatively high friction velocity and relatively high pressure in the axial direction, i.e. lower volumetric velocity and deformation through a larger depth in the central part of a sample, coarser particles are transferred from steel R6M5 to steel 60. Further on the joining process in the friction plane occurs between the transferred coarse particles of steel R6M5 and the remaining particles, develops up to their deformation at a complex path of movement of the particles and, in parallel, up to their forcing out from the friction plane [3, 7]. Because of a rapid increase in the contact surface, the friction moment reaches its maximal value already at the beginning of phase I (Figure 6), which leads to increased heat release and increased temperature in the friction plane.

In phase II of the friction process, metal of the contact zone under conditions of high temperatures, increased depth of the zone heated to a high temperature and decreased resistance to plastic deformation is deformed to a high degree. A change in thermal-deformation conditions is accompanied by a change in character of the metal flow in the high-plasticity zones. In a region immediately adjoining the friction plane the highly plastic metal moves by the mechanism of not only rotational but also vortex (laminar and turbulent) flow. The rotational flow is caused by the nature of a physical model of the process, whereas the turbulent flow is mostly a result of peculiarities of BM.

Steel R6M5 is a material that contains about 20 % of the carbide phase with carbide precipitates of a

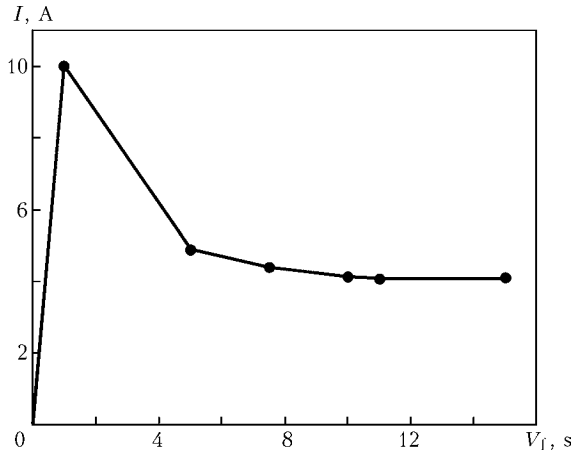

Figure 6. Dependence of current of the motor (friction moment) upon friction time V_f in FSW of steel R6M5 to steel 60

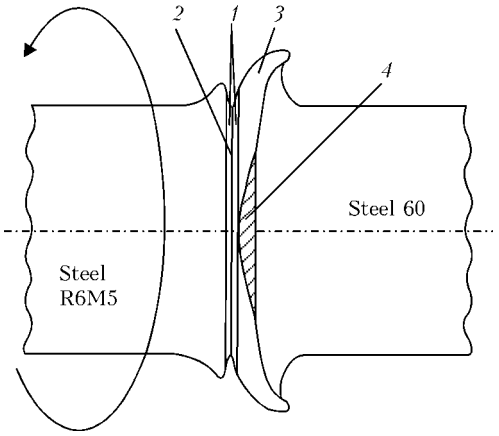

Figure 7. Schematic of characteristic zones in friction plane (phase III) of the process of FSW of steel R6M5 to steel 60: *1* — viscous layer; *2* — carbide layer (d = 0.001–0.006 mm) formed near the friction plane; *3* — layer of steel R6M5 deposited on steel 60; *4* — mixing zone

different type and size. Displacements of highly plastic particles of steel R6M5 in a layer deposited on steel 60 and in a remaining part of steel R6M5 also cause displacements of hard particles of the carbide phase. As the friction phase becomes longer, the content of the carbide phase decreases due to dissolution in solid solution and retention on a rotating side of the friction plane [9–11].

Another important cause of formation of the turbulent flow is that mixed particles of both BM with different mechanical and thermal-physical properties exist in the high-plasticity zone.

Increase in the friction time leads to decrease in the effect of the above two factors, while the effect of nature of the process proper on the type of the turbulent flow grows.

Phase III begins when the layer of steel R6M5 characterised by high plasticity and low resistance to thermal plastic deformation widens over the entire friction plane. Plastic deformation in this phase develops mostly in thin contact layers of steel R6M5, and equilibrium is established between the amount of released heat and heat transferred to BM [9]. Because of a high deformation degree, the so-called polishing of thin contact layers of steel R6M5, maximal temperatures and a state of high plasticity are achieved in them [2, 4], resulting in a decrease of the friction coefficient and friction moment to a lower constant level. In this phase of the process of FSW of steel R6M5 to steel 60 the started diffusion processes are accelerated and restrict conditions for mixing of the BM particles, and a metal layer in the viscous state is formed in the friction plane [9, 30].

In the initial phase of its formation the viscous layer contains more than 10 % of the hard carbide phase particles. At the same time, as the process becomes longer, the content of non-dissolved carbides decreases because of their dissolution in solid solution, retention at the viscous layer boundary on the rotating side [9] and forcing out from the friction plane. Carbides retained on the end surface of a rotating sample of steel R6M5 form a flat front of carbides on the friction plane. Schematic of characteristic zones in the friction plane in phase III of the process of FSW of steel R6M5 to steel 60 is shown in Figure 7.

It can be concluded on the basis of the above mechanism of joining of the steels tested that a mixing zone (Figure 7, zone *4*) 50–150 μm thick is formed in steel R6M5. Mixing of particles of both BM begins and deformation of a high level takes place in this zone. After air cooling, this zone has a high-strength martensite-austenite-carbide structure (Figure 8). This zone is formed in a layer of steel R6M5 deposited on steel 60 (Figure 7, layer *3*) and is in contact with the layer of steel R6M5 on the other side of the rotating friction plane (Figure 8). The latter may be of a wavy form, which proves the fact that in the friction phase the material joined displaces in a somewhat turbulent manner (Figure 9). More detailed explanations of formation of the deposited layer are given in [12].

The carbide layer with a flat front is often formed in the friction plane on the end surface of a rotating sample of steel R6M5 during the FSW process. At the same time, carbides on the other side are squeezed into the sample of steel R6M5 (Figure 10). On the side of the steel R6M5 layer deposited on the sample of steel 60, which was not rotated, no solid or continuous carbide plane is seen.

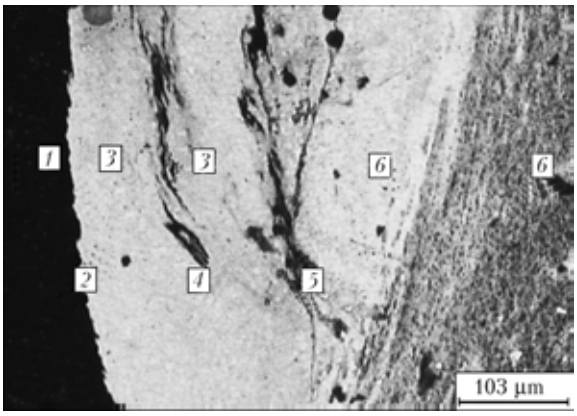

Figure 8. Microstructure of characteristic zones in region of the friction plane between steel R6M5 and steel 60 (without forging, V_f = 12 s): *1* — steel 60; *2* — joining line between steel R6M5 and steel 60; *3* — layer of steel R6M5 deposited on steel 60; *4* — particles of steel 60 remaining in the layer of steel R6M5 deposited on steel 60; *5* — friction plane; *6* — steel R6M5

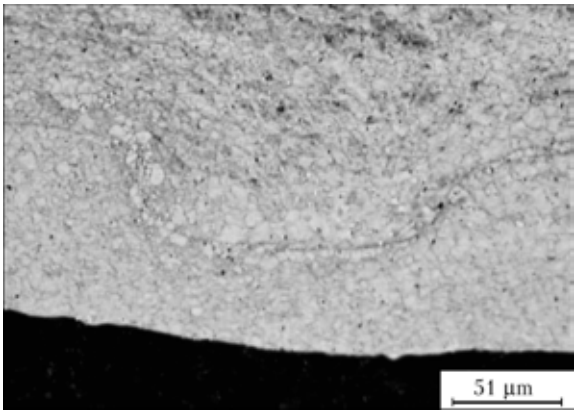

Figure 9. Microstructure of steel R6M5 in friction plane region

The presence of a narrow layer with a low content of the carbide phase and coarser crystalline grain, compared with the neighbouring zones, was revealed on both sides of the friction plane (Figure 11). According to the results given in studies [9, 30], this layer is formed in cooling of the viscous layer formed in phase III of FSW.

Investigation of processes occurring in viscous layer and neighbouring zones. Detailed analysis of microstructure, chemical and phase composition of the welded joint region, particularly the viscous layer and friction plane regions, was performed by the optical and quantitative optical microscopy, electron microscopy and EDS methods. The analysis covers mostly phenomena occurring in phase III of the FSW process.

Microstructure of viscous layer. As reported in studies [9, 30] and according to the authors' investigation results, a viscous metal layer is formed in phase III of the FSW process (Figure 12). This is a boundary layer, and processes occurring in it can be regarded as a continuous medium flow in the boundary layer.

After phase III and air cooling (solidification and transformation in solid state), the viscous layer is a narrow layer on both sides of the friction plane with a lower content of the carbide phase, compared with the neighbouring layers. The viscous layer, especially in the central portion of a sample, is divided by a clearly defined friction plane (rotating plane) into two parts. The carbide layer, the so-called carbide plane, is often formed immediately near the rotating friction plane on the side of steel R6M5.

Under the FSW conditions the viscous layer in the central portion of a sample is formed in the majority of cases in parallel or almost in parallel to the rotation axis (Figure 12, *a–c*), whereas in remote portions of the samples it is formed at a certain angle (radius) to the rotation axis (Figure 12, *d, e*). This is indicative of the fact that the flow of a viscous metal mass takes place in the viscous layer in the friction phase, along with the rotational and laminar flows, and that this flow takes place by a different mechanism.

Electron microscopy (JEOL microscope JSM-5300, Japan) shows that the viscous layer of a certain width is formed on both sides of the friction plane, the viscous metal mass and hard carbide particles describing a complex path when moving in this layer. As noted, after solidification (Figure 13) the metal is in a solid-liquid (viscous) state with a relatively low viscosity. This state of the metal leads to retention of hard carbide and other particles in a viscous mixture of a two-phase solid-liquid metal (Figure 14).

Therefore, a partial or full detachment of carbide and other particles from their initial position and their rotation to a certain angle parallel to the friction plane were seen immediately near the friction plane, in a zone subjected to a high plastic deformation. Figure 15 shows cavities near a partially detached carbide, which can be formed in a complex process

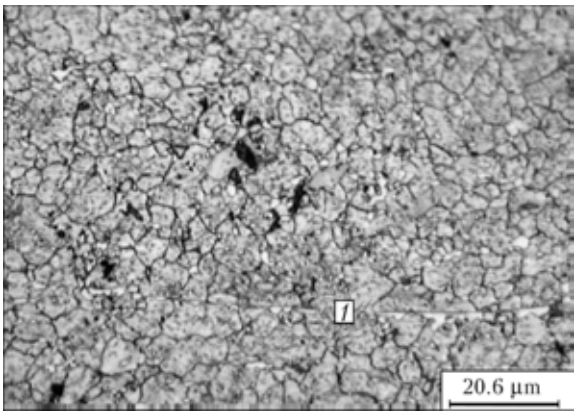

Figure 10. Microstructure of metal of bonds in friction plane region with a formed carbide plane (*1*) (FSW without forging, V_f = 18 s)

of high plastic deformation or in a zone from which a carbide or any other hard particle was previously pulled out.

Examinations performed in the immediate proximity to the friction plane or in the plane proper reveal the presence of individual non-carbide particles.

Results of EDS analysis. Along with analysis of microstructure, the EDS method (Link-DX 2000 instrument manufactured by Oxford Institute, England) was used to analyse composition of metal in a region spaced at 1 mm from the sample axis (rotation axis), in the friction plane and in the zone of mixing of both BM, as well as to analyse individual particles in the immediate proximity to the viscous layer and in the layer proper. The FSW parameters were as follows: V_f = 15 s, no forging, air cooling.

As shown by the EDS analysis results, the viscous layer immediately near the friction plane contains the same alloying elements as alloyed BM (steel R6M5), whereas chemical composition of the mixing zone may vary in a direction from one to the other measurement point, and at some points the metal base of the zone may contain a considerable amount of steel 60. The EDS spectra of individual particles in the friction plane region of steel R6M5 show that they are alloyed with vanadium (probably with carbides VC [11]). The presence of inclusions alloyed with aluminium and silicon was proved.

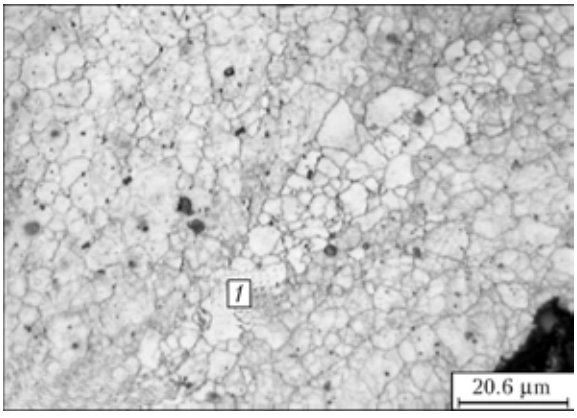

Figure 11. Microstructure of viscous layer (*1*) (FSW without forging, air cooling)

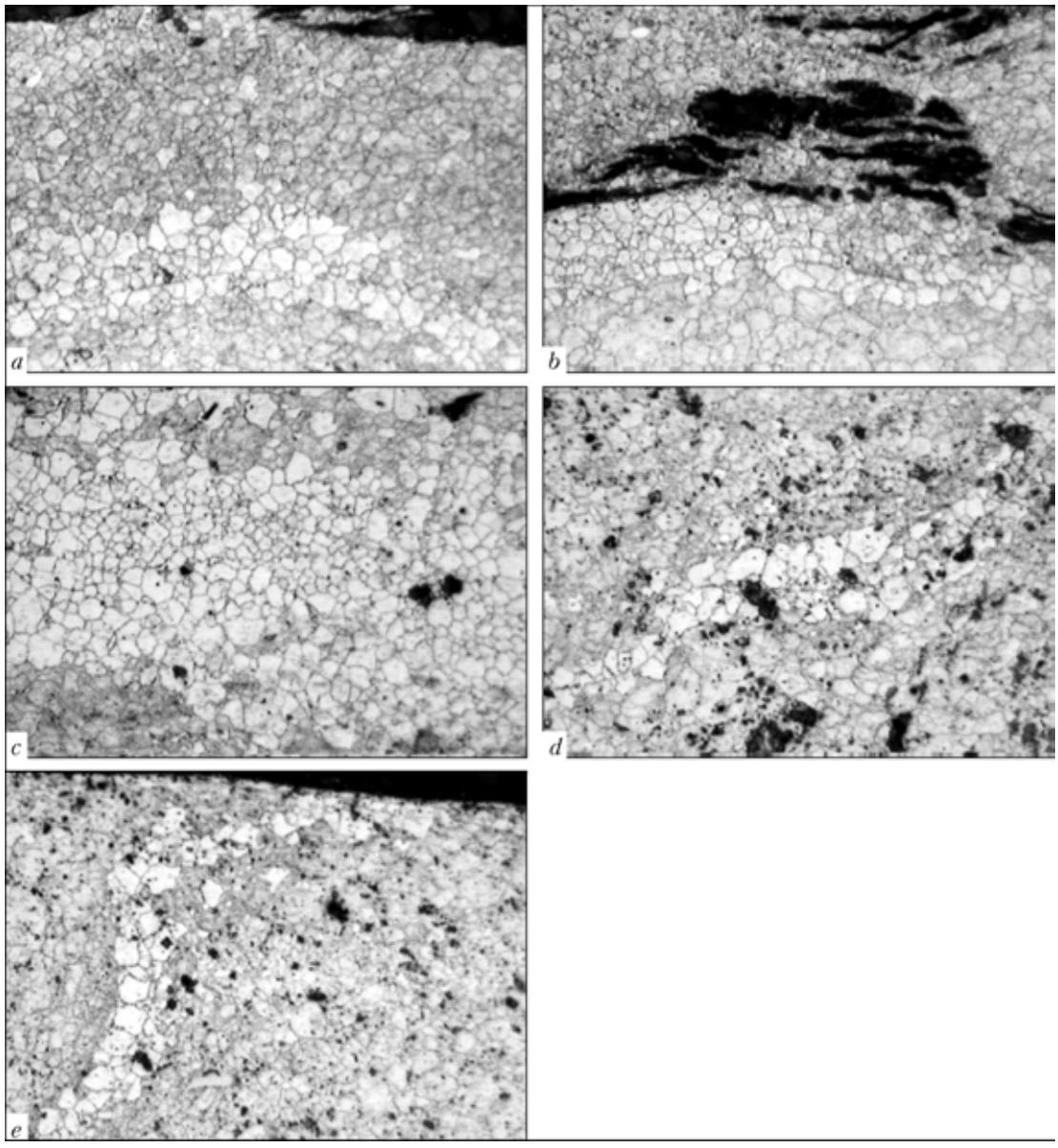

Figure 12. Microstructure of viscous layer across the FSW joint between steel R6M5 and steel 60 at different distances from the rotation axis: *a* — rotation axis; *b* — 1250; *c* — 2500; *d* — 3750; *e* — 5000 μm

Figure 13. Microstructure of metal of the joint in friction plane region (×5000)

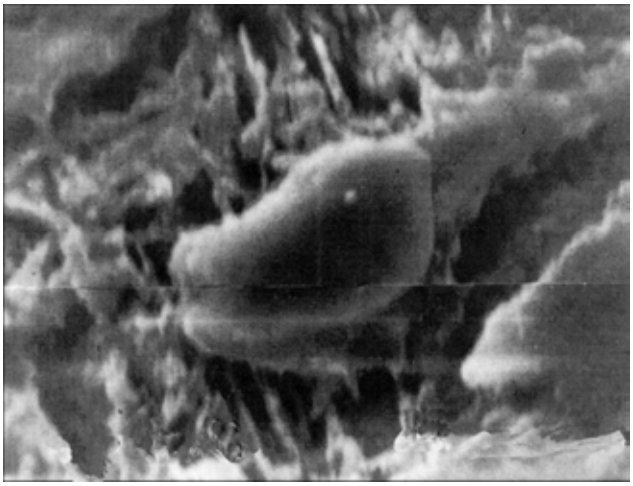

Figure 14. Carbide particle retained in viscous layer (×7500)

Table 3. Volume content and mean size of carbide particles in the FSW joint between steel R6M5 and steel 60

Zone	*Content of non-dissolved carbides, vol.%*	*Mean size of carbide particles, μm*
Friction plane	24.05	0.93829
Viscous layer (outside friction plane)	5.70	0.63780
Zone of mixing of both BM	9.38	0.97125
HAZ in steel R6M5	10.43	0.91381
Steel R6M5 BM	26.90	0.63597

Content and size of carbide phase and austenite grain. The purpose of the tests was to measure content and size of the carbide phase and austenite grain in the viscous layer and neighbouring zones. The tests were conducted on samples produced by FSW of steel R6M5 to steel 60 (V_f = 15 s, no forging, air cooling) with an optical microscope using the image analyser of the Quantimet 500 MC type manufactured by the Leice Company.

Content, size and location of carbide particles affect the character of the process in the characteristic zones and vice versa. Thus, non-dissolved carbides, i.e. hard particles in solid-liquid metal (viscous layer) and in high-plasticity zones (outside the layer), may have a substantial effect on the character of metal displacement. At the same time, thermal-deformation conditions have a substantial effect on the dissolution phenomena and probable mechanical fractures of the carbide phase, etc.

The volume content of non-dissolved carbide particles after FSW without forging was measured at a distance of 1 mm from the rotation axis in the viscous layer, friction plane, zone of mixing of both BM,

Figure 15. Illustration of detachment of a carbide particle from solid solution in the FSW process (×7500)

HAZ metal in steel R6M5 and in steel R6M5 outside the HAZ metal. The mean measured content of the carbide phase and mean size of the carbide particles in characteristic zones are given in Table 3. The probability density of size distribution of the carbide particles is shown in Figure 16.

It can be concluded on the basis of the obtained results that the highest volume content of the carbide phase is in steel R6M5 outside the HAZ metal (26.90 vol.%). In the latter, thermal-deformation conditions immediately near the viscous layer cause dissolution of a major part of the carbide phase (10.43 vol.% is left) during the FSW process, which is much lower compared with its content in BM (steel R6M5). The zone of mixing of both BM contains a smaller amount of the carbide phase (9.38 vol.%), which is a result of extra mixing of particles of both BM. The lowest amount of carbides is contained in the viscous layer (5.70 vol.%), which is almost 5 times as low as in steel R6M5. At the same time, the content

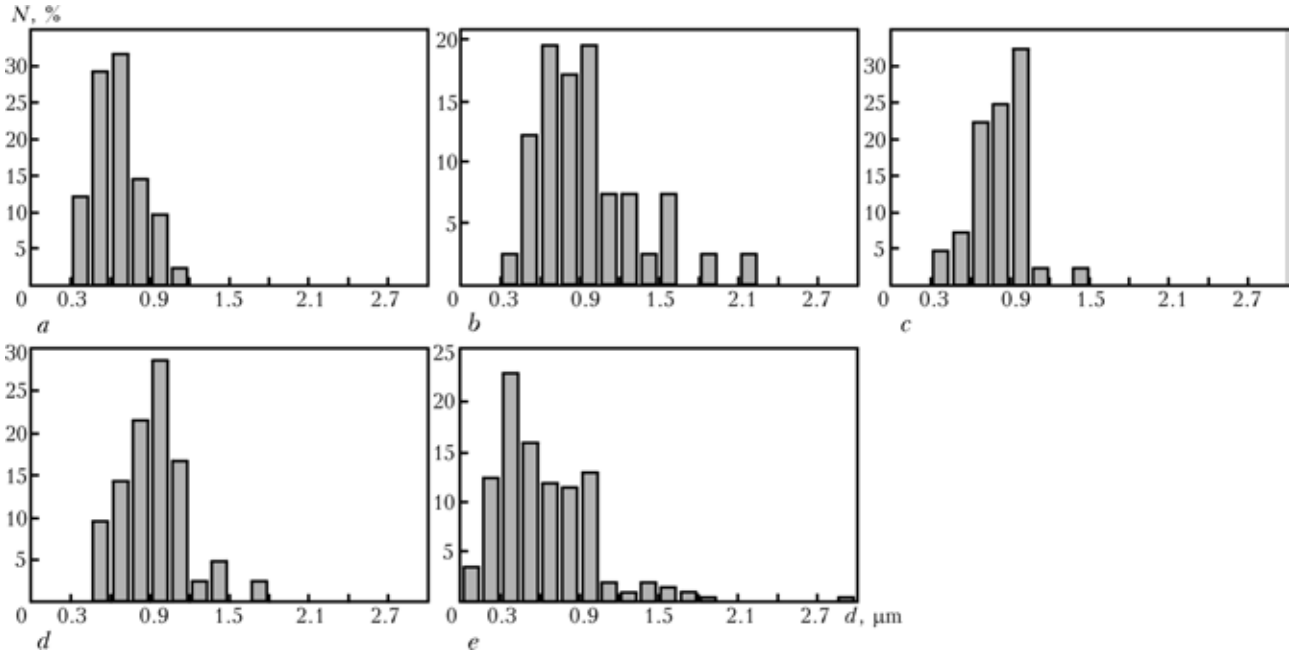

Figure 16. Density of distribution of carbide particles in viscous layer (*a*), friction plane (*b*), zone of mixing of both BM (*c*), HAZ metal in steel R6M5 (*d*) and BM of steel R6M5 (*e*)

Table 4. Mean size of austenite grain in selected zones

Zone	*Mean size of austenite grain, μm*
Viscous layer	2.96131
Steel R6M5 and steel 60 mixing zone	3.46284
HAZ metal in steel R6M5	2.66309

of carbides in the friction plane in the viscous layer amounts to 24.05 vol.% (almost at a level of the content of carbides in steel R6M5 and much lower than in other neighbouring zones). As noted, carbides in the above plane are oriented mostly in parallel to the friction plane. The results obtained are indicative of the probability of the fact that increase in the carbide phase in the friction plane proper is a consequence of retention of carbide particles in viscous metal near the friction plane with a simultaneous decrease in the content of the carbide phase in the rest of the zones.

On the average, carbide particles in the characteristic zones of the HAZ metal in steel R6M5 and in the zone of mixing of both BM are coarser than in BM. The cause is dissolution of finer carbides in solid solution during the FSW process. At the same time, the presence of a major part of finer carbides in the viscous layer may be a result of retention of the major part of coarser carbides immediately near the friction plane and retention of fine non-dissolved particles in the viscous layer. Results of measurement of distribution of the carbide phase allow calculation and prediction of some processes occurring in the friction phase during the FSW process.

Mean size and distribution of austenite grains after FSW (V_f = 15 s, no forging, air cooling) were measured at a distance of 1 mm from the rotation axis in the viscous layer, mixing zone and HAZ metal in steel R6M5 (Table 4, Figure 17).

It can be seen from the Table that mean austenite grain after the friction phase and air cooling (without forging) has the largest size in the steel R6M5 and steel 60 mixing zone. This zone is characterised by the lowest alloying degree and lowest resistance to grain growth. Mean austenite grain in the viscous layer is a bit coarser than in the hottest zones of the HAZ metal immediately near the viscous layer. Formation of the measured austenite grain in the viscous layer was affected by a low content of the non-dissolved carbide phase, thermal-deformation conditions and, to a large degree, nature of the viscous layer. In the friction phase the viscous layer consists of austenite and carbides, formation of δ-ferrite is also probable. According to the constitution diagram [31], carbides of the type of M_6C and MC exist at a temperature of 1260 °C, and a melt containing no insoluble carbides, in addition to austenite and δ-ferrite, exists at a temperature of 1360 °C, while at 1430 °C there is only the melt.

It can be concluded on the basis of analysis of phase composition of the viscous layer after cooling (martensite and austenite with a low content of the carbide phase) that temperature of the viscous layer in the friction phase is in an upper region (immediately near the upper limit) of existence of insoluble carbides in steel R6M5.

It could be noted in conclusion that, according to the results on displacement of the measured points in steel R6M5, under the used FSW conditions the radial displacements are much larger than the tangential ones, the $\Delta r / \Delta s$ ratio growing with increase in the distance from the rotation axis. Increase in the friction time under a constant friction pressure leads mainly to increase in values of the plastic deformation parameters (Δr, Δs, γ, ε and ε').

Expression (5) is suggested to calculate the family of the curves describing radial displacements as a function of distance from the friction plane and initial radial distance from the rotation axis.

The described mechanism of joining steel R6M5 to steel 60 during the friction phase process is in good agreement with the experimental results.

Under the used FSW conditions the viscous layer of a certain width is formed in the friction phase on both sides of the friction plane. Movement of the viscous metal mass and hard carbide particles in it describes a complex path. Based on appearance of the viscous layer after solidification, it can be concluded that retention of a substantial amount of the carbide phase takes place in this phase, in addition to formation of areas of viscous metal in a region located immediately near the rotation plane.

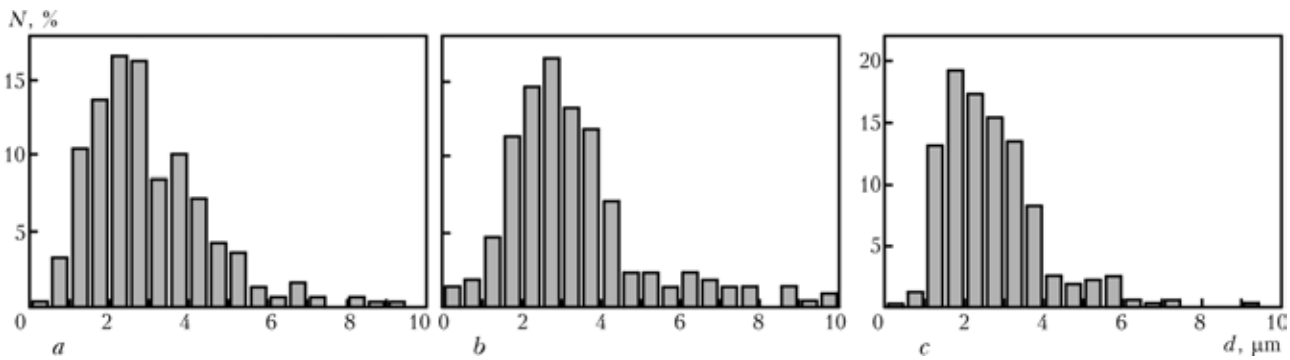

Figure 17. Density of distribution of austenite grain size in HAZ metal in viscous layer (*a*), steel R6M5 and steel 60 mixing zone (*b*) and HAZ metal in steel R6M5 (*c*)

Analysis confirms the presence of the same alloying elements in the friction plane as in the initial steel R6M5 (chromium, tungsten, molybdenum, vanadium), as well as particles with a high vanadium content and individual particles of other chemicals.

Quantitative optical microscopy revealed a high volume content of carbide in steel R6M5 outside the HAZ metal and in the friction plane (24.05 vol.%), and the lowest content of carbide in the viscous layer outside the friction plane (5.70 vol.%). At the same time, the content of carbide in the zone of mixing of both BM and in the HAZ metal in steel R6M5 is 9.38 and 10.43 vol. %, respectively. Supposedly, the cause of a low content of the carbide phase in the viscous layer is its dissolution in solid solution.

Mean austenite grain in the viscous layer after FSW and air cooling is a bit coarser than in the hottest zones of the HAZ metal in steel R6M5 immediately near the viscous layer, and finer than in the steel R6M5 and steel 60 mixing zone.

Phase composition of the viscous layer in steel R6M5 is represented by austenite, carbides of the M_6C and MC type and δ-ferrite, while after cooling the viscous layer also contains martensite, carbides and austenite.

The results obtained on characteristics of the viscous layer and region immediately adjoining the layer allow calculation and prediction of the processes occurring during FSW.

1. Vil, I.V. (1970) *Friction welding of metals*. Moscow: Mashinostroenie.
2. Dennin, G. (1979) Optimierung von Einstellwerten fuer das Reibschweissen mit kontinuierlichem Antrieb. *Fachinformationen von KUKA*, **32**.
3. Kreye, H., Wittkamp, J. (1975) Gefuegeaenderungen und Bindemechanismus beim Reibschweissen. *Fachinformationen von KUKA*, **19**.
4. Khazanov, I.O. et al. (1997) Structure and properties in friction welded joints produced under superplasticity conditions in R6M5 steel. *Welding Int*., **11**, 64–66.
5. Hasui, A. (1998) Effect of faying surface gradient in friction welding. *Ibid*., 10(**12**), 761–768.
6. Fukukasa, K. (1996) On the characteristics of the rotational contact plane ---- a fundamental study of friction surfacing. *Ibid*., 7(**10**), 524–529.
7. Hasegawa, M., Ieda, T. (1999) Effect of welding condition on initial joining phenomena. *Q. J. JWS*, 1(**17**), 24–34.
8. Horn, H. (1987) Untersuchungen zum Bindemechanismus reibgeschweisster Wolframhartmetall-Stahl-Verbindungen. *Schweissen und Schneiden*, **10**, 513–516.
9. Benzsak, G.J., North, T.H. (1996) Modelling of viscosity and fluid dynamics in similar friction joints. *Transact. of JWRI*, 25(**2**).
10. Ciric, R. (1986) P*rilog analizi osobina trenjem zavarenog spoja celika C7680 sa C1730: magistarski rad*. Beograd: Tehnolosko-metalurski fakultet Un-ta u Beogradu.
11. Ciric, R., Raic, K., Cantrak, S. *Strukturne promene i mehanizam spajanja kod rotacionog zavarivanja trenjem razlicitih celika* (u pripremi).
12. Popandopulo, N.A., Tkachevskaya, D.G. (1977) Structure of metal in bright rings of lack of penetration in friction welding of high-speed steels. *Metallovedenie i Term. Obrab. Metallov*, **2**, 64–65.
13. Seryogin, A.S. (1976) Plastic deformation degree in friction welding of metals. *Svarochn. Proizvodstvo*, **8**.
14. Roberts, W. (1986) *ICSMA*. Ed. by H.J. McQueen et al. Oxford: Pergamon Press.
15. Roberts, W. (1983) *In deformation, processing and microstructure*. Ed. by G. Krauss. Ohio: ASM, Metals Park.
16. Johnson, W.A., Mehl, R.F. (1939) *Transact. of AIME*, **135**, 416.
17. Avrami, M. (1939) *J. Chem. Phys.*, **7**, 103.
18. Avrami, M. (1941) *Ibid.*, **9**, 177.
19. Kolmogorov, A.N. (1937) *Izvestiya AN Ukr. SSR. Series Matematics*, **1**, 335.
20. Burke, J. (1980) *The kinetics of phase transformations in metals*. Oxford: Pergamon Press.
21. Radovi, N. (2000) *Deformaciono i rekristalizaciono ponasanje mikrolegiranih selika na visokim temperaturama:* Dokt. dis. Beograd: Tehnolosko-metalurski fakultet Un-ta u Beogradu.
22. Roberts, W. et al. (1979) Dynamic recrystallization kinetics. *Metals Science*, **3/4**, 195–203.
23. Fernandez, A.I. et al. (2002) Static recrystallization mechanisms in a coarse-grained Nb-microalloyed austenite. *J. Metallurg. and Materials Transact*., 33A(**10**), 3089–3098.
24. Devadas, C. et al. (1991) *Metallurg. Transact*., **22A**, 321–333.
25. Baragar, D.L. (1987) *J. Mech. Working Techn*., **14**, 295–307.
26. Sankar, J. et al. (1979) *Metals Techn*., **6**, 325–330.
27. Sellars, C.M., McTegart, W.J. (1966) *Acta Metallurg.*, **14**, 1136–1138.
28. Polukhin, I.P., Gun, Ya.G. (1976) *Resistance of metals and alloys to plastic deformation*. Refer. book. Moscow: Metallurgiya.
29. Suckjao, Na et al. (1984) Temperaturermittlung beim Reibschweissen ungleichartiger Werkstoffe in zylindrische Form-Messung und Berechnung. *Schweissen und Schneiden*, 4(**36**).
30. Fomichyov, I.N., Imshennik, P.K. (1981) Influence of intermediate layer formed in friction welding of high-speed steels to structural steels on strength of the joints. *Svarochn. Proizvodstvo*, **2**, 21–22.
31. Rodic, J. Razvoj orodnih jekel (1978) *Eljezarski zbornik*, **4**.

PROPERTIES OF WELD METAL AT INDUCTION BRAZE-WELDING OF STEEL 20

A.S. PISMENNY, D.P. NOVIKOVA, A.S. PROKOFIEV and **V.V. POLUKHIN**
E.O. Paton Electric Welding Institute, NASU, Kiev, Ukraine

The paper gives the results of studying the microhardness of the metal of the weld and HAZ produced by the method of induction-press welding (braze-welding) with application of activating materials. It is established that the weld metal is an alloy based on the parent metal of the parts being joined. It is determined that deformation coefficient required for performance of sound welds is within k_d = 0.025–0.050. It is shown that during performance of braze-welding with contact trajectory along a closed cylindrical surface, up to 25 % of the joint zone is not visualized and the billets are joined over the base metal.

Keywords: *braze-welding, tubular and flange joints, induction heating, deformation, weldability, metallographic examination, express-procedure*

Braze-welding process is used to produce butt joints of pipes of the oil production range of up to 325 mm diameter, as well as drill pipes [1–8]. Features of the technology of producing such joints have been quite well studied, and criteria are known which should be satisfied to ensure the high quality of welds [5, 6].

The braze-welding process is usually conducted as follows. If required, preliminary machining of the surface of the edges of parts to be joined is performed. Then the billets are installed in the welding fixture clamps, induction heating of the part edges is performed up to the temperature of melting of the activating materials, which are placed in the weld zone before the process. Then, pressure is applied to the parts to be joined, and at the same time the counter plastic deformation of the edges to a controlled level (upsetting) is performed, during which the part joint forms. The weld forms during plastic deformation of the heated edges, which is accompanied by pressing the low-melting phase of the activating material out of the weld right up to formation of a strong joint of the parts.

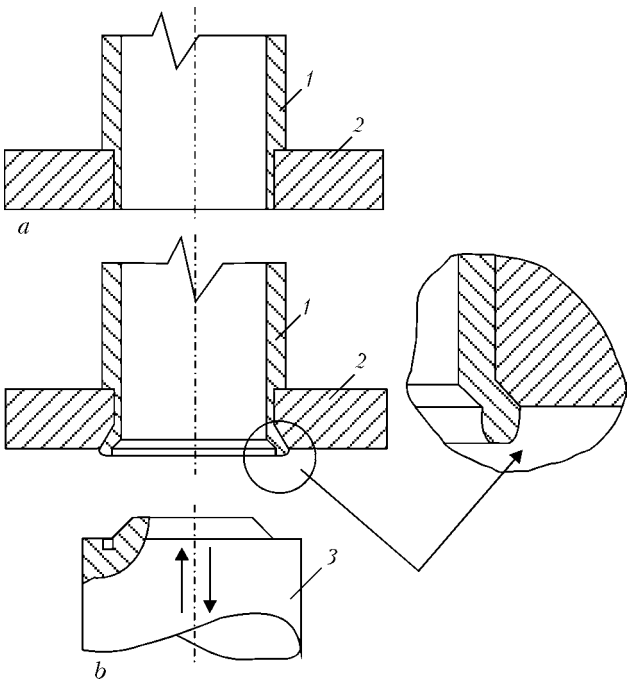

Figure 1. Schematics of a rigid flange joint (*a*) and its braze-welding with pipe flanging over the inner surface (*b*): *1* — pipe; *2* — flange; *3* — welding die

Braze-welding of pipe joints of the end and intermediate pipe fittings has become widely accepted lately [9, 10]. The process of weld formation in these joints differs from that proceeding in butt braze-welding of pipes. This is chiefly related to a more complex mode of displacement of the heated edges metal during upsetting.

This paper is devoted to analysis of the results of studying the welds produced by braze-welding on special samples, using the developed express method [11], which allows simulation of welds, characteristic for joints of pipe–flange type and T-shaped pipe joints [9, 10]. The influence of plastic deformation level of weld zone on weld properties was studied.

Figure 1 shows the schematics of traditional flange structure [12], made by braze-welding with upsetting around the pipe inner diameter.

Such joints of flanges to thin-walled tubes (up to 70 mm diameter and diameter to wall thickness ratio of 12–20 and higher) are widely used in manufacture of bicycles, motor cycles, rehabilitation means for disabled, and medical equipment.

Figure 1, *b* gives the schematic of braze-welding of a flange joint with cone-shaped flanging of the pipe over the inner surface of the flange, and shows the possibility of formation of a sealing lip or groove by applying the welding die. Such joints are often made in tubesheets, where flange thickness *h* is usually greater than tube wall thickness by 5 or more times, for instance in heat-exchanger structures.

In the above-mentioned procedure, special pin *1* and washer *3* (Figure 2) are used, which are made of a certain material and the design of which allows

simulation and study of the process of joint formation between the parts making up the sample.

This allows studying the dependence of the properties of the produced joints on the specified levels of plastic deformation of the sample parts being joined. In order to simulate the above process, after sample heating is over cylindrical insert *4* of a specified size with a cone-shaped sharpening (Figure 2, *a*), is pressed into the technological opening in the pin. As the pin goes deeper, it first deforms the opening wall up to sealing of the gap accommodating the activating material, and at further movement the pin applies to the sample parts a simultaneous plastic deformation up to a specified level.

Samples joined by braze-welding according to the express method, were prepared for studies by the following procedure. In order to study the changes in the shape and dimensions of the parts and the produced weld, resulting from plastic deformation, the made samples were machined over the end face and ground.

For metallographic examination the samples were cut along the axis (Figure 2, *b*) and polished. Sample etching was performed in 4 % alcohol solution of nitiric acid (nital) [13].

If required, this procedure enables selection of activating materials (braze alloys, fluxes and binders) for braze-welding of sample parts of the specified material. Performance of welds, formation of which was simulated by the express method, should be evaluated depending on upset parameters, influencing the part joining process.

Performance of butt joints of pipes made by braze-welding used to be evaluated by certain numerical values expressing the influence of the process and its parameters on weld quality. In determination of the degree of plastic deformation ε in the butt plane deformation coefficient $k_d = \delta_y / \delta$ was introduced, where δ_y is the geometrical dimension showing pipe wall thickening in the butt area and determined as the difference between the newly formed weld reinforcement and pipe wall thickness δ [5].

For the proposed type of samples (see Figure 2), simulating formation of joints of the pipe end fittings, such as joints of flanges to pipes around a closed cylindrical (contact) surface, the parameter determining degree of deformation ε, is the diameter of contact surface d_c, which undergoes changes, depending on the diameter of the cylindrical part of a cone-shaped insert, which, when pressed-in ensures joint plastic deformation of the sample parts to a specified level.

Deformation coefficient corresponding to this parameter for the given case can be defined as follows:

$$k_d = \frac{d_c - d_1}{d_1}, \qquad (1)$$

where d_1 is the outer diameter of the pin determining the initial location of the contact surface.

Dependence of k_d on upset parameters of the edges can be determined.

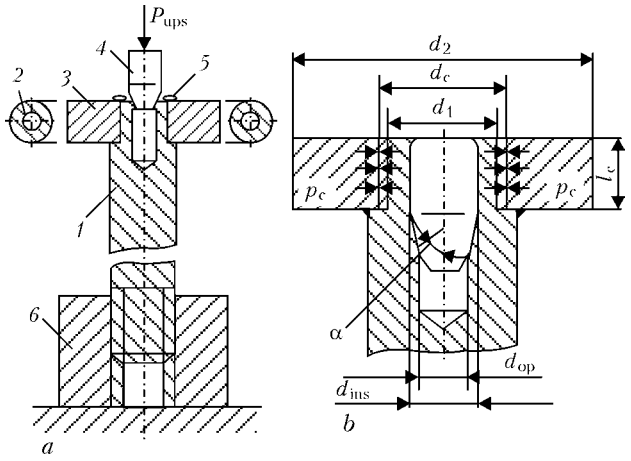

Figure 2. Schematic of simulation of the process (*a*) of braze-welding on samples (*b*): *1* — pin; *2* — inductor; *3* — washer; *4* — cylindrical insert; *5* — activating material; *6* — rest

Contact pressure in the weld, p_c, induced at pressing-in of the cone-shaped insert, can be defined as follows [14]:

$$p_c = \frac{E\delta(1 - k_2^2)}{2d_c}, \qquad (2)$$

where E is the modulus of elasticity for a given steel grade (steel 20 to GOST 8733–87) equal to $2 \cdot 10^5$ MPa; δ is the tightness (mm) formed in the sample, determined from expression $\delta = d_c - d_1$; k_2 is the coefficient of non-uniformity of pipe thickness, calculated by formula $k_2 = d_c / d_2$; d_2 is the outer diameter of the washer.

Expression δ / d_c included into equation (2) can be presented in the form of $d_c - d_1 / d_c$ or considering that according to (1) $d_c = d_1(k_d + 1)$, it can be expressed as

$$\frac{\delta}{d_c} = \frac{d_c - d_1}{d_c} = \frac{d_1(k_d + 1) - d_1}{d_1(k_d + 1)} = \frac{k_d}{k_d + 1}.$$

Substituting this expression into formula (2), the latter can be written as

$$p_c = \frac{Ek_d(1 - k_2^2)}{2(k_d + 1)}. \qquad (3)$$

In this case, dependence of contact pressure on the degree of plastic deformation becomes obvious from expression (3):

$$p_c = f\left(\frac{k_d}{k_d + 1}\right).$$

Figure 3 shows the dependence of k_d on the specified p_c.

The force required for contact crushing and development of plastic deformation in metals and alloys can be determined, using the results of the fourth theory of strength, from which it follows that

$$\sigma_{max} = 5\sigma_y, \qquad (4)$$

where σ_{max} is the maximum contact compressive stress normal to the weld surface [15].

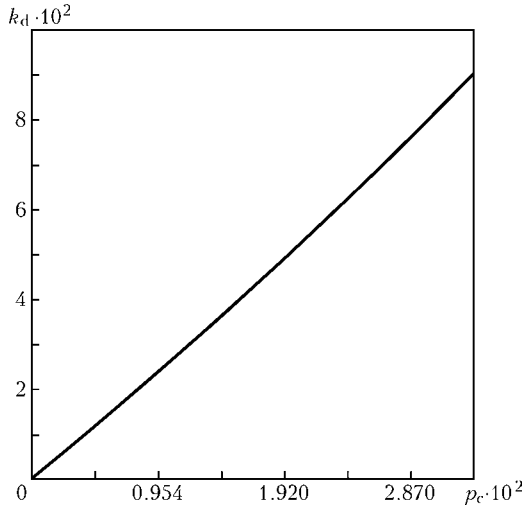

Figure 3. Dependence of deformation coefficient k_d on specified contact pressure p_c

This comparison allows evaluation of the influence of plastic deformation on weld formation, its properties at the applied contact pressure p_c, and enables optimizing the braze-welding process, allowing for σ_y of the joined materials and used activators.

In order to determine the mechanical capacity of the upset drive and upset force P_{ups}, contact pressure in the weld, p_c, calculated from expression (3) was compared to stress σ_{max}, which should be achieved to produce the plastic deformation and contact crushing in metals and alloys.

To determine the upset force, let us use the expression given in [9]:

$$P_{ups} = \frac{P_n}{\cos\alpha} = \frac{S_c p_c}{\cos\alpha} = \frac{\pi d_{ins} l_c p_c}{\cos\alpha}, \qquad (5)$$

where P_n is the force normal to the crushing surface; S_c is the contact surface area; p_c is the contact pressure at upsetting and temperature of conducting the process, usually p_c = 5–50 MPa; d_{ins} is the cylindrical insert diameter; l_c is the axial length of the contact surface; α is the angle between the axis of the cylindrical insert and the normal to the contact surface.

In the above experiments, the sample parts were made of carbon steel (GOST 8733–87) with the following composition specified to group B (GOST 1050–74), wt.%: 0.16–0.24 C; ≤ 0.65 Mn; 0.15–0.30 Si; ≤ 0.25 Cr and up to 0.005 P. Brass foil of grade L-63, as well as flux Na_2BrO_7 (borax) was used as the activating material.

Results of measurement of pin and washer dimensions over the total machined end face showed that braze-welding had changed them. For instance, when the diameter of the cone-shaped insert was equal to 5.0 mm, diameter of the technological opening in the pin increased from 3.5 up to 5.0 mm, while the average diameter of weld surface (practically coinciding with the pin outer diameter and inner diameter of the washer opening) changed from 8.0 (diameter d_1) up to 8.44 mm (diameter d_c). Outer diameter of washer d_2 was unchanged. In this case the coefficient of weld deformation was 0.055 (5.5 %).

As a result of deformation, the wall thickness between the surface of technological opening and average weld surface decreased from 2.25 to 1.72 mm, i.e. by 24 %. This led to increase of weld surface area ΔS_w by 5 %, compared to the initial joint area.

Change of the above dimensions can be interpreted as follows. Proceeding from the geometrical dimensions of the samples (see Figure 2), contact pressure in the cooled weld induced in braze-welding and calculated from expression (3) varies in the following range $p_c \cong$ 2000–4250 MPa along the axial weld length.

Comparison of the calculated contact pressure p_c in the cooled weld to the maximum contact compressive stress σ_{max} determined from expression (4) showed that p_c is more than 2–4 times greater than σ_{max} and more than 7–15 times greater than σ_y (σ_y is the yield point for the given steel grade at 20 °C). It should be noted that for steel 20 at ambient temperature T = 20 °C, σ_y = 200–245 MPa, and σ_{max} = = 1000 MPa. The same relationships are observed also at the temperature of running of the braze-welding process, but at lower absolute values of stresses. At the melting temperature of the activating material (T_m = 880–950 °C) σ_{max} is on a level close to σ_y under the conditions of weld formation, σ_y being in the range of 5–50 MPa. Contact pressure values p_c will be much lower, respectively.

Achievement of the activating material melting temperature determines the start of the joining process, usually running in the temperature range of 1000–1100 °C for Cu-containing activating materials. In this range the process of edge upsetting proceeds in the case of the appropriate p_c application, as well as weld formation.

These pressures lead to formation of flows in the molten interlayer, directed along the contact surfaces being joined and promote pressing of the low-melting phase of the activating material out of the weld. In addition, these pressures cause changes of the contact surface diameter d_c in the formed sample, and promote formation of the welded joint.

The thus obtained data allow determining from expression (5) the upset force P_{ups} equal to 5060 N, this corresponding to p_c = 8 MPa at the temperature of conducting the process. These data were used in experiments.

Structure of the metal of the weld and HAZ was analyzed, using the above procedure of sample preparation. Enrichment of steel parts in copper was found in weld zones adjacent to the contact surface of the joint (dark traces in Figure 4).

Figure 5 shows that the solidified weld interlayer has an intermittent structure along the mating surfaces of the edges being joined, and is not visually observed approximately on 25 % of its total boundary. Here the part edges are probably joined in the solid phase.

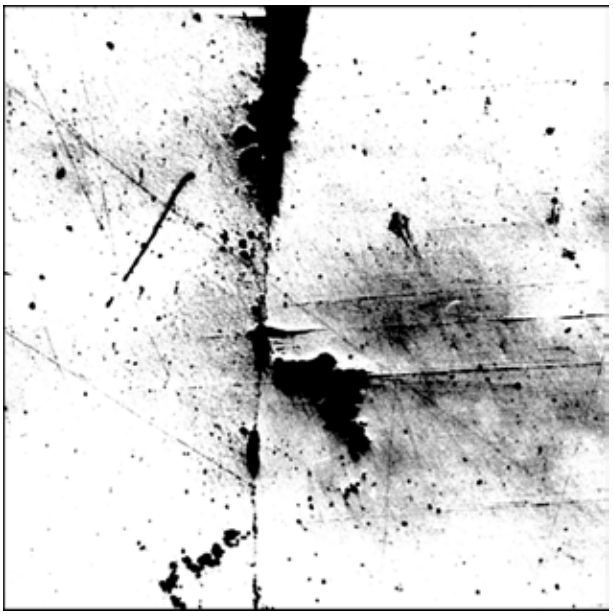

Figure 4. Enrichment of steel parts with a Cu-containing molten interlayer in weld zones adjacent to the contact surface of the joint (×25)

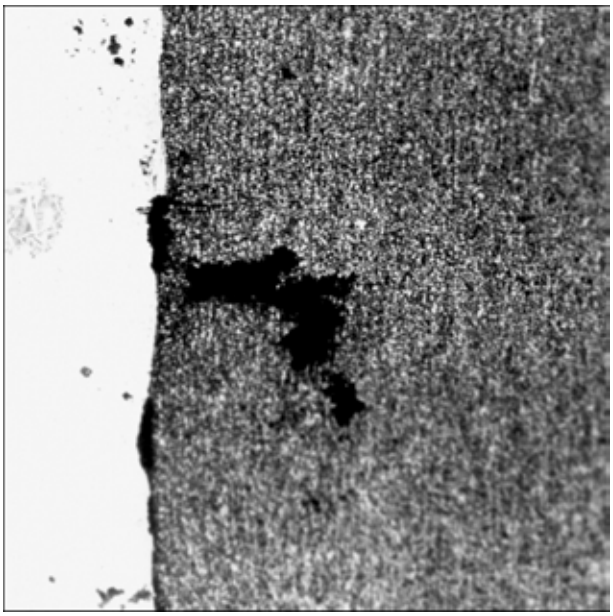

Figure 6. Filling of a microcracks with the solidified interlayer material to the depth down to 0.4 mm (×63)

In Figures 6 and 7 it is seen that the Cu-containing material of the solidified weld interlayer penetrates during braze-welding along the grain boundaries into the part bulk to up to 0.4 mm depth, filling the imperfect zones of the edge surface (microcracks).

More detailed metallographic examination of the same samples did not reveal any visible defects in the weld.

Analysis of microhardness of these zones in the samples by the known procedure was performed to determine the comparative characteristics of the metal of the weld and the HAZ [16–21].

Microhardness distribution in the weld zone was studied using LECO microhardness meter. In those areas where no visible weld was observed (solid-phase joints), and isolated inclusions of unpressed-out interlayer up to 2.5 μm thick were found (Figure 8, *a*) the instrument recorded the hardness *HV* 2540 MPa, which is higher by 9.4 % than that of samples of steel 20 in as-delivered condition (*HV* 2320 MPa).

Also measured was the hardness of weld metal with up to 18 μm grain size near its central part (Figure 9, *a*). Instrument readings were *HV* 2190 MPa, which is by 6 % lower than that of sample material.

Microstructure of the same weld zone at an even greater magnification of this weld section image (Figure 10) is indicative of the absence of lacks-of-fusion, discontinuities, pores or other defects.

Microhardness values obtained when studying the boundary of the weld of the interlayer and the edge are equal to *HV* 2190–2510 MPa, their scatter from the average measured weld hardness of *HV* 2320 MPa reaches +10 % and does not exceed 10 % of base metal hardness. These data are indicative of the similarity between the strength properties of the weld and base metal [22].

X-ray microprobe analysis of the joint zone in Camebax instrument SX-50 was conducted to study the weld composition and distribution of the main

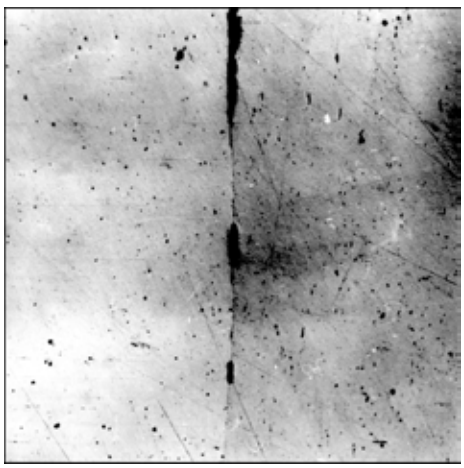

Figure 5. Intermittent structure of the solidified interlayer in weld zone (×25)

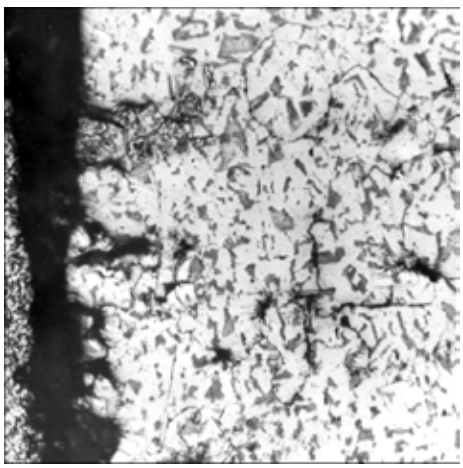

Figure 7. Penetration of interlayer material along grain boundaries into the part bulk (×100)

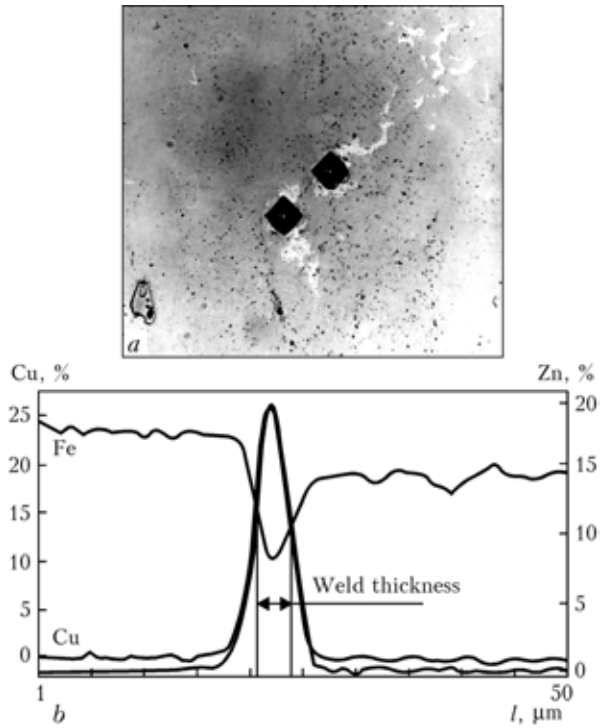

Figure 8. Microstructure of the joint section with isolated inclusions of the interlayer (*a*) and distribution of iron, copper and zinc in it (*b*) (×320)

components of the activator (copper and zinc) in the metal of the weld and the HAZ under the conditions of the occurring edge deformation. Investigations were conducted with microprobe displacement to a distance of 50 μm (1.02 μm step). It is established that the content of activating material elements dissolved in weld metal (in the case of L-63 braze alloy and borax) is as follows:

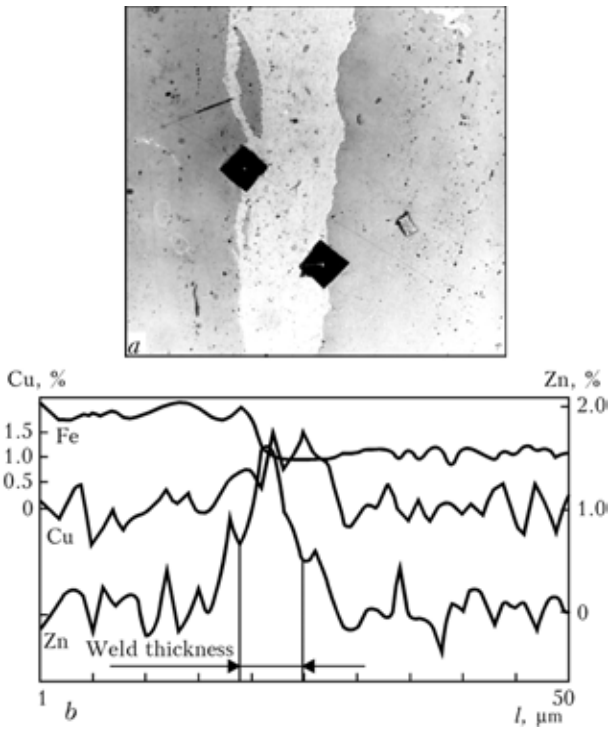

Figure 9. Microstructure of the joint section with weld thickness up to 18 μm (*a*) and distribution of iron, copper and zinc in it (*b*) (×320)

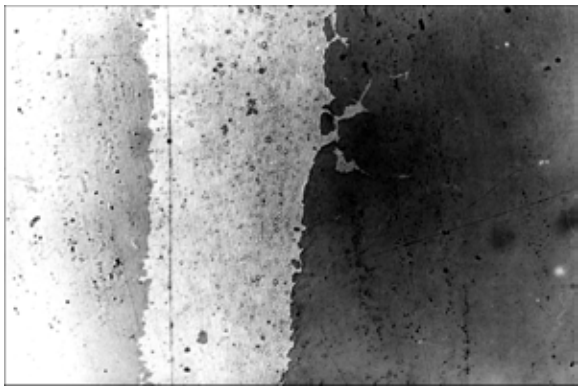

Figure 10. Microstructure of weld zone (see Figure 9) at a great magnification (×680) (five-fold)

• in places where no visible weld was observed, but isolated inclusions of unpressed-out interlayer were found (Figure 8, *a*): 0.018 wt.% Cu, 0.015 wt.% Zn at 99.967 wt.% Fe; 0.02 at.% Cu, 0.01 at.% Zn at 99.97 at.% Fe (Figure 8, *b*);

• in sections near the weld central part: 1.510 wt.% Cu, 1.698 wt.% Zn at 96.792 wt.% Fe; 1.33 at.% Cu, 1.46 at.% Zn at 97.21 at.% Fe (Figure 9, *b*);

• in the weld periphery, where there are sections of unpressed-out interlayer (Figure 6): 26.190 wt.% Cu, 18.162 wt.% Zn at 55.648 wt.% Fe; 24.44 at.% Cu, 16.47 at.% Zn at 59.08 at.% Fe.

It is established that the weld metal is an alloy of base metal, i.e. iron. Even in the peripheral regions of the weld, in the place of fillet formation, where the degree of plastic deformation and the contact pressure is 2.5 times lower than in the middle, iron content is above 50 %. This is indicative of the dependence of the composition of the solidified weld metal on the degree of plastic deformation ε and contact pressure p_c, applied to the weld interlayer in case of solidification under constrained conditions.

Thus, in order to obtain sound welds over the close cylindrical surface by braze-welding it is necessary to ensure k_d = 0.025–0.050.

Mechanical shear testing of samples was conducted (Figure 11), simulating making of a flange joint with formation of a cone-shaped flanging of the pipe over the inner surface of the flange (see Figure 1, *b*). In the experiments, edge deformation coefficient k_d was equal to 0.04 to 0.14 in different sections along the weld height. Cone-shaped striker *5* (Figure 11, *a*) was used instead of a cylindrical insert of the specified size with a conical sharpening (see Figure 2). Furtheron the sample, made by the schematic in Figure 11, *b*, was treated by the schematic in Figure 11, *c*. Results of sample testing are given in the Table.

As is seen from the Table, the lowest shear stress $\tau_{av.sh}$ is found in the samples made without applying the activating materials. For samples, in which the welds are made with activating materials, shear stress $\tau_{av.sh}$ is 3 and more times greater than in samples without activating materials at the same specified degree of deformation of the weld and HAZ metal.

Shear stress $\tau_{av.sh}$ in the samples with application of brass L-63 with borax as the activating material

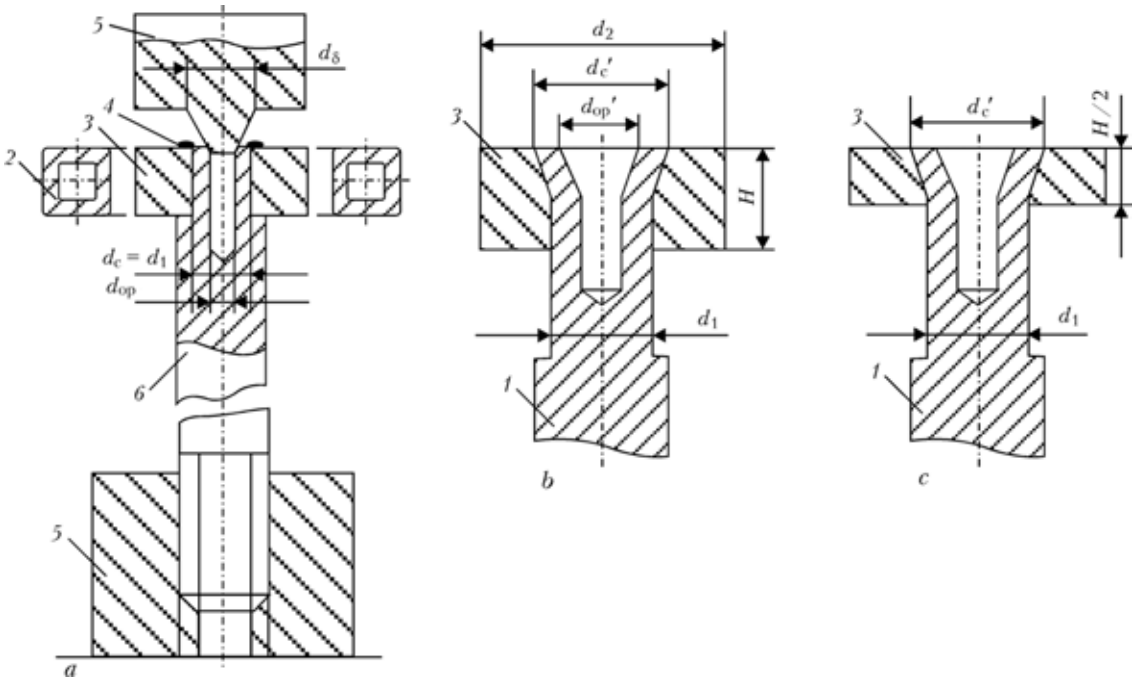

Figure 11. Schematic of simulation of the process of braze-welding of a flange joint with pipe flanging: *a* ---- process schematic; *b* ---- sample; *c* — sample after machining for shear testing; *1* — pin; *2* — inductor; *3* — washer; *4* — activator; *5* ---- cone-shaped striker; *6* ---- rest

was equal to 218 MPa, which is close to the specified shear stress for steel parts brazed with the brass braze alloy, which reaches approximately 200 MPa. This also corresponds to the lower boundary of the yield limit $\sigma_y \cong 200$–245 MPa for steel 20 (GOST 1050–52).

An even higher shear stress (425.2 MPa) was obtained when using a mixture of borax and PAN-3 braze alloy (TU 14-1-2991–80) as an activating material. This value was almost 1.5 times higher than the shear stress of brass of L-63 grade and 1.2–1.3 higher than the specified value of shear stress in brazing welds with PAN-3 braze alloy. In this case, part of the samples (Nos. 7 and 8) could not be tested to fracture for the reason of twist-off of the thread from the sample tail part.

These results are indicative of the fact that the strength values of the weld and base metal are close.

As follows from [3–7], the deformation coefficient required for making sound welds by braze-welding in the butt joints of pipes is higher than that in the considered joints and is equal to 0.4–0.5 of the pipe wall thickness in the joint area. This is attributable to displacement of the heated metal of the edges in the considered joints both in the axial and tangential directions along the weld surface, thus promoting improvement of the joint mechanical properties [8, 23].

Thickness of visually recorded weld is commensurate with the roughness depth of the billet edges, which results from machining the sample parts prior to welding. This is exactly why the weld consists of alternating sections of different thickness, right up to disappearance of the boundary between the edge surfaces.

Results of shear testing of samples made by braze-welding

Sample No.	*Activator*	F_{av}, *Í*	d_1, *mm*	d_c, *mm*	S_w, mm^2	τ_{av}, *MPa*	$\tau_{av.sh}$, *MPa*
1	–	2660	8.0	10.18	101.36	26.24	–
2	–	4850	8.0	10.18	101.36	47.85	–
3	–	3751	8.0	10.18	101.35	37.01	37.0
4	L-63	18400	8.1	10.18	102.24	179.9	–
5	Same	22000	8.0	10.18	101.34	217.0	–
6	»	25980	7.9	10.18	100.52	258.5	218.0
7	PAN-3	38400	No failure				
8	Same	37700	Same				
9	»	17200	7.9	10.18	50.65	339.6	–
10	»	30600	8.0	10.18	58.13	526.4	–
11	»	22850	7.8	10.18	55.79	425.2	425.2

Notes. 1. Here d_1 is the contact surface diameter measured on the sample before making the joint; $\tau_{av} = F_{av} / S_w$. 2. Shear stress was determined by the current procedures from expression $\tau_{av.sh} = \tau_{av1} + \tau_{av2} + \ldots + \tau_{avn}) / n$, where n is the number of samples for determination of average value of shear stress. In our experiment $n = 3$. 3. No activating material was used, when making sample Nos. 1–3. 4. Borax was a component of the activating material used in the experiments.

CONCLUSIONS

1. Data of X-ray microprobe analysis are indicative of the fact that the weld metal is an alloy of the base metal of the parts being joined, i.e. iron. When a weld is made by braze-welding along a closed cylindrical surface, up to 25 % of the joint zone is not visualized, and the billets are joined in the solid phase.

2. Comparative studies of microhardness of metal of the weld and HAZ indicate that metal similar to the base metal in its properties is produced.

3. Deformation coefficient required for making sound welds by braze-welding along a closed cylindrical surface, is 0.025–0.050. This is lower than k_d of butt joints of pipes and rods (0.4–0.5), which is attributable to displacement of the heated metal of the edges both in the axial and tangential directions along the weld surface.

1. Lebedev, V.K., Tabelev, V.D., Pismenny, A.S. et al. (1989) Brazing of tubes for geology exploration drilling. *Avtomatich. Svarka*, **5**, 28–30.
2. Pismenny, A.S., Shinlov, M.E., Buzhenetsky, A.I. (1995) Application of induction braze-welding for joining oil pipe grades. *Ibid.*, **12**, 35–38.
3. Lebedev, V.K., Tabelev, V.D., Pismenny, A.S. (1983) Butt pressure brazing of steel pipelines. *Ibid.*, **9**, 25–27.
4. Tabelev, V.D., Kareta, N.L., Panasenko, A.I. et al. (1985) Structure and phase composition of welds made by capillary and pressure brazing. *Ibid*., **11**, 26–29.
5. Pismenny, A.S. (1990) Synthesis of induction systems for butt welding and brazing of tubes. *Ibid.*, **5**, 11–15.
6. Lebedev, V.K., Pismenny, A.S., Kasatkin, O.G. et al. (1990) Physical modeling of upset in butt welding or brazing of pipes. *Ibid.*, **8**, 17–20.
7. Tabelev, V.D. (1991) Special features of joint formation in brazing with plastic deformation of parent metal. *Ibid.*, **7**, 5–9.
8. Pismenny, A.S., Prokofiev, A.S. (2002) Press welding of pipes using activating materials. *The Paton Welding J.*, **7**, 19–23.
9. Prokofiev, A.S., Pismenny, A.S. (2000) Technology of braze-welding of flanges to tubes. *Ibid.*, **5**, 48–50.
10. Prokofiev, A.S., Pismenny, A.S., Bondarev, V.A. et al. (2001) Induction braze-welding of T-joints without fittings in pipes. *Ibid.*, **4**, 43–47.
11. Pismenny, A.S., Polukhin, V.V., Prokofiev, A.S. et al. (2002) Express-method for development and verification of pressure brazing technologies. *Ibid*., **1**, 47–50.
12. Dolginov, L.Sh., Prokopov, V.K., Samsonov, Yu.A. (1972) *Calculation and design of flange joints of ship piping and vessels*. Leningrad: Sudostroenie.
13. Grabin, V.F., Denisenko, A.V., Novikova, D.P. et al. (1977) *Reagents for examination of macro- and microstructures of steel and alloy welded joints*. Kiev: Naukova Dumka.
14. (1955) *Reference book of a mechanical engineer*. Vol. 3. Moscow: Mashgiz.
15. (1973) *Resistance of materials*. Ed. by G.S. Pisarenko. Kiev: Vyshcha Shkola.
16. Davidenkov, N.N., Belyaev, S.E., Markovets, M.P. (1945) Producing base mechanical characteristics of steel using hardness measurements. *Zavod. Laboratoriya*, **10**, 964–973.
17. Sichikov, M.F., Zakharov, B.P., Kozlova, Yu.V. (1947) About evaluation of mechanical properties of steel without testing of fracture specimens. *Ibid*., **12**, 1463–1471.
18. Kuchuk-Yatsenko, S.I., Kazymov, B.I. (1967) Optimal thermal cycle in resistance butt welding of steel 12Kh1MF. *Ibid*., **6**, 24–27.
19. Forostovets, B.A. (1972) Peculiarities of metal structure of joints in flash-butt welding. *Ibid.*, **4**, 9–13.
20. Markovets, M.P. (1979) *Evaluation of mechanical properties of metal by hardness*. Moscow: Mashinostroenie.
21. Gulyaev, A.P. (1989) On the problem of mechanical properties of structural steels. *Metallovedenie i Term. Obrab. Metallov*, **7**, 23–25.
22. Shmykov, A.A. (1956) *Reference book of a heat-treaters*. Moscow: Mashgiz.
23. Sakhatsky, G.P., Dudnik, G.P. (1972) Properties of butt welded joints made in forming devices. *Avtomatich. Svarka*, **4**, 56–58.

IMPROVEMENT OF THE STRUCTURE AND PROPERTIES OF WELDED JOINTS IN LARGE-DIAMETER OIL AND GAS PIPES

Yu.N. SARAEV[1], **V.P. BEZBORODOV**[1], **I.M. POLETIKA**[1], **A.V. TYUTEV**[1], **I.V. NIKONOVA**[1], **N.V. KIRILOVA**[1] and **S.P. SEVASTIANOV**[2]

[1]Institute of Strength Physics and Materials Science of SD of RAS, Tomsk, Russia
[2]OJSC «Tyumentransgas», Yugorsk, Russia

Effect of a pulsed welding process on the structure and mechanical properties of welded joints in large-diameter (1420 mm) pipes of manganese low-alloy steels, intended for manufacture of oil and gas pipelines, has been studied. It is shown that the pulse welding conditions make it possible to improve the homogeneity of the structure and reduce the grain size of metal of the weld and HAZ zones. Structural changes at a positive temperature (20 °C) lead to increase of 8–27 %, and at a negative temperature (–60 °C) to increase of 15–24 % in ductility and impact toughness of the welded joint zones.

Keywords: *pulsed welding, low-alloyed steels, welded joints, electrodes, mechanical properties, structure, pipes, oil and gas pipelines, strength, ductility, impact toughness*

Pipes of 1420 mm diameter with 16 mm wall thickness of steel X67 made in Germany (Russian analog is 10G2S steel) are used under the difficult service conditions at alternating loads and low temperatures. Welding of such a steel with a steady arc leads to overheating of the metal of the weld and HAZ, causing pronounced coarsening of the grains. In order to avoid it, welding has to be performed at a lower heat input and in narrow limits of heat conditions.

Requirements to the mechanical properties, reliability and fatigue life of welded joints of pipes in oil and gas pipelines, as well as structures and tanks in chemical engineering have greatly increased over the recent years. In a number of cases minimum admissible indices of the mechanical properties are specified for such pipes and structures, which primarily concerns the strength, impact toughness and ductility. Properties of welded joints in structures should usually be equivalent to those of the base metal [1].

A feature of steels of 09G2S, 10G2S, 17G1S type widely used in the oil and gas industry is their proneness to softening in welding, which results in lower structural strength of welded joints.

Low-alloyed steels in the thermally improved condition (after quenching and high-temperature tempering) are often used now. Such treatment is applied, for instance, to steels 17G1S, 16GS, 30KhGSNA, etc. In their welding, softening of the section heated above the temperature of 550 °C proceeds in the near-weld zone. The properties of HAZ metal in such welded joints can be completely restored only using post-weld heat treatment, namely quenching with high-temperature tempering. The mode of such a treatment should be similar to that of the earlier conducted heat treatment [1].

Heat treatment is also mandatory in some other cases, envisaged by OST 26-291–79. However, heat treatment of welded joints always complicates the welding technology, particularly during construction or repair welding operations in the field.

In order to improve the strength and service properties of welded joints, the Institute of Strength Physics and Materials Science of Siberian Division of the Russian Academy of Sciences uses a new approach, based on controlling the process of electrode metal melting and transfer in pulsed welding. This is achieved by application of systems of a flexible energy process, which ensures control of a complex electrodynamic system of the power source–electrode–arc–weld pool, depending on the instant values of energy characteristics, using feedback channels and subsequent study of the influence of the parameters of adaptive pulsed welding on the structure, physico-mechanical, special and service properties of welded joints on high-strength steels [2–4].

The purpose of this study is investigation of the influence of the process of pulsed welding of pipes of low-alloyed steels X67 and 17G1SU on the structure and physico-mechanical properties of welded joints (strength under tensile static loading, microhardness of the structural components and its distribution in the welded joint zones, impact toughness at temperatures of +20 and –60 °C) and their compliance to the main requirements made of welded joints of pipes for oil and gas pipelines.

Samples were prepared by welding 140 × 300 mm plates 16 mm thick cut out of pipes (steel X67), as well as 150 × 300 mm plates of steel 17G1SU 14 mm thick, cut out of pipes of 1420 mm diameter. Welding was performed in the steady and pulsed modes. In welding in the steady mode by the standard technology an inverter-type power source MP 200, Kemppi, Finland, was used, and welding in the pulsed mode was performed using VD-306E rectifier in the set with a specialized UDI-205 attachment, providing an adaptive technological process.

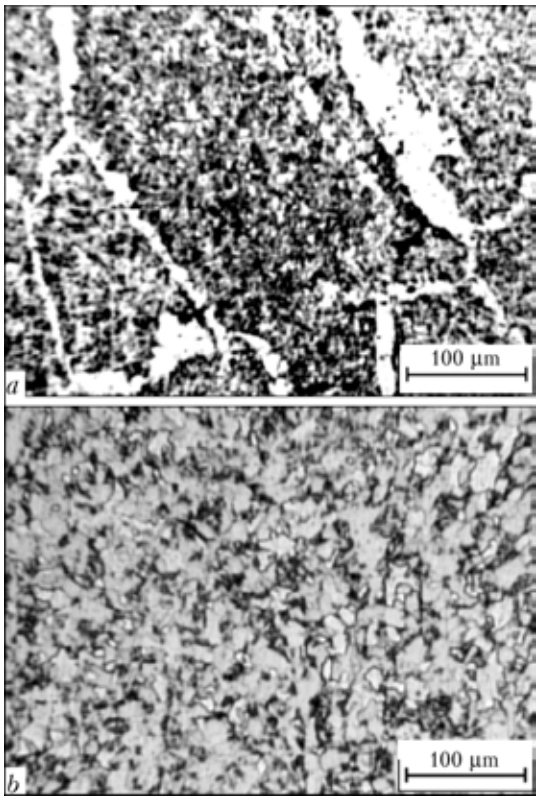

Figure 1. Microstructure of weld metal in the facing layer of a welded joint of steel of 10G2S type after welding in the steady (*a*) and pulsed mode (*b*) (×170)

Welded joints of steel X67 were made using Swedish electrodes of OK series, and steel 17G1SU was welded with Russian electrodes of MTG grade, as well as German Kessel electrodes.

The following mechanical properties were determined: ultimate tensile strength, yield point, relative elongation and relative reduction in area. Samples for mechanical testing in the form of two-sided blades were cut out across the welded joint so that the weld were in the middle of the sample test portion (GOST 1497–73). Testing was performed in Instron type unit.

Sample testing for impact toughness was conducted in a pendulum hammer of MK-30A type at temperatures of +20 and –60 °C. A concentrator in the form of a V-shaped notch was made in the weld (GOST 9454–78).

Qualification of the structure of welded joint zones after mechanical testing of samples for impact toughness was conducted in an optical microscope of MIM-9 type. Microhardness of metals in the welded joint zones was measured in PMT-3 instrument at loads of 0.5 and 1.0 N on the indentor.

As follows from [1], steels of 09G2, 09G2S type have a very high critical cooling rate, exceeding 100 °C / s, therefore, post-weld cooling does not cause any martensite structure formation in the metal of the weld and HAZ. Structure of the metal of different HAZ sections changes from the coarse-grained ferrite-pearlite (often of Widmanstatten type) in the near-weld zone to the fine-grained ferrite-pearlite structure in the incomplete recrystallization zone. Hardness of the metal of the weld and near-weld zone of the HAZ usually is not more than 2000 MPa.

Table 1. Mechanical properties of welded joints on steel of 10G2S type produced in welding in the stationary and pulsed modes

Welding mode	$\sigma_{0.2}$, *MPa*	σ_t, *MPa*	δ, *%*	ε, *%*
Steady	454	540	20.3	62.8
Pulsed	448	536	24.6	60.8

Metallographic analysis of samples of steel of 10G2S type showed that when welding in the pulsed mode is used, metal with more disperse, homogeneous and equiaxed structures forms in all the weld sections by height (root, filing and facing) and near the line of fusion with the base metal, as well as in the HAZ, compared to those obtained in the steady mode (Figure 1).

Mechanical testing of welded joint samples at static tensile loading demonstrated the high strength of the welds, formed by both the technologies (necking and fracture ran through the region of HAZ boundary with the base metal). Welded joints produced in the pulsed mode demonstrate the same values of ultimate strength, yield point, as well as relative reduction in area of the materials as in the steady mode.

Relative elongation of samples rises by about 20 % (Table 1), which is related to formation of much more finely dispersed structures in pulsed welding, which promote improvement of ductility of the metal in all the zones of the welded joint.

Influence of the pulsed welding process of steel 17G1SU on formation of the metal structure of the weld and HAZ was studied with the aim of structural optimization of high-strength welded joints. Investigations showed that as a result of a controllable heat input into the item [2], the pulsed welding mode ensures a considerable refinement of the structure of weld metal and the HAZ, which is the most prone to structural changes, this preventing the abrupt deterioration of microhardness and strength in this zone, and thus reducing the possibility of development of dangerous stress raisers here, which would promote formation and propagation of cracks leading to fracture (Figure 2).

Grain size in the metal of the zones of the weld formed in the pulsed mode is reduced 2.5 to 3 times, and in the HAZ by approximately 2 times, compared to those obtained in the steady mode (Figure 3). This promotes lowering of post-weld deformations and increase of the impact toughness of welded joints. For instance, the impact toughness of welded joints formed using electrodes of grades MTG and Kessel, increased by 8 to 27 % during testing at +20 °C and by 15–24 % at –60 °C (Table 2). Values of σ_t of welded joints made with these electrodes, almost did not change (compared to those characteristic of the steady mode) and were equal to about 560 MPa.

In keeping with the currently valid Russian standards on edge preparation of items to be welded for gas and petrochemical equipment (OST 26-291–79), limiting the welding heat input and conducting post-weld heat treatment, the joints produced by manual arc welding, mechanized submerged-arc and gas-

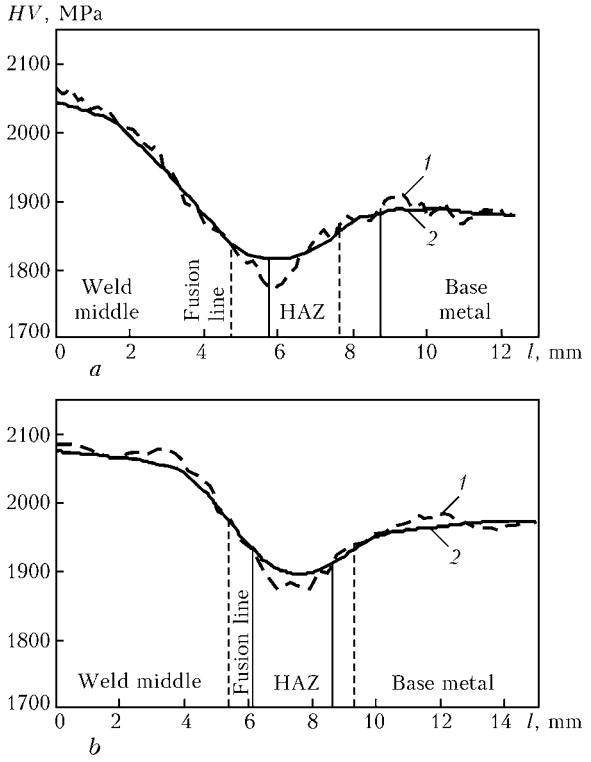

Figure 2. Microhardness distribution in the filling layer of welded joints of steel of 17G1SU type produced by welding with MTG (*a*) and Kessel (*b*) electrodes in the steady (*1*) and pulsed (*2*) modes (*l* ---- distance to fusion center)

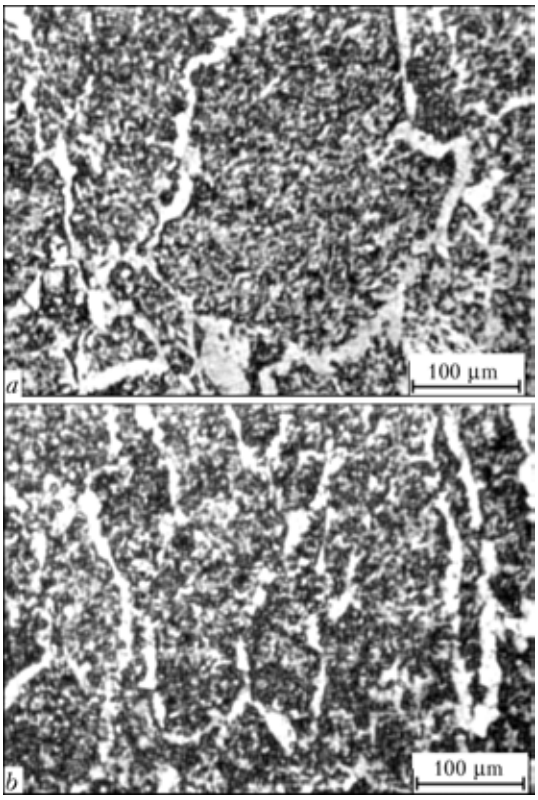

Figure 3. Structure of weld metal in the facing layer of the joint on steel 17G1SU after welding in the steady (*a*) and pulsed (*b*) modes (×170)

shielded arc welding, should meet the following requirements. Minimum *KCV* value of welded joints of low-alloyed manganese and silicon-manganese steels at temperature below –20 °C should be 0.3 MJ / m^2. Ultimate tensile strength of welded joints at +20 °C should be equal to or exceed σ_t of the metal being welded (base metal).

Analysis of the values of ultimate strength of the metal of welded joints of steels 10G2S and 17G1SU showed that after welding in the pulsed mode, σ_t of the metal of near-weld zone is in all the cases higher than the strength level of base metal of the above-mentioned steels. Impact toughness of weld metal at T_{test} = –60 °C after welding in the pulsed mode of steel 17G1SU, using Kessel and MTG electrodes, is 1.7 and 2 times higher, respectively, than the level required by the standard (0.3 MJ / m^2) and by 24 and 15 % higher than this value for joints produced by welding in the steady mode. It is important to note that the above-mentioned values of impact toughness were obtained on welded joints not subjected to heat treatment (normalizing or refinement) usually conducted for samples and items of this class of low-alloyed steels [1, 5]. By the strength level the joints of the studied steels after welding in the pulsed mode meet the requirements of the standard for welded joints of pipes for oil and gas pipelines. This allows eliminating the post-weld heat treatment.

Table 2. Impact toughness of weld metal of 17G1SU steel welded joints produced in the steady and pulsed modes with different electrodes

Used electrode	*Welding mode*	*KCV, MJ/m^2, at Ò, °Ñ*	
		+20	*–60*
Kessel	Steady	1.30	0.41
	Pulsed	1.40	0.51
MTG	Steady	1.18	0.52
	Pulsed	1.50	0.60

CONCLUSIONS

1. Application of a pulsed mode of welding large-diameter pipes (1420 mm) of manganese steels of 10G2S and 17G1SU type designed for oil and gas pipelines, allows improvement of structural homogeneity and 2 to 3 times refinement of the grain size of metal of the weld and HAZ.

2. Structural changes after application of the pulsed welding mode lead to increase of ductility of the metal of welded joint zones, as well as its impact toughness by 8 to 27 % at +20 °C and by 15 to 24 % at –60 °C.

1. Livshits, L.S., Khakimov, A.N. (1989) *Metals science of welding and heat treatment of welded joints*. Moscow: Mashinostroenie.
2. Saraev, Yu.N. (1994) *Pulsed technological processes of welding and surfacing*. Novosibirsk: Nauka.
3. Saraev, Yu.N., Makarova, L.I., Kirilova, N.V. et al. (2001) Ways of improvement of efficiency of construction, service and repair of oil and gas industrial equipment and main pipelines on the base of adaptive pulsed technologies of welding and hardfacing. *Svarochn. Proizvodstvo*, **5**, 31–37.
4. Saraev, Yu.N., Poletika, I.M., Kozlov, A.V. et al. (2002) Influence of welding conditions on structure, hardness distribution and mechanical properties of steam pipeline welded joints. *Ibid.*, **8**, 3–8.
5. Goldshtejn, M.I., Grachyov, S.V., Veksler, Yu.G. (1985) *Special steels*. Moscow: Metallurgiya.

CHARACTERISTICS OF MODERN UNITS FOR MECHANISED GMA WELDING

M.V. KARASYOV[1], E.M. VYSHEMIRSKY[1], V.I. BESPALOV[1], D.N. RABOTINSKY[1], I.M. ZAKHAROV[1], A.E. BELYAEV[1], G.V. PAVLENKO[2] and V.V. SOLYANIK[2]

[1]Closed Joint Stock Research-Production Association ITS, St.-Petersburg, Russian

[2]Open Joint Stock Company «Electric Machine Building Plant SELMA», Simferopol, Ukraine

Described are modern types and characteristics of application of new mechanised welding technologies using solid (small diameter) and flux-cored wires. It is shown that allowance for the dynamic properties of welding sources is important for analysis and comparison of mechanised welding units.

Keywords: *mechanised arc welding, new technologies, units, comparative analysis, solid wires, flux-cored wire, welding sources, dynamic properties*

Semi-automatic welding processes have received a wide acceptance in the last five years in welding fabrication of Russia. In current welding-related industries (mechanical engineering, ship building, oil and gas production) the share of semi-automatic welding using solid and flux-cored wires, including self-shielding wire, is 75–85 % [1].

It should be noted that this is not just a mere widening of application of the known process, but a wide introduction of new technologies using old and new equipment available at enterprises. The main objective of introduction of new technologies is to raise labour productivity and improve quality of welded joints. Trade training centres are very active in providing a relevant training of welders.

The new technologies include:

- method for deposition of filling and facing beads in position butt welding of pipelines using self-shielding wire (providing increase of not less than 1.4 times in productivity, compared with manual arc welding, according to the data of the All-Russian Research Institute for Pipeline Transport (VNIIST);
- method for gas-shielded manual welding with back bead formation using no backing with 1.2–1.6 mm solid wire in all spatial positions [2] (providing increase of not less than 2 times in speed of making a root pass, compared with basic-electrode welding, and not less than 50 % compared with welding using electrodes with cellulose covering);
- method for re-welding of a welded joint on the back side (minimising the content of diffusible hydrogen in the weld (to 1.34 ml / 100 g), which is 3 times as low as in welding using basic electrodes, and 10 times as low as in welding using electrodes with cellulose covering);
- method for gas-shielded welding using flux-cored wire (providing increase of not less than 2 times in impact toughness, compared with solid wire welding, and increase of not less than 1.8 times in process productivity, according to the data of the Production Association SEVMASh);
- method for controlled short-circuiting welding for making root gap passes and joining thin-sheet metal [2], as well as many other welding methods.

Advancement of the forced short-circuiting (FSC) welding method [2] is causing a rebirth of interest in using 1.6 mm solid wire (providing increase in welding speed from 25 m / h using 1.2 mm wire to 50 m / h using 1.6 mm wire in all spatial positions, the high weld quality being maintained and spattering being kept at no more than 3 %). These aspects are sufficiently comprehensively described in study [1].

It is just natural that the wide application of new mechanised welding technologies involves new techniques (extension of wire tip over the nozzle exit section [2]; oscillatory motion of the torch along and normal to the weld, rather than across the weld; downward welding instead of traditional upward welding, etc.).

This extensive advancement of new gas-shielded mechanised welding technologies and techniques [3] requires a more deliberate approach to selection of welding equipment. Study [4] describes an attempt to systematise welding rectifiers and feeding mechanisms as to application fields, designs and welding properties.

Properties of modern mechanised welding units can be analysed and compared more accurately on the basis of typical oscillograms of current and arc voltage with a reference to stages of transfer of the electrode metal drops to the weld pool. It should be borne in mind in this case that these properties must be different for solid and flux-cored wire welding.

Typical shapes of the welding current and arc voltage curves for the case of traditional CO_2 welding are shown in Figure 1, *a*, those for FSC welding are shown in Figure 1, *b*, and those for the STT-process — in Figure 1, *c*. As seen from the Figure, the main difference of the new types of equipment lies in increased dynamic properties of welding sources. The characteristic short-circuiting time of traditional units of the type of VDU-506, VS-300, etc. (Figure 1, *a*)

is 10–20 ms, that of the DK units (Figure 1, *b*) for the FSC method is 5–7 ms, and that of the Invertec STT II unit (Figure 1, *c*) for the STT-process is 2–5 ms.

With traditional units (Figure 1, *a*) the short-circuiting frequency is no more than 30–50 Hz and substantially changes during welding, as in the years when those units were made there was no task to give priority development to welding processes with controlled short-circuiting. Breaking of the bridge between the welding wire and pool at the end of the short-circuiting period occurs at the arc current close to maximum. This, correspondingly, leads to a substantial spattering (more than 5 %) caused by a considerable impact by electrodynamic forces, chaotic changes in size of the electrode metal drops in welding, and to impossibility of controlling the welding process in a stable manner and within the range of wide variations in process parameters.

With the DK type units (Figure 1, *b*) the typical oscillogram is similar to the previous one, except for the time and slope of the leading and trailing edges of the arc current line, especially in a region of end of the short-circuiting period. This leads to qualitative changes during welding. Breaking of the bridge between the welding wire and pool occurs at a much lower arc current (decreased to 40–50 A). This is accompanied by a dramatic decrease in electrode metal spattering (to 3 % and lower). The short-circuiting frequency in this case is 120-150 Hz (for VD-506DK-4) and 70–80 Hz (for VD-306DK). Size of the electrode metal drops becomes stabilised and is controlled through adjusting the process parameters [4]. The process is characterised by stability and is easy to control. Diameter of the wire used is 1.6 mm or less.

With the Invertec STT II units (Figure 1, *c*) the oscillogram is substantially different from the two previous ones. Breaking of the bridge between the welding wire and pool occurs at a yet lower welding current, compared with the previous unit. Here spattering of the electrode metal is less than 2 %. The short-circuiting frequency is about 130–140 Hz. The process is stable and easy to control. Diameter of the wire used is 1.2 mm or less.

Units of the last two types reliably provide gas-shielded welding of the root and other layers of the weld using solid wires. Study [2] considers main technological differences between the last two processes and a technique of welding of the root layers using solid wire. It should be emphasised that with the units of the last types the wires used have different diameters and, hence, the welding process has a different linear speed.

The use of welding under the short-circuiting conditions offers a serious advantage in quality of welded joints, compared with other technologies. Figure 2 shows macrosection of the welded joint with a back bead and microstructure of the weld and HAZ metal.

As follows from analysis of Figure 2, structure of the root weld metal (Figure 2, *b*) is close to that of the weld and HAZ metals (Figure 2, *c*). The coarse grain zone, which is present as a rule in welding of this grade of steels, is almost unnoticeable. This is attributable to the fact that the arc current decreases in the short-circuiting period, which decreases heat input into a workpiece. The main advantage of a decreased heat input is rise of the level of mechanical properties of the workpiece.

The following mechanical properties can be achieved in steels of the above type: σ_t = 618–659 MPa (600 MPa is required according to SP 105-34–96), bending angle — more than 120°, impact toughness

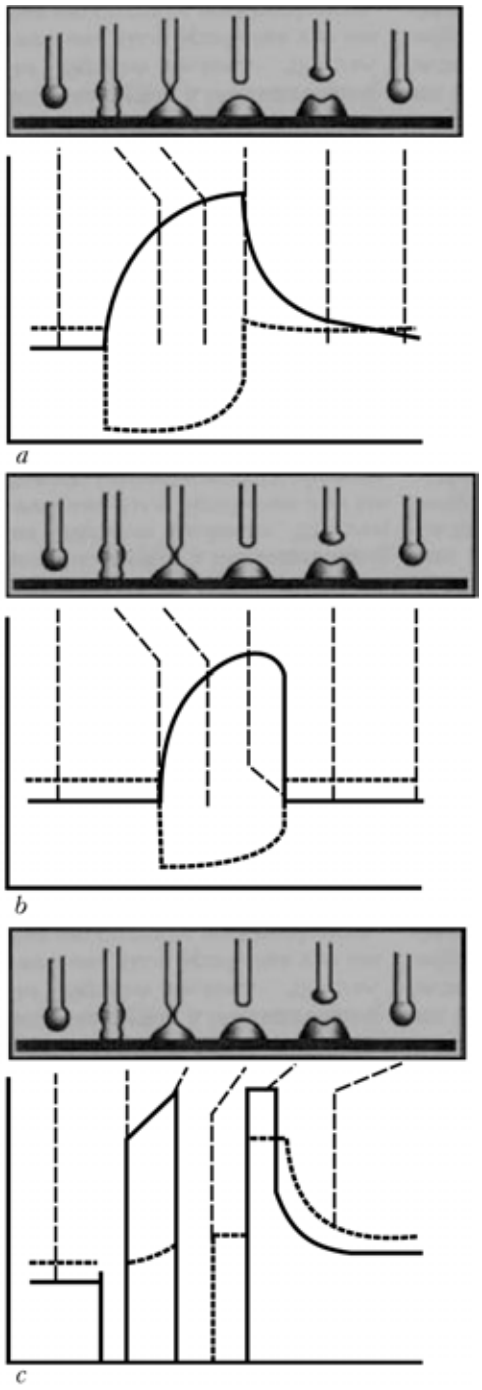

Figure 1. Typical shapes of curves of welding current (*bold curve*) and arc voltage (*dashed curve*) for traditional CO_2 welding (*a*), FSC welding (*b*) and STT-process (*c*) (courtesy of the Moscow Office of Lincoln Electric Company)

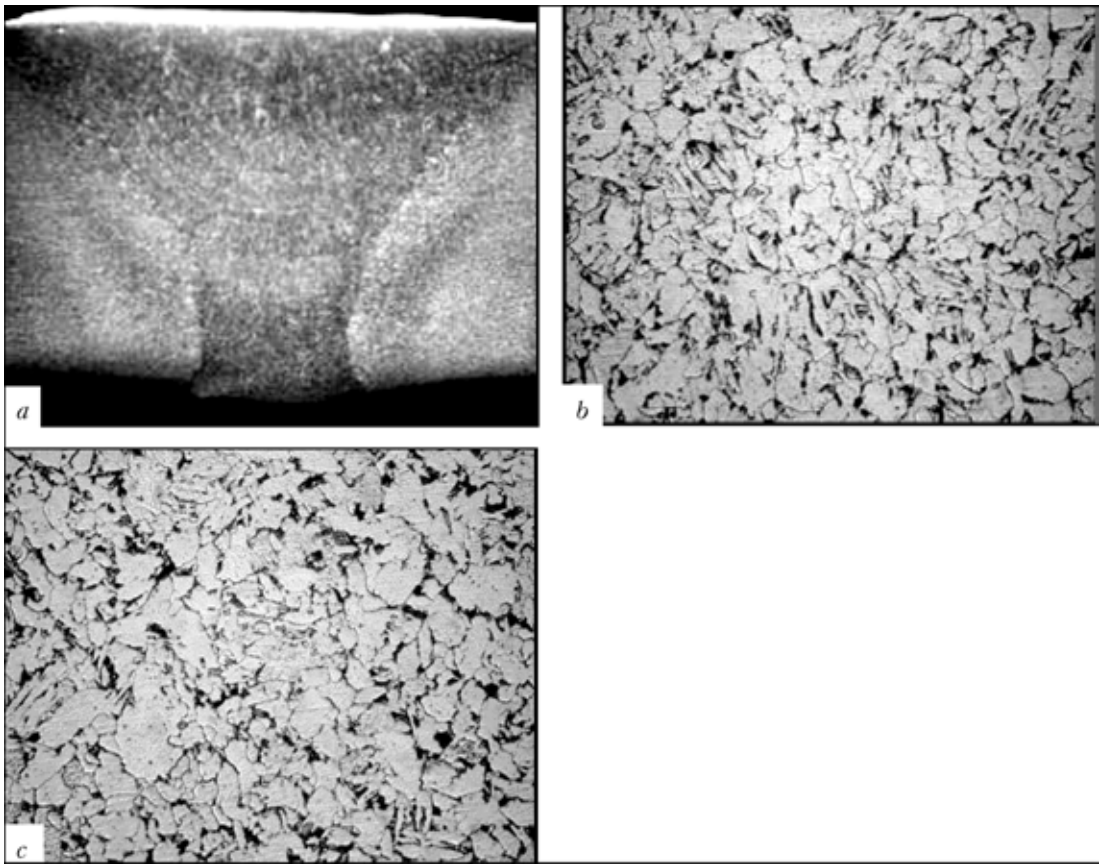

Figure 2. Macrosection (*a*) of welded joint in steel 10G2FBYu (welding was performed with the VD-306DK unit and the PDGO-511 feeding mechanism; the root pass was made using the 1.2 mm wire Sv-08G2S, and filling and facing layers were deposited using 1.7 mm wire NR-207); *b* ---- microstructure of the root pass weld metal (×500); *c* — microstructure of the HAZ metal (overheated region) (×550)

KCV at –20 °C ---- 76–142 J / cm^2, depending upon the notch location (34 J / cm^2 is required according to SP 105-34–96).

The method of welding with short-circuiting of the arc gap minimises burnout of alloying elements. The following was obtained in welding of stainless steels of the 18-10 type using the VD-306DK unit and the PDGO-511 feeding mechanism:

Figure 3. Thyristor-type rectifier VD-506DK

• steel 12Kh18N10T, butt welded joint, test specimen of the XIII type according to GOST 6996–66;

• σ_t = 590–610 MPa, bending angle ---- more than 120°, hardness of base metal---- *HV* 204–210, hardness of weld metal ---- *HV* 212–218.

Results of spectral analysis of a reference welded specimen are given in the Table.

Requirements to welding units are substantially different in cases of using a flux-cored wire. This is caused by the fact that in welding using flux-cored welding consumables, like in the case of using electrodes with cellulose covering, short-circuiting leads most often to formation of defects. Welding in this case, unlike welding by the FSC or STT methods, is performed with the «long» arc. Another difference of the welding units is that length of the arc should be as stable as possible to avoid non-uniform burnout of

Results of spectral analysis of reference welded specimen

Material	*Content of elements, wt.%*					
	C	*Ni*	*Mn*	*Cr*	*Ni*	*Ti*
Steel 12Kh18N10T, GOST 5632–72	<0.12	<0.80	<2.00	17.0–19.0	8.0–9.5	0.5–0.80
Test piece base metal	0.11	0.73	1.65	17.10	8.87	0.74
Weld metal	0.08	0.77	1.48	18.6	9.1	0.17

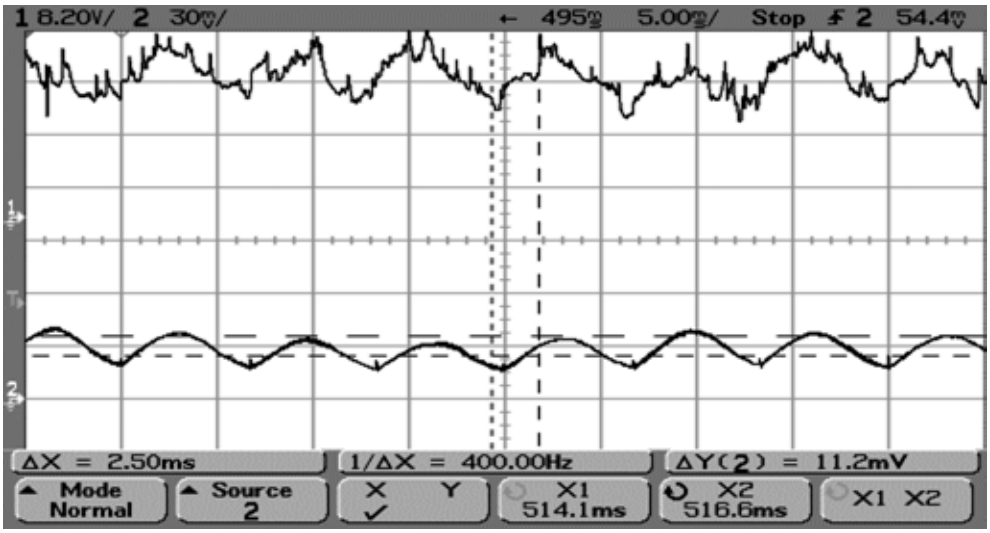

Figure 4. Typical oscillogram of welding using 1.7 mm self-shielding flux-cored wire of the NR-207 type, VD-506DK unit and PDGO-511 feeding mechanism (upper oscillogram — arc voltage, lower oscillogram ---- arc current)

alloying elements. This imposes certain limitations on the relationship between inductance of the choke and constancy of the external volt-ampere characteristic.

Thyristor-type rectifiers VD-506DK (Figure 3) (ITS, St.-Petersburg) and DC-400 (Lincoln Electric, USA) are most often applied in the last years in Russia for welding using flux-cored welding consumables. These rectifiers meet most fully a set of requirements imposed on such units. The possibility of employing the DK type rectifiers for welding by the FSC method and for flux-cored wire welding is provided by the fact that it is possible to switch the types of external volt-ampere characteristics. The scopes of application amount to more than 5000 of each of the rectifiers. The Production Association SEVMASh alone uses more than 1000 units of the VD-506DK type with the PDG-322M feeding mechanisms for flux-cored wire welding. As seen from Figure 4, the process is of the spray type and stable. The current and voltage curves copy the mains pulsations, which corresponds to requirements of welding consumables manufacturers.

It should be noted in conclusion that the process of introduction of new technologies has been intensified in the last years in Russia. This predetermines new requirements to the applied welding equipment. Above we have made an attempt to analyse applicability of mass-produced equipment to meet requirements imposed by new technological processes and conditions of utilisation of new welding consumables.

1. Karasyov, M.V., Isakov, S.V., Rabotinsky, D.N. et al. (2002) Analysis of the most effective application of different types of welding equipment and consumables in fabrication of metal structures. *Svarka v Sibiri*, **1 / 2.**
2. Karasyov, M.V., Rabotinsky, D.N., Pavlenko, G.V. et al. (2004) New developments of Production Association SELMA-ITS in the field of gas-shielded arc welding. *Avtomatich. Svarka*, **5**, 40–46.
3. Karasyov, M.V., Rabotinsky, D.N., Pavlenko, G.V. et al. (2003) Comparative analysis of welding-technological properties of advanced rectifiers for gas-shielded welding. *Svarka v Sibiri*, **2**, 17–22.
4. Karasyov, M.V., Kopilenko, E.A., Pavlenko, G.V. et al. (2002) Main tendencies of development of welding equipment manufacture in SELMA-ITS Association and its application in Russia and CIS countries. *The Paton Welding J.*, **5**, 41–45.

APPROXIMATE CALCULATION OF CHOKE INDUCTANCE IN DC WELDING CIRCUIT

N.I. POSTOLATY
Kakhovka Plant of Electric Welding Equipment, Kakhovka, Ukraine

A procedure is described for determination of the required inductance of DC welding circuit and design of welding circuit choke by the admissible rate of current increment.

Keywords: *arc welding, voltage, welding current, flat external characteristic, electrodynamics of source, fluctuations of voltage and current, drop transfer of molten metal, law of control, inductance, flux linkage, magnetic flux, choke, geometry of magnetic core*

One of the main elements of welding rectifiers is a choke at the rectified side of the power source. Welding properties of the source depend on the choke inductance. The routine of setting the parameters of welding thyristor (smoothly controlled) and inverted (with a step control) rectifiers confirmed the determinant role of electrodynamics of welding circuit on the quality of formation of deposited metal and minimizing of losses. Requirements of GOST 25616–83 are, undoubtedly, necessary, but are insufficient for optimum selection of ratios of design parameters of the sources. Subjective evaluation by experienced operators-welders of the process nature (up to acoustics) remains quite necessary.

If there is also law of control in the disposal of the designers, besides the selection of RL relations of a mains–transformer–bridge–choke path [1], then the proper selection of choke diagrams in combination with inductance of the transformer short-circuiting (reduced to the secondary side) is determinant in the inverter power sources. In operation of two rectifiers for a parallel load in one source (KIG-401, KIG-601) it is necessary to optimize each parallel path.

An experience has been gained at the Kakhovka Plant of Electric Welding Equipment for determination of the required inductance of DC welding circuit by a preset initial rate of current increment and approximate calculation of design parameters of the choke at their optimum ratio (section of magnetic core, number of turns, non-magnetic gap). The practice shows that the choke, set for the universal sources by criteria for the condition of flat external characteristics (FEC), is quite suitable also for falling characteristics. Therefore, we shall be limited by the power sources with FEC.

As follows from work [2], the welding condition at currents 250–350 A is most unfavorable as to formation and losses, accompanied by coarse-drop short-circuits of arc gap (arc voltage is approximately 25–30 V). A step «dip», equal to U_{weld}, was fixed on the oscillogram of electrode voltage.

It is evident that this stage of voltage at the initial period is distributed successively in areas of the entire path proportionally to their inductance. It can be written for the entire path at the initial moment

$$-U_{weld} = L \frac{di_{max}}{dt}, \quad (1)$$

where L is the total inductance of the path reduced to the secondary (welding) circuit; di_{max} / dt is the maximum (initial) rate of current increment.

Later on, the rate is decreased by exponent with a time constant $\tau = l / R$, where R is the total ohmic resistance of the path reduced to the secondary (welding) circuit.

From the one hand, very quick increment in welding current due to a low inductance will lead either to a drop break, or to the pool fluctuations and poor formation. From the other hand, the excessive inductance will cause the delayed (sluggish) drop transfer, and, consequently, a poor formation.

The effect of a total resistance R consists, probably, in the fact that the steady value of short-circuit current, to which the transition process at small R is tended, is so high that the curvature of a shape of current increment will lead either to the drop break or to fluctuations of the pool.

The contradiction consists also in the fact that taking into account the efficiency factor, it is necessary to tend to R, as low as possible. As R defines the curvature of external static characteristics of the source (i.e. capability to self-control of arc at constant speed of electrode feed), then this parameter should be compromised.

It follows from the above-given that all the complex of parameters influences the welding properties, and a single parameter cannot characterize these properties. However, the highest rate of current increment is remained to be the main parameter.

According to work [2], the power sources are divided by dynamic characteristics as follows: inertia (10–30), medium- (30–60), low- (70–200) and extra-high speed (above 200 kA / s).

In accordance with this classification, let us determine the total inductance for each group with allowance for formula (1) and at $U_{weld} \approx 25$ V:

$$L = U_{\text{weld}} / \frac{\mathrm{d}i_{\max}}{\mathrm{d}t}.$$

For inertia sources L is $(2.5\text{--}1.0)\cdot 10^{-3}$, medium-inertia ---- $(0.8\text{--}0.4)\cdot 10^{-3}$, low-inertia ---- $(0.36\text{--}0.125)\cdot 10^{-3}$ H.

According to technical characteristics of 13 sources [2], their efficiency factor is 70–72 %, and, consequently, their short-circuit resistance is approximately similar, and short-circuit current (in particular, at drop transfer) has a similar order.

Inductance of chokes of the sources (except dynamoelectric) is 0.16–0.56 mH, that allows them to be referred to medium- and low-inertia. Experience of short-circuiting of power source KIG-401 by Y / Y–bridge path at minimum and maximum stages shows a short-circuit inductance within the 0.10–0.11 mH.

The experience of short-circuit of the same power source by Y / Δ–bridge path shows the inductance of these sources equal to 0.234–0.345 mH. The check-out of welding properties using Y / Δ–bridge (without choke) gives a good result. It was established in check-out of KIG-401 using Y / Y–bridge path (without choke) that welding is impossible.

Similar results were obtained in source KIG-601. The output circuit of these sources has a non-symmetric diagram by choke, which leads to a mutual symmetry of electrodynamics of two parallel paths.

Inductance of choke KIG-401 using Y / Y–bridge–choke path is 0.11 + 0.45 = 0.56 mH; using Y / Δ–bridge–choke path is 0.345 + 0.125 = 0.47 mH.

Consequently, sources KIG-401 and KIG-601 can be refered to medium-inertia.

It follows from the above-mentioned that for determination of a required inductance of choke after presetting of admissible rate of increment and determination from experiment of short circuits or calculation of internal inductance (leakage) of the transformer

$$L_{\text{ch}} = L_{\text{path}} - L_{\text{sh.c}},$$

where L_{ch} is the choke inductance; L_{path} is the total required inductance of path by the condition of admissible rate of current increment; $L_{\text{sh.c}}$ is the inductance of short circuit of transformer from the experiment of short circuits (or calculation).

The following designations are used for calculation: δ is the total gap from material with a relative magnetic permeability, close to vacuum; l_{st} is the mean length of magnetic field lines along the steel magnetic core, m; I is the current in coil, A; ω is the number of turns in coil; S_{st} is the section of magnetic core, m^2; B is the inductance in magnetic core (and in gap), T; H_{st} is the intensity of magnetic field in steel, A / m; Φ is the magnetic flux in steel section, Wb; $\psi = \Phi\omega$; ψ is the flux linkage, Wb.

Figure 2 gives a family of curves of magnetizing of magnetic cores, containing different non-magnetic gaps δ_{air} up to an open magnetic core where the curve

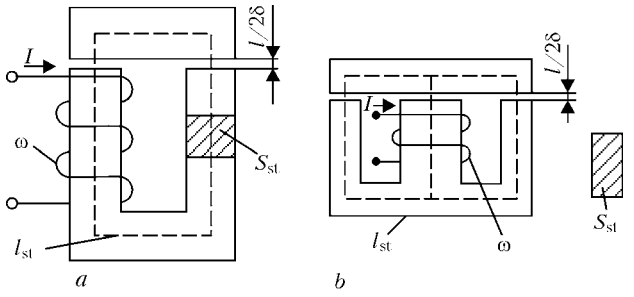

Figure 1. Electromagnet schemes of choke with a Ï- (*a*) and E-shaped (*b*) magnetic core

is transformed into a linear relationship of air magnetizing:

$$B_{\text{air}} = \mu_{\text{air}} H_{\text{air}}, \quad \mu_0 = 4\pi\cdot 10^{-7} \text{ H / m};$$

$$1/\mu_0 = 796; \quad \frac{\mu_{\text{air}}}{\mu_0} \approx 1 \text{ [3]},$$

where μ_{air} is the magnetic permeability in a gap; H_{air} is the intensity of magnetic field in a gap, A / mm.

As the curves *2*, *3*, ... , *n* reflect the dependence of induction B in two media, it is more convenient to regard them in coordinates $B = f(I)$, where I is the current in choke winding.

Let us consider the link between the curve of choke magnetizing $B = f(I)$ and its inductance. We shall write the expression for inductance L_{ch} of coil with magnetic core without a gap in any point of its curve of magnetizing as

$$L_{\text{ch}} = \frac{\mathrm{d}\psi}{\mathrm{d}I}. \qquad (2)$$

Let us make the following equivalent changes and substitutions in formula (2) [4]:

$$L_{\text{ch}} = \frac{\mathrm{d}\psi}{\mathrm{d}I} = \frac{\mathrm{d}}{\mathrm{d}I}\omega\Phi = \frac{\mathrm{d}}{\mathrm{d}I}\omega B S_{\text{st}} = \frac{\mathrm{d}}{\mathrm{d}I}\omega\mu\mu_0 H S_{\text{st}} =$$

$$= \frac{\mathrm{d}}{\mathrm{d}I}\omega\mu\mu_0 \frac{\omega I}{l_{\text{st}}} S_{\text{st}} = \frac{\mu\mu_0\omega^2 S_{\text{st}}}{l_{\text{st}}} = \frac{\mu_0\omega^2 S_{\text{st}}}{l_{\text{st}}/\mu}, \qquad (3)$$

where μ is the relative dynamic magnetic permeability of medium in its operating point. Here $\mu = f(B)$ and is, as a result, a linear function.

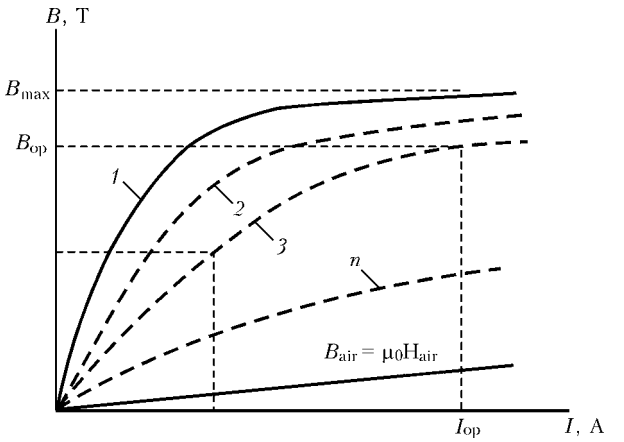

Figure 2. Dependence of magnetization of a closed magnetic core, made from ferromagnetic material, on current at different gaps

Analyzing the formula (3) it is possible to consider conditionally that the ferromagnetic magnetic core of l_{st} length was replaced by a linear medium of length l_{st} / μ with an absolute magnetic permeability μ_0, and inductance L_{ch} is written for the operating point of the magnetic core. In addition, when the curve of magnetizing of electric steel is considered [4], where $\mu = (dB / dH) / \mu_0 = f(B)$ has at the beginning the order $(5.0–4.5)\cdot 10^3$, in the middle (in the region in front of «elbow») the order $(2.0–1.5)\cdot 10^3$, and at the saturation region it is tended to unity; the coil inductance with steel is decreased with magnetizing up to a negligible minimum. Thus, the closed magnetic core is saturated at low currents and at welding currents the choke will not operate.

If to add some area (gap) δ into magnetic core, then the magnetizing curve in coordinates $B = f(I)$ will spread along the current axis, curves *2*, *3* ... , *n* will tend, with increase in a gap, to the «curve» of vacuum magnetizing, taking more and more linear nature.

With account for formula (3) for calculation of inductance of choke of such a design the expression will take the form [4]

$$L_{ch} = \frac{\mu_0 \omega^2 S_{st}}{\delta + l_{st}/\mu}. \quad (4)$$

It is seen from formula (4) that in a non-saturated choke the inductance does not almost depend on the length of magnetic core due its relatively small equivalent length l_{st} / μ. Until magnetic core saturation starting, the inductance depends only on steel section, number of turns and gap size.

Consequently, the problem consists in the fact that except the calculation of a preset inductance in an operating point of a ferromagnetic medium it is necessary to occur to be in this point at preset welding current and optimum ratio of steel section, number of turns and gap. Formula (4) does not provide the adequate solution, the additional conditions are required.

It is possible to preset B_{op} as an operating point, coming from maximum admissible inductance (saturation) B_{max}.

Analysis of design parameters of chokes of known sources shows that their operating point B_{op} is at the level

$$B_{op} \approx 0.75 B_{max},$$

that is sufficient in practice for resistance against the welding current fluctuations.

In a non-saturated magnetic core with a gap the point B_{op} is determined adequately by the intensity of magnetic field H_{op} in a gap

$$B_{op} = \mu_0 H_{op}.$$

Magnetomotive force of magnetizing $I_{op}\omega$ of a magnetic circuit is spread by the law of full current in a gap δ and ferromagnetic region l_{st}

$$I_{op}\omega = \delta H_{op} + l_{st} H_{st}. \quad (5)$$

Let us substitute the ferromagnetic region by the region of additional gap, equivalent to it by the magnetic resistance, in mathematical model by formula (5)

$$l_{st} H_{st} = \frac{l_{st}}{\mu} H_{op}$$

(as follows from curves of magnetizing the electric steels [5], this parameter in operating regions is in the ranges $1.5\cdot 10^3 \le \mu \le 5.0\cdot 10^3$).

δ, *mm*	ω	S_w, mm^2	S_{st}, mm^2	L, *mH*
		I_{op} = 150 A		
1	8	800	560	0.0391
2	15	1500	1050	0.138
4	31	3100	2170	0.631
8	61	6100	4270	2.45
10	76	7600	5320	3.80
12	91	9100	6370	5.45
		I_{op} = 300 A		
1	5	100	700	0.0191
2	9	1800	1260	0.059
4	16	3200	2240	0.174
8	31	6220	4340	0.642
10	38	7600	5320	0.95
12	46	9200	6440	1.41
		I_{op} = 500 A		
1	3	1000	700	0.00688
2	5	1666	1167	0.017
4	10	3332	2332	0.0706
8	18	6000	4200	0.21
10	23	7667	5370	0.352
12	27	9000	6300	0.475
		I_{op} = 600 A		
1	2	800	560	0.0025
2	4	1600	1120	0.0105
4	8	3200	2240	0.0434
8	16	6400	4480	0.177
10	19	7600	5320	0.235
12	23	9200	6440	0.35
		I_{op} = 1000 A		
1	--	–	--	–
2	3	2000	1400	0.0074
4	5	3330	2330	0.017
8	9	6000	4200	0.052
10	12	8000	5600	0.099
12	14	9330	6530	0.132

Substituting the drop of magnetic potential at the additional gap into formula (5) we shall obtain

$$I_{op}\omega = \delta H_{op}\frac{l_{st}}{\mu} H_{op} = H_{op}\left(\delta + \frac{l_{st}}{\mu}\right).$$

Taking into account the relationship (5) we have

$$I_{op}\omega = \frac{B_{op}}{\mu}\left(\delta + \frac{l_{st}}{\mu}\right),$$

hence,

$$\omega = \frac{B_{op}}{I_{op}}\frac{\delta + l_{st}/\mu}{\mu_0}. \quad (6)$$

From the experience of design of chokes l_{st} / μ lies within the ranges of 0.1–0.2 mm that allows it to be taken equal to δ_{add}, i.e. about 0.15 mm, in the first approximation.

By presetting operating point $B_{op} = 0.75B_{max}$, it is possible to determine the number of turns depending on a gap at operating current I_{op} using formula (6):

$$\omega \approx \frac{0.75B_{max}}{I_{op}}\frac{\delta + 0.15}{\mu_0}. \quad (7)$$

For example, $B_{max} = 1.8$ T is supposed for steel 3414.

To calculate inductance by formula (3) it is necessary to know the sizes of a magnetic core.

$$S_w = \frac{I_{op}\omega}{\Delta K_f}, \quad (8)$$

where S_w is the window section, mm^2; Δ is the current density in winding from the heating conditions (for copper $\Delta = 2.5$ A / mm^2 is taken with allowance for an artificial ventilation); K_f is the coefficient of window filling; $K_f = 0.6$.

From the experience of design of magnetic cores we assume

$$S_{st} \approx 0.7S_w. \quad (9)$$

Calculation of dependence of number of turns ω, size of window S_w, magnetic core section S_{st}, choke inductance L_{ch} on non-magnetic gap δ (at operating point $B_{op} \approx 0.75B_{max} = 1.4$ T) by formula (4) will be shown in the Table.

Analysis of Table shows that to obtain the required choke inductance at the preset current by a simple increment in number of turns is impossible due to saturation of the choke magnetic core.

It follows, therefore, coming from the Table that, first, it is necessary to find a gap, then the number of turns (7), then section of magnetic core (8), (9), then to check the choke inductance L_{ch} by formula (4). The next clarifications of the design to obtain the preset L_{ch} using condition of operating point preserving are possible only at the expense of steel section.

After selection of plate profile the more precise calculations by formulae (6) and (4) should be made.

1. Postolaty, N.I., Glushchenko, A.D., Dukh, S.V. et al. (2002) On welding properties of thyristor rectifiers. *The Paton Welding J.*, **10**, 38–40.
2. Potapievsky, A.G. (1984) *CO_2 welding*. Moscow: Mashinostroenie.
3. Chertov, A.G. (1990) *Physical values*. Moscow: Vysshaya Shkola.
4. Pentegov, I.V., Meshcheryak, S.N., Turty, M.V. et al. (1997) Procedure of calculation of chokes of input and output filters of welding invertor power sources using standard magnetic conductor. *Avtomatich. Svarka*, **4**, 34–39.
5. Kopylov, I.P. (1980) *Design of electrical machine*. Moscow: Energiya.

SOURCES OF FLAME HEATING FOR BRAZING

A.M. ZHADKEVICH
E.O. Paton Electric Welding Institute, NASU, Kiev, Ukraine

Retrospective description of development of the equipment and technique of heating during brazing with application of hydrocarbon and hydrogen fuel is given. The technological features and capabilities of flame of different composition in acetylene, hydrogen-oxygen and atomic-hydrogen brazing are analyzed. The role of a number of specialists and organizations in the history of gas and gas-electric brazing is demonstrated.

Keywords: *oxygas, hydrogen-oxygen, atomic-hydrogen brazing, hydrocarbon fuel, gas torches, heat sources, electric arc*

The most important classification features of brazing are the degree and temperature of melting [1], which are closely connected with physical-chemical characteristics of heat sources. Over several centuries the majority of methods of brazing and forge welding of metals was based on use of the heat generated in combustion of wood (peat, coal). To intensify the process of combustion, increase in temperatures and concentration, the artificial blowing was used. Here, the feasibility of control of the brazing conditions was limited by a comparatively low heat-generating capacity of the fuel and a low intensity of air entering.

At present, the number of brazing methods, classified by the heat sources, is counted by several dozens. The aim of the present work was to analyze the genesis of brazing, its technical capabilities, specifics of application and a role of heat sources in the development of brazing alloys and technologies of brazing.

Since the ancient times the combustion of coal, wood and other hydrocarbons was used in metallurgy for three main purposes, such as heat generation, reduction of metals from oxides and (more seldom) alloying [2]. In brazing by a hydrocarbon flame only the first function is used completely, similar to metallurgy, and the second function is more seldom used. In addition, the specific functions are also often originated, such as providing and maintaining of temperature conditions for chemical-metallurgical reactions between the brazing alloy and surface layers of workpieces, improvement of physical conditions (improvement of fluidity, increase in an admissible gap, etc.). It should be noted that these features are typical not only of the methods of brazing using hydrocarbon flame, but also of a number of other methods of brazing (with other heat sources, for example, based on reaction of hydrogen oxidation).

Since the beginning of the VIII century the metals science and metal working attracted attention of specialists in the Middle East.

A great contribution to the fundamentals of chemistry was made by the Arabian scientist Jabir ibn Haijan (Latin name Heber). In particular, depending on the behavior of metal in air and in flame, he divided them into «noble» and «non-noble». Scientists of Caliphate, who melted, evaporated, distillated, performed various reactions using different substances, have discovered, in particular, the method of hydrogen producing in reaction of metals with acids, established the melting points (comparative) of different metals, developed the technology of air-hydrogen and oxy-air brazing [3]. Naturally, the brazing was the most important technology of manufacture of intricate articles made of metals, known at that time.

The wide application of gold in everyday life and architecture by Eastern people attracted attention of Europeans. Crusades of West European knights and monks for grabbing the wealth of Arabians resulted, except other things, in the appearance of alchemists [4]. The first alchemists were mainly monks, taken knowledge from Arabians. They modified the designs of torches, apparatuses for producing combustion gases and oxygen. Their achievements, though did not lead to a significant progress in metallurgy, technology of melting and brazing, but made premises for the progressing of many handicrafts, related to metal working. Skill of foundry men, smiths, tinsmiths and other specialists of metal working ceased to be a secret of separate Middle Age workshops [5].

Knowledge gained by the middle of the XVI century and experience were described in 12-volume encyclopedia «About metals» (De re metallica) by the famous German physician, public figure George Bauer (Latin name Agricola) [6]. In this work, published in 1556, he generalized the experience in the field of metallurgy.

By the middle of the XIX century the optimum designs of apparatuses were developed for producing hydrogen, evolving in reaction of nitric acid with zinc, and torches for brazing and welding. Temperature of hydrogen-oxygen flame reached 2600 °C, that exceeded the temperature of melting not only of silver and gold, but also of platinum [7]. At similar volume ratio of hydrogen and oxygen three zones of flame are distinguished, namely internal cone of blue color *1*, middle zone of light blue*2* and flame tongue of faintly-pink *3* colors (Figure 1).

Transition to the new, more efficient and effective type of brazing is connected with application of natural gases and methods of industrial production of acetylene and oxygen, their compression, transportation and storage.

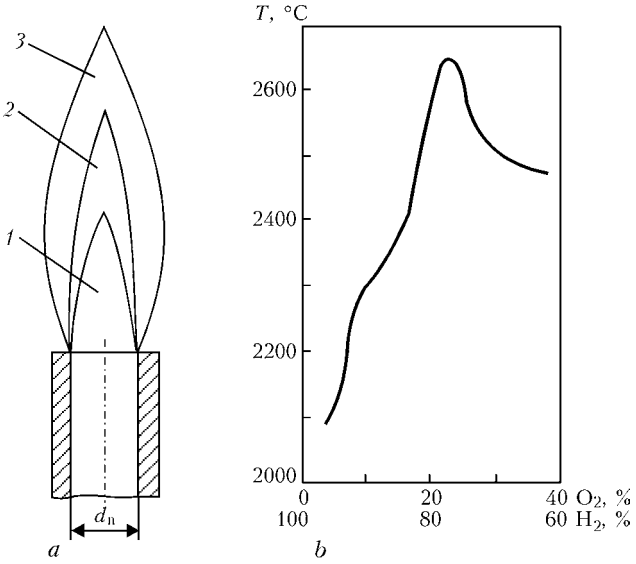

Figure 1. Schematic diagram of hydrogen-oxygen flame (*a*) and change of its temperature depending on mixture composition (*b*)

In 1835, the English scientist Devi produced for the first time the acetylene (C_2H_2) from calcium carbide (CaC_2); reaction of calcium carbide interaction with water $CaC_2 + 2H_2O = C_2H_2 + Ca(OH)$ was synthesized from coal and hydrogen in 1860 by French chemist Bertelo [8] (Figure 2).

At that time, to provide lighting of large cities, public buildings, shops and separate houses, the gas lanterns were used, to which the gas was supplied from the central line. However, the acetylene was not used due to high cost of calcium carbide, produced in laboratory electric furnaces. Only in 1892, Wilson, the employee of US company «Wilson Aluminium», conducted the first melting of calcium carbide using the technology, effective enough for the industrial application [9]. Simultaneously, the inexpensive method of melting of calcium carbide from coke was developed by Moissan, the French scientist. The cost of a product was several times decreased [10]. Nevertheless, acetylene as a technological (but not illuminating) gas attracted attention of specialists only after representation of Chatelier in 1895, who stated that temperature of combustion of acetylene in oxygen reaches 4000 °C [11].

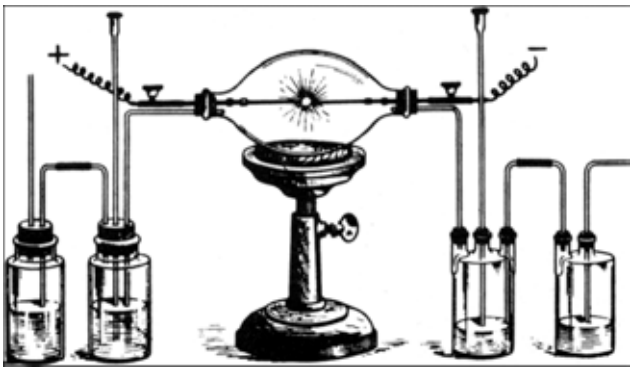

Figure 2. Apparatus Bertelo for producing acetylene (1862)

At exothermal reaction $C_2H_2 + 2.5O_2 = 2CO_2 + H_2O + Q$ the amount of generating heat 5 times exceeded the amount of heat generated in hydrogen combustion and more than 1.5 times in combustion of natural gas [12] (Table). The wide application of acetylene became feasibility after feasibility of acetylene dissolution in liquid, stated by Cloud, the engineer of the French Branch of company «Thomson–Houston». Acetylene began to be pumped under the 2.5 MPa pressure into cylinders with acetone and transported, being protected from explosion [13] (Figure 3).

Thus, by the beginning of the XX century the elementary design and technological solutions were found for use of the flame brazing and it occupied the leading place among other methods of brazing.

The application of acetylene-oxygen flame in brazing prevailed over other gas and vaporous hydrocarbon combustion mixtures. However, coke, pyrolized, natural oil gas, vapors of benzene and kerosene were also used for the flame brazing (as well as for gas welding).

However, the acetylene-oxygen flame from the point of view of heat generation is most effective among all hydrocarbon heat sources, and brazing with brass, copper, bronze and steel brazing alloys competed with thin-coated electrode arc welding as to the quality and efficiency.

In use of flame for welding and brazing, it is necessary to take into account that the processes of acetylene decay and oxidation of carbon and hydrogen are

Heating value and temperature of flame of gas mixture with oxygen

Description of gas mixture and its approximate composition, vol.%	*Lower heating value at 20 °C and 760 mm Hg, kcal/m³*	*Fame temperature in mixture with oxygen, °C*
Acetylene C_2H_2	12600	3150
Hydrogen H_2	2400	2100–3100
Coke gas 50–60 H_2, 25–30 CH_4, 5–7 Co, 6–13 N_2, CO_2	3500–4200	2000
Natural gas 96–98 CH_4, 0.6–1.0 C_2H_6, C_3H_8, 1.0–1.5 N_2, CO_2	7500–7900	2000
Oil gas 12 H_2, 28 C_2H_2, C_3H_8, 50 CH_4, 10 CO, CO_2	9800–13500	2300
Benzene	10200–10600*	2500–2600
Kerosene	10000–10200*	2450–2500

Note. Data marked with * for benzene and kerosene are given in kcal / kg.

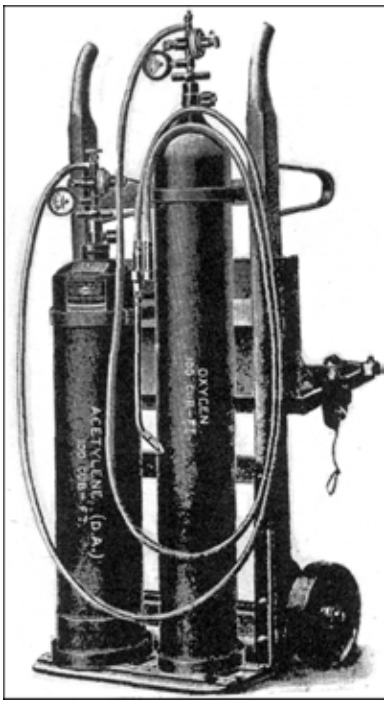

Figure 3. Mobile equipment for gas welding and brazing (1916)

passing several stages. Neglecting the chain of chemical transformations, described in works of Khrenov [13], Klebanov [14], Glizmanenko, Evseev et al., it should be noted that there are H, H_2, C, CO in definite areas of the flame. Flame (Figure 4) has three zones (*I–III*) with different temperatures, the acetylene decay ($C_2H_2 = 2C + H_2$) is occurred in the external envelope of the cone and the real temperature in the cone envelope does not exceed 1500 °C. Zone of flame located just beyond the cone is more often «used» for brazing, where hydrogen is formed as a result of reaction ($C_2H_2 + O_2 = 2CO + H_2$), possessing the reduction properties as regards to oxides of many metals. Moreover, it is the zone which has the highest temperature of the flame.

There is no information about the period of appearance of brazing methods without a direct contact

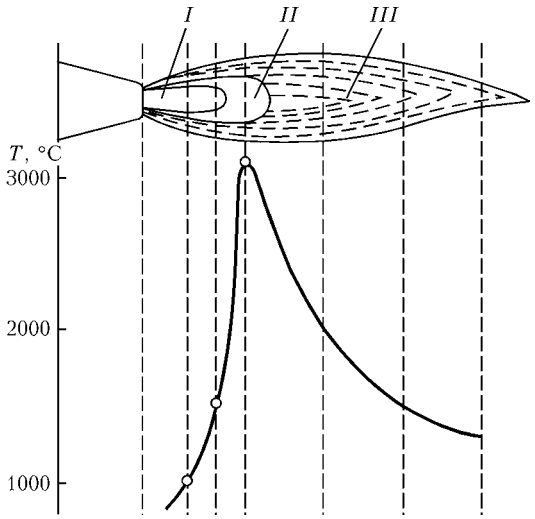

Figure 4. Structure of acetylene-oxygen flame and temperature distribution in its length

with open flame. Nevertheless, it can be assumed that brazing and tin plating with use of heat of heated gases (in furnaces), and also heat transferred through the support or tinning tool, have appeared much earlier than the methods of the flame brazing.

The effectiveness of flame brazing depends greatly on the design of torches. For a long time, the blowing was realized using bellows (like forge bellows) or pumps and mechanical air blowers. The spreading of gas lighting and, especially, struggle of «gas-lighting» companies with «electrolighting» companies, started at the end of the XIX century, stimulated the modification of equipment [15]. Mixture of combustion gas and air (and then oxygen) should not be exploded, neither inside nor outside the torch and should provide the high concentration of heat [16]. As far back as the first half of the XIX century the devices were designed, preventing the return stroke of combustion gas flow inside the channel, firstly, for the hydrogen-oxygen flame, and then also for hydrocarbon-oxygen flame. It was more difficult to fulfill the second condition, i.e. to find the design of the torch in which the hydrocarbons could burn out completely. For a long time the dense deposit of carbon was precipitated on the channel walls and contaminated the nozzle.

Pikard from the company «French Acetylene Dissolved» found the integrated solution: the combustion gas and oxygen were mixed inside the torch, and the acetylene was supplied from cylinders under the excessive pressure [16]. Gas from generators was coming out at normal pressure, therefore, another employee of the same company (Fouché) developed the torch in 1909 in which the oxygen was supplied at pressure, and the acetylene was sucked during injection [17]. These two principles became the basis for the improvement of gas torches over the next years [18]. Simultaneously, the acetylene generators were intensively updated and by the end of the XIX century the European countries and the USA produced tens of thousands of generators of three types («carbide into water», «water on carbide» and mixed type), whose significant part was used not only for welding, but also for brazing (Figures 5 and 6).

Application of flame working in machine building in Russia and West Europe started simultaneously. In 1906 the gas welding and brazing were demonstrated in Moscow Technical College. By 1911 the gas welding stations (where also brazing was used) were available in railway workshops, factories of Petersburg, Moscow, Ekaterinoslav, Ural and in other regions. At the same time the joint stock company «Perun» founded plants for manufacture of equipment in Petersburg, Warsaw and Ekaterinoslav [19, 20].

The rapid progress of the Russian industry in the pre-war and also in the years of the World War I demanded for training the specialists. In Petrograd Technological Institute the school of «lead-soldering mastering and autogenous welding» was organized. Professor Kurbatov wrote a manuscript in 1918, which

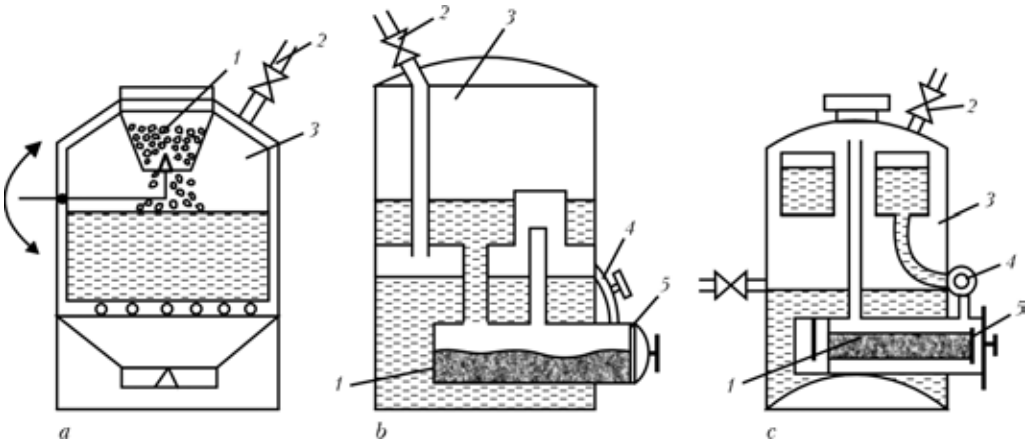

Figure 5. Schemes of acetylene generators: *a* — calcium carbide feeding into water; *b* — supply of water portions into retort with carbide; *c* — at periodic interaction of carbide with water (mixed type); *1* — calcium carbide; *2* — gas sampling; *3* — gas collector; *4* — water supply; *5* — retort

became a manual for the specialists [20]. At the factories of Russian-US joint stock company «Ragas» (in Rostok and other cities) 2074 pieces of acetylene generators, 5782 pieces of welding torches and 4632 pieces of reducers were manufactured over the 1927–1930 period. The more intensive development of the autogenous industry started in the 1930s after liquidation of the joint foreign-Soviet enterprises.

Oxygen industry was also rapidly developing, the furnaces for melting carbide and shops for manufacture of gas-welding equipment were constructed, production of propane-butane from oil and methane, from the natural gas was organized. Over 10 years of industrialization (by 1938) the USSR occupied the first place on oxygen production in Europe and second place, behind the USA, in the world. In 1934, when the import of equipment was interrupted, the specialists selected the heat sources, coming from the optimum conditions of brazing. In parallel with acetylene-oxygen brazing the vapors of liquid fuels were used to save funds [21].

In selection of combustible gases, their heat capacity and flame temperature were taken into account (see the Table) [12]. In accordance with these characteristics the brazing with fusible (soft) brazing alloys was recommended to be performed using the natural gas, vapors of benzene and kerosene [21]. The volume of application of autogenous metal working was 53 % by the end of the 1930s of a total volume of welding jobs.

Brazing found the wide application in the Great Patriotic War years. In 1944 a specialized research institution (VNIIAvtogenmash) was established for the development of technologies, based on application of a gas flame, and as far back as at the beginning of the 1950s the flame brazing of non-ferrous and ferrous metals became one of the activities of this Institute. One of the first works was devoted to the study of causes of porosity in capillary brazing of brasses using silver brazing alloy, creation of fundamentals for selection of flux and brazing alloy in flame welding (brazing) of cast iron [22]. For a long period of time the research works were supervised by A.N. Shashkov, the director of the Institute, and then by G.A. Asinovskaya, K.V. Vasiliev, I.I. Iljina, N.I. Nikiforov [23]. Technologies of gas-flux brazing of brass, not requiring the cleaning of joints from remnants of flux and slags, have been developed and a number of other works on brazing technique has been performed [24].

One of the main directions in the activity of VNII Avtogenmash was the design of the new equipment, suitable for advanced flame technologies. Thus, even by the end of the 1940s the designs were developed for multi-flame torches, used in brazing pipes or cylindrical parts of 30–170 mm diameter at operating pressure of acetylene up to 1.5 kgf / cm^2 and oxygen up to 6.0 kgf / cm^2, using maximum number of nozzles (44) [25]. For brazing workpieces of rectangular section a multi-flame torch was designed, whose upper and lower tips (with a total number of nozzles up to 74) were hinge-connected to a distributing chamber.

The challenging developments of VNIIAvtogenmash are the equipment and technology of gas-flux

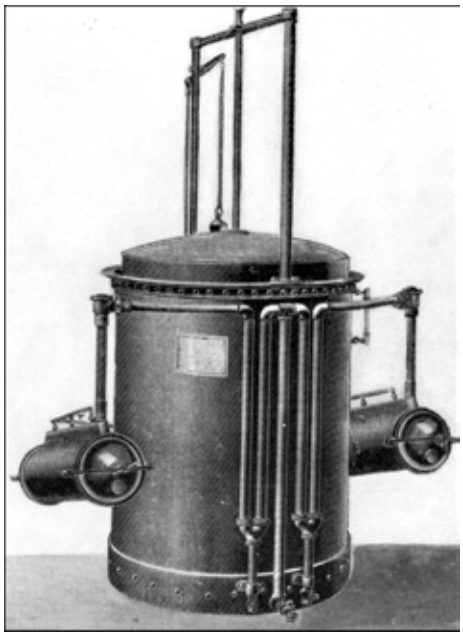

Figure 6. Acetylene generator of Kay design (1897) is one of the first automatic apparatuses of a mixed type

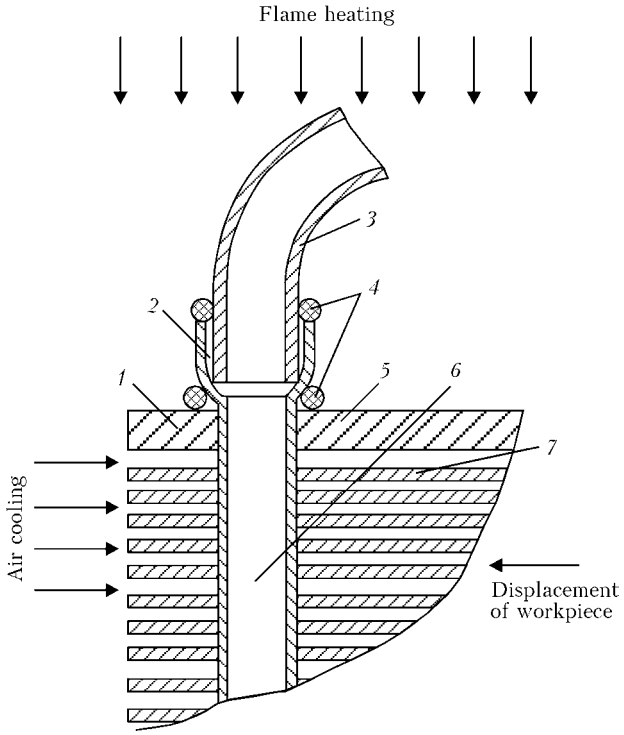

Figure 7. Scheme of heat exchanger sub-assembly being brazed: *1*, *2* — points of arrangement of thermocouples; *3* — return bend; *4* — brazing alloy; *5* — tube plate; *6* — finned tube; *7* — plates for fins

brazing, at which the vapors of boron-containing liquid are introduced directly into the flame. Here, the high air-tightness of joint from some alloys is provided without cleaning the sites of joining [23].

To widen the production of equipment for the flame working the plants of avtogenous machine building were constructed in Odessa in 1952 («Avtogenmash») and in Kirovakan in 1958 («Kirovakanavtogenmash», now «Vanadzoravtogenmash»). In the 1950–1970s the annual increase in output of this equipment in the USSR was on average 13.1 % [19]. In these and next years, great contributions to the improvement of flame technique were made, except VNIIAvtogenmash and N.E. Bauman Moscow High Technical College, by teams of the Branch of VNIIAvtogenmash in Voronezh, Giprokislorod, plant «Krasny avtogen» No.1 (Moscow), Voronezh experimental plant and others.

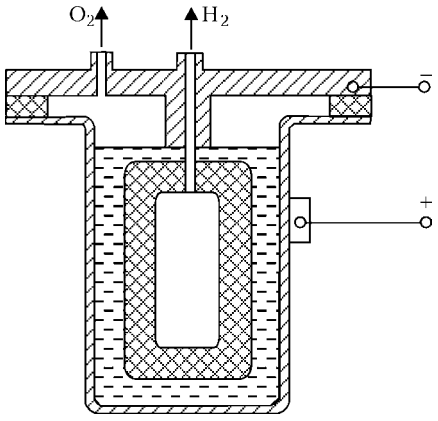

Figure 8. Scheme of separate producing of hydrogen and oxygen in electrolyzer

At the last quarter of the XX century the efforts of specialists in the field of flame brazing were directed to the mechanization of the process of brazing of serially-manufactured products of especially intricate design. Thus, for example, a unique scheme of flame feeding with a simultaneous air cooling was developed at the Institute of Gas of AS of Ukr. SSR [26] (Figure 7). Tubes and return bends of heat exchangers were manufactured of copper or German silver, and the tube plates were made from corrosion-resistant steel or brass, the brazing alloy in assembly was placed in the form of rings. The application of furnace brazing was eliminated due to presence of coating (tin plating) from fusible alloy on plates. Therefore, simultaneous heating of the entire surface of tube plate was realized by a group of flames; in addition, the equipment provided the reciprocal movement of heat exchanger and combustion products, and tinned plates were air cooled additionally.

When regarding the methods of application for brazing of the hydrocarbon fuel, it should be noted about one of the most ancient simplest soldering iron: a copper sharpened bar fixed in the holder. This tool, heated by the heat of an open flame, was used for brazing (welding) of lead pipes of the famous Roman pipeline, roofs of palaces and lining of ships. The copper soldering iron in the form of a bar or rod is used widely until now by tinsmiths in workshops where the fusible solders are used. This method can be referred to brazing with heated blocks, as the «heating of materials being brazed and brazing alloy is realized by their contacting the heated bodies» [1].

In the XX century the technique of application of hydrogen for brazing (as well as for welding) was progressing in two directions: the first one was based on water electrolysis and the second one was based on dissociation of atomic hydrogen.

The suggestion of Lachinov, the known Russian physicist, to use the heat of reaction between two gases, hydrogen and oxygen obtained in electrolyzers [27], was regarded several times (Figure 8). Thus, in the 1930s attempts were made in different countries to use also the electrolyzing welding in parallel with gas and atomic-hydrogen welding [28]. In the USSR the manufacture of multi-polar generators of capacity of 1.3 m^3 / h oxyhydrogen gas at 200 A optimum current was organized. Generators as attachments to the electric welding equipment were used in machine-tractor stations [29].

The improvement of electrolysis-water generators and technique of welding and brazing by hydrogen-oxygen flame was regarded again at the end of the 1960s. The attention was paid to the fact that the volume of the gas mixture, forming in water electrolysis, 1868 times increased the volume of initial water. There were no need in storage and transportation of explosive gases, as the consumption of gas mixture at direct its use could correspond to the volume produced. The foreign experience showed that generators can generate several hundreds of liters of

gas mixture, it is possible to realize welding, brazing and cutting of wires, foils, ceramics, glass and so on. The high-temperature ecologically clean flame is suitable for high- and low-temperature brazing [30].

In Germany at the end of the 1960s a water-oxygen generator of efficiency up to 170 l / h [29–31] (model Water-Welder, Figure 9) was developed and found an application for processes of brazing and microwelding of products of electric and electron industry. In 1971 the specialists of VNIITEM (Moscow) designed a simplified unit (SMO-3275) which found an application in jewelry and electron industry.

Industrial electrolyzers, available in the USSR, for separate producing of hydrogen and oxygen from water could not be used for conductance of technological operations due to a number of problems of technical and organizing nature. The main of them were stationariness of design of electrolyzers, necessity in separate specially-equipped room for their mounting, robustness (mass of electrolyzer is more than 1 t), too high efficiency for supply of one welding station (10 m^3 / h and more), higher requirements to explosion safety. At the same time, the use of cylinders with hydrogen was prohibited for flame method of materials working due to high degree of explosion hazard of its mixtures with oxygen.

In 1973 Prof. V.K. Lebedev from the E.O. Paton Electric Welding Institute suggested to start the works on the creation of national small-sized gas-generators of combustible mixture for the processes of brazing and welding of micro-products, for producing the hydrogen-oxygen mixture by the water electrolysis [32]. Two variants were developed: filter-press electrolyzer with separate producing of hydrogen and oxygen and electrolyzer of a monopolar type for producing mixture of hydrogen with oxygen (methane).

In the development of electrolyzers of a bipolar type by V.I. Balakin, the impossibiity of copying the technical solutions used in designs of electrolyzers of capacity up to 10 m^3 / h and more, in those of electrolyzers of up to 0.1 m^3 / h capacity was revealed. Thus, the «modification» of known designs of electrolyzers consisted in searching for an optimum shape of electrodes, providing the sufficient degree of leak-tightness of electrolytic cells, and also for a variant of uniform distribution of electrolyte between the cells and the solution of other not less important problems.

As a result of works, carried out at the E.O. Paton Electric Welding Institute by V.M. Kislitsyn, A.G. Musin, I.M. Melnichenko, V.P. Shevchenko and others, several models of gas generators of a bipolar type were designed and manufactured [32] (Figure 10).

At present the developments in this direction are made at the enterprises of Moscow, manufacturing gas generators of types «Moskva» (OJSC NPP «Gas welding machines –– XXI century»), LIGA (St.-Petersburg) and others.

At the same time the E.O. Paton Electric Welding Institute has developed several models of gas generators of hydrogen-oxygen mixture with a monopolar

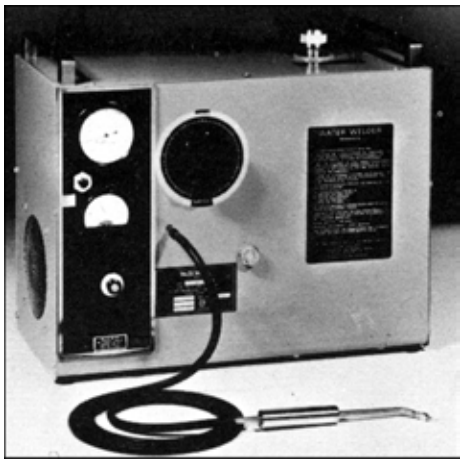

Figure 9. Electrolysis-water generator of Kager company (Water-Welder)

electrolyzer, and also technologies of welding and brazing of products from different metals and alloys [33–37]. The distinguished feature of the suggested design of electrolyzer is the use of electrodes in the form of two strips, coiled in spiral around a central current connector, moreover, one of the strip was wound with insulating thread of about 1 mm diame-

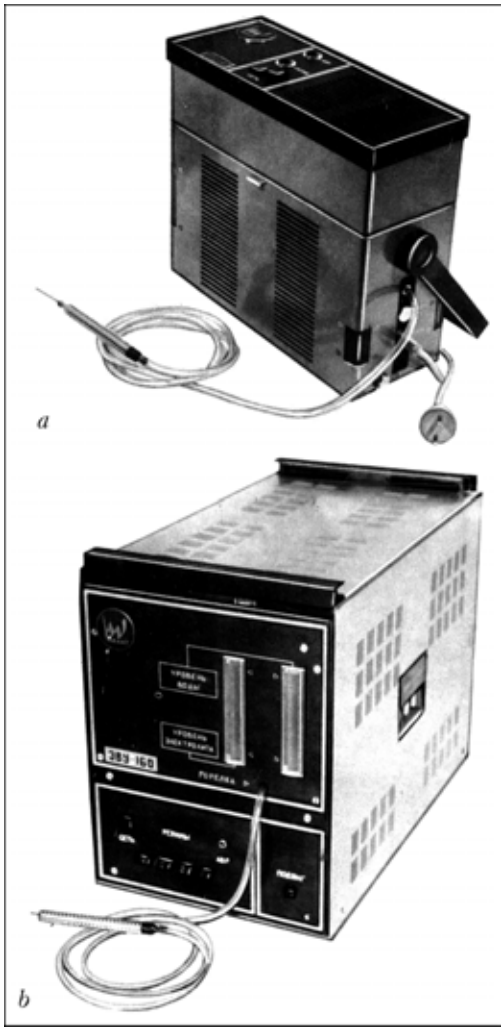

Figure 10. Generators of hydrogen-oxygen mixture with electrolyzer of a bipolar type: *a* — EVU-40; *b* — EVU-160

ters at 5–10 mm pitch, providing the necessary gap between electrodes [38].

On the base of gas generator GVK-1.5 the gas generator of hydrogen-oxygen mixture of efficiency up to 1.8 m^3 / h was developed, which was then serially-manufactured at Brovary pilot plant of equipment («Fakel», Ukraine) since 1980 to 1990.

The gas generators of different series were implemented at Artyom PO (Kiev) in the technological production line for manufacture items of radio-technical purposes, at several enterprises of pharmaceutical industry in production line for sealing glass ampoules with drugs, and also at the enterprises in many research institutes for brazing of microelements.

Abroad, in the 1990s, the attention was also paid to the developments of this direction. For example, the leading company «Hydrox» (USA) at that time mastered the manufacture of several models of gas generators of hydrogen-oxygen mixture of efficiency from 0.3 to 5 m^3 / h using electrolyzer of a monoplar type. Developments of the E.O. Paton Electric Welding Institute were not only inferior by mass and dimension characteristics to the developments of company «Hydrox» (Figure 11), but also superior by technological characteristics and reliability. It should be noted that neither in Europe nor in the USA any of companies were dealing with the development of gas generators of hydrogen-oxygen mixture using electrolyzer of a bipolar type.

Technological processes of brazing using heating by hydrogen-oxygen mixture were developed at several Moscow enterprises [39, 40], moreover, the important results were obtained for flame brazing by hydrogen-oxygen flame of aluminium alloys using brazing alloys of Al–Zn system without fluxes.

It should be noted that experimental investigations of specifics of operation of gas generators, theoretical grounds and recommendations for the selection of optimum variants of sources for flame working of metals, including also brazing, were made by V.N. Korzh et al. (Kiev Polytechnic Institute) [41], V.M. Nerovny et al. (E.N. Bauman MGTU), V.I. Stolbov et al. (Toliatti Polytechnic Institute) [42], V.F. Kvasnitsky et al. (Admiral Makarov Ukrainian State Navy Technical University) [43].

To increase the sizes of the reduction zone of the flame it is necessary to add the hydrocarbon additions (vapors of alcohol, acetone, benzine), which reduce the flame temperature, to hydrogen oxygen flame (see the Table).

As to the torches, so they represent, in principle, a usual tube to which the ready mixture is fed. The tube diameter is selected depending on the flame power (for welding and cutting the acetylene-oxygen torches are also used). The application of gases, produced in electrolyzing-water generators for the purpose of brazing, does not cause great problems, and the brazing technique is not differed from the technique of brazing with other gas flame [35]. The interesting technical solution is the suggestion to perform heating by two co-axial gas flows. In accordance with this technical suggestion the hydrogen-oxygen mixture of a stoichiometric composition (providing the temperature of flame of order of 3400 °C) is supplied through a central nozzle, and through the channel, embracing the central nozzle, the shielding gas is supplied, for example, the same hydrogen-oxygen mixture, but enriched with vapors of a hydrocarbon liquid, providing the reduction atmosphere around the central zone of heating. The devices are known [44], allowing dosing of heat energy, introduced into the zone of brazing (welding), that guarantees the high reproducibility of quality of brazed or welded joints [45].

The very challenging is the development of equipment for a separate producing of hydrogen and oxygen

Figure 11. Gas generators of hydrogen-oxygen mixture with a monopolar electrolyzer: *a* — of company «Hydrox», 0.6 m^3 / h efficiency; *b* — of E.O. Paton Electric Welding Institute (A-1803), 1.6 m^3 / h efficiency

from water for technological application in the processes of welding and brazing.

The another direction of application of hydrogen as an energy carrier can be referred to the type of brazing only conditionally. The method of atomic-hydrogen welding (brazing) is based on the phenomenon of hydrogen dissociation in electric arc, discovered in 1911 by Langmuir, the outstanding American scientist. Welding and brazing are performed by a torch with two non-consumable electrodes (tungsten), the arc is burning between them. Hydrogen is supplied into the arc zone, where the two-atomic molecules of this gas are dissociated [46]. Atoms (ions) of hydrogen, entering the comparatively cold metal, are recombined with a generation of energy $H + H = H_2 +$ + 436 kJ / mol. Workpiece and filler (brazing alloy) are heated both by the heat of arc (by convection and radiation), and also by exothermal heat.

In the 1930s the atomic-hydrogen welding and brazing were widely used in aircraft, electric engineering and other branches of industry, providing the most quality joints (as compared with methods known at that time) of aluminium, copper, bronze. These technologies were developing at Moscow Mechanical Machine Building Institute (now N.E. Bauman MGTU), at Leningrad Industrial Institute, in laboratories of Aviaprom, etc. The technology found the widest spreading in the USA (more that 3000 stations). In the 1940s the technologies based on «hydrogen arc», were forced out by other, more effective technologies, and at present it is used in exclusive cases, for example, in welding of T-joints from thick-walled tubes of up to 20 mm diameter in aircraft construction, providing a «spike» heating across the thickness of the tube, that is impossible in realizing arc method of welding in a very narrow gap.

CONCLUSIONS

1. Gas-air and gas-oxygen brazing originated in the period of the Middle Ages. High-efficient methods of producing calcium carbide, the first industrial designs of acetylene generators and gas torches were developed and updated by the inventors and scientists of many countries of Europe and the USA at the second half of the XIX–beginning of the XX centuries.

2. In the 1920–1930s the machines, manufactured for atomic-hydrogen welding, were used for brazing products of aircraft and electric industry.

3. In the first half of the XX century the investigations of gas flame were carried out; in the USSR the manufacture of equipment and materials for gas brazing was organized, specialized institute (VNII Avtogenmash) and several laboratories were created. At the second half of the XX century the task was to update the equipment and to automate the brazing processes.

4. In the XX century the technique of brazing by hydrogen-oxygen flame was progressing. Designs of electrolyzing-water generators, reliable and effective in industrial application, were developed.

1. *GOST 17325–79*. (1979) Brazing and tinning. Main terms and definitions. Moscow: Standart.
2. Peren, T. (1998) Role of carbon in ancient metallurgy. *Chyorn. Metally*, **2**, 68–71.
3. Figurovsky, N.A. (1969) *Outlines of general history of chemistry. From ancient times to beginning of the 19th century*. Moscow: Nauka.
4. Gua, M. (1975) *History of chemistry*. Moscow: Mir.
5. Stillman, M. (1960) *The study of alchemy and early chemistry*. New York.
6. Agricola, G. (1978) *Zwoelf Buecher vom Berg- und Huettenwesen*. Duesseldorf: VDI.
7. Fletcher, T.A. (1888) New commercial application of oxygen. *J. Soc. Chem. Ind.*, **3**, 182–185.
8. Musabekov, Yu.S., Chernyak, A.Ya. (1971) *Prominent chemists of world*. Bibliography. Moscow: Znanie.
9. Smith, K.S. (1998) A history of the oxyfuel and electric arc welding processes. *Practical Welding Today*, March / April, 19–22.
10. Lebrun, M. (1954) Fifty years of welding in France. *British Welding J.*, **7**, 25–28.
11. Le Chatelier, H. (1895) Sur la combustion de l'acetylene. *Comptes rendus de l'Academie des sciences*, **27**, 1144–1147.
12. Bagryansky, K.V., Dobrotina, Z.A., Khrenov, K.K. (1968) *Theory of welding processes*. Kharkov: KhGU.
13. Khrenov, K.K. (1970) *Welding, cutting and brazing of metals*. Moscow: Mashinostroenie.
14. Klebanov, N.N. (1947) *Autogenous welding and cutting of metals*. Moscow: Mashgiz.
15. Kornienko, A.N. (1996) Thermochemical processes in welding. *Avtomatich. Svarka*, **7**, 42–50.
16. Lebrun, M. (1961) *La soudure, le brasage et l'oxycoupage des metaux. 3500 ans d'histoire*. Paris: Academie de Marine.
17. Weirs, S.A., Orn, T. (1935) An early history of oxyacetylene welding and cutting in the United States. *Welding Eng.*, **6**, 22–24.
18. (1927) *Choice and arrangement of oxyacetylene installation*. Leningrad: Nauka i Shkola.
19. Antonov, I.A. (1976) *Flame treatment of metals*. Moscow: Mashinostroenie.
20. Kurbatov, V.Ya. (1918) *Self-welding and different methods of brazing of metals*. Petersburg: VSNKh Sci.-Techn. Dep.
21. Miloslavsky, S., Glizmenko, D. (1933) Combustibles gases for autogenous treatment of metals. *Avtogennoe Delo*, **7**, 18–24.
22. Shashkov, A.N., Asinovskaya, G.A., Ilyina, I.I. (1970) Low-temperature soldering-welding of cast iron with tin plate. In: *Transact. of VNIIAvtogenmash*. Issue 16.
23. Nikiforov, N.I., Vasiliev, K.V., Smirnov, A.Kh. (2001) Developments of the FGUP «VNIIAvtogenmash» in field of equipment and technology of flame brazing. In: *Brazing, current technologies, materials, structures*. Coll. 1. Moscow: Dom Znany.
24. Asinovskaya, G.A. (1963) *Flame brazing of metals*. Moscow: Mashgiz.
25. (1953) Circular multiple-flame torches KG for gas-pressure welding of transverse butts of tubes and rod-iron. *Inform. Listok VNIIAvtogenmash*, **41**.
26. Erinov, A.E., Soroka, V.A., Petishkin, S.A. et al. (1982) Mechanized brazing of heat exchangers with brazing alloy using natural gas burned in air mixture. *Avtomatich. Svarka*, **12**, 49–51.
27. Yakimenko, L.M., Modylevskaya, I.D., Tkachek, Z.A. (1970) *Electrolysis of water*. Moscow: Khimiya.
28. Popov, S.M. (1938) Application of electrolysis welding in conditions of repair of airplanes. *Aviapromyshlennost*, **4**, 18–24.
29. Lashko, N.F., Lashko-Avakyan, S.V. (1959) *Brazing of metals*. Moscow: Mashgiz.
30. (1972) Wasser-Schweisser. *Produktion*, **8**, 104.
31. (1968) Mikroschweissgeraet «Water-Welder». *Technische Rund.*, **7**, 49.
32. *Protocoles of technical meetings*. Archives of E.O. Paton Electric Welding Institute.
33. Balakin, V.I. (1986) Application of electrolysis-water generators in brazing, cutting and welding. *Avtomatich. Svarka*, **8**, 57–61.
34. Kislitsyn, V.M., Musin, A.G. (1974) Small-sized portable units for brazing and welding with oxyhydrogen flame. In:

Welding and brazing of elements of semiconductor devices and integrated circuit. Kiev: Znanie.
35. Rossoshinsky, A.A., Kislitsyn, V.M., Musin, A.G. et al. (1976) *Unit for pulsed flame brazing of micropieces*. Kiev: PWI.
36. Rossoshinsky, A.A., Kislitsyn, V.M., Musin, A.G. et al. (1975) *Unit U-853 for microflame brazing*. Kiev: PWI.
37. Kislitsyn, V.M., Musin, A.G., Shevchenko, V.P. (1981) *Generators of hydrogen-oxygen mixture GVK-1.5 and GVK-0.2*. Kiev: PWI.
38. Lebedev, V.K., Rossoshinsky, A.A., Kislitsyn, V.M. et al. *Electrolyzer for producing of oxyhydrogen gas from water and water solutions*. USSR author's cert. 507668. Publ. 1976.
39. Latypov, R.A., Khromov, V.N., Semeshin, A.L. (2001) Repair of motor cooling systems of autotractor engineering by flame brazing. In: *Brazing, current technologies, materials, structures*. Coll. 2. Moscow: Dom Znany.
40. Khromov, V.N., Semeshin, A.L., Latypov, R.A. (2000) Repair of radiators of cooling systems by flame brazing. *Svarochn. Proizvodstvo*, **9**, 44–49.
41. Korzh, V.N., Dykhno, S.L. (1984) *Treatment of metals by hydrogen-oxygen flame*. Kiev: Tekhnika.
42. Frolov, V.P., Markova, I.Yu., Pevzner, B.N. (2000) Brazing and tinmans during the 30th later years. In: *Proc. of Sci.-Techn. Conf. on Brazing 2000*. Toliatti: TPI.
43. Romanovsky, G.F., Kvasnitsky, V.F., Safonov, A.I. et al. (1999) 40th anniversary of chair of UGMTU welding production. *UDMTU Zbirnyk Nauk. Prats*, **6**.
44. Zhogol, V.T., Reznichenko, V.F., Melnikov, V.P. et al. *Method of flame treatment*. USSR author's cert. 1449268. Int. Cl. B 23 K 7 / 08. Publ. 1986.
45. Dykhno, S.L., Kislitsyn, V.M., Musin, A.G. et al. *Device for flame microwelding and brazing*. USSR author's cert. 721289. Int. Cl. B 23 K. Publ. 1980.
46. Weinman, A., Langmuir, J. (1926) Atomic hydrogen welding. *General Electric Rev.*, **29**, 160–163.

WEAR RESISTANCE OF DEPOSITED METAL WITH INCREASED SHARE OF TITANIUM CARBIDES

V.N. KALIANOV and **A.N. PETRENKO**
Kharkov Ukrainian Engineering Pedagogical Academy, Kharkov, Ukraine

The paper gives the results of laboratory studies of wear resistance and technological strength of three types of deposited metal (boron–titanium, austenite-martensite and martensite-austenite). It is shown that steels with a high content of metastable austenite, strengthened by dispersed precipitation of titanium carbides, have the best complex of properties.

Keywords: *abrasive wear resistance, carbide phase, titanium carbide, technological strength, self-shielding flux-cored wire, boron–titanium deposited metal, metastable austenite*

The resistance of deposited metal against the abrasive wear is defined mainly by the hardness, structural state and degree of base metal alloying, and also by composition, amount and hardness of the strengthening carbide phase (carbonitride, carboboride, intermetallic). Increase in a share of the carbide phase increases the wear resistance to a certain limit. Here, the change in amount of the carbide phase influences greater the wear resistance than the aggregate hardness, produced only by increase in the matrix hardness. The wear resistance is also increased with increase in hardness of the strengthening phase [1–5]. Titanium carbide TiC is referred to thermodynamically resistant carbides, has a high temperature of melting and hardness (about 32 GPa). In this case, the cost of ferrotitanium in comparison with ferroalloys of other strong carbide-forming elements (vanadium, tungsten and others) is lower, moreover, it is not so scarce.

Adding of alloying elements into the deposited metal to increase the wear resistance can lead to the decrease in technological strength and service characteristics. Carbon has the greatest effect on the above-mentioned properties [6]. The aim of the work is to study the wear resistance and technological strength of the deposited metal of different structural classes, containing a large share of thermodynamically resistant carbides.

The deposited metal, studied in the work, can be divided into three groups: boron–titanium (180T3R, 250Kh3T3NR and others), austenite-martensite (100Kh10G10T4S, 100Kh10G8T4S, 75Kh6G9M3T3S), martensite-austenite (150Kh6T4M [1], 100Kh3G9T4S). The appropriate self-shielding flux-cored wires are manufactured for hardfacing of metal of the mentioned compositions. Hardfacing of specimens was performed on plates from steels 20, 45 and 5KhNM without preheating. Before testing, the working surfaces of the specimens (10 mm diameter, 35 mm length) were polished and cleaned.

Wear resistance tests were made at reciprocal movement on a carborundum abrasive paper with a size of abrasive grain of 200–160 and 80–63 μm, rated pressure of 1.37 MPa. The speed of specimen movement over the paper surface is 0.086 m / s. Heating of specimens in testing was negligible. As a reference for tests a specimen of steel 45 of about *HV* 200 hardness was used.

Wear was defined as a ratio of reference mass loss to the loss in mass of the material examined. Additionally, the microhardness on the surface after wear (P = 0.5 and 1.0 N) and near the friction surface of «taper» sections was examined (Table).

Resistance to hot crack formation (with allowance for content of alloying and impurity elements, wt.%) was determined by the value of criterion

$$\text{H.C.S.} = \frac{C\left(S + P + \frac{Si}{25} + \frac{Ni}{100}\right)10^3}{3Mn + Cr + Mo + Ti}$$

and in machine LTP-6 [7], susceptibility to formation of cold cracks was in compliance with GOST 26388–84.

As to the deposited metal of the first group, then with increase in boron content the share of a B-containing eutectic and its microhardness are increased [5]. Due to a possible formation of fusible eutectic Fe–B and significant content of carbon in products of decomposition of solid solution this metal possesses a great susceptibility to the formation of different types of cracks and tears in the fusion zone (Figure 1). The structure of the latter is the «light band» with an acicular structure.

According to data of work [5] the metal of 250Kh3T3NR, 250T5N2R type has the higher wear resistance as compared with metal 350Kh27N4S2. The advantage of metals of this group is their low cost,

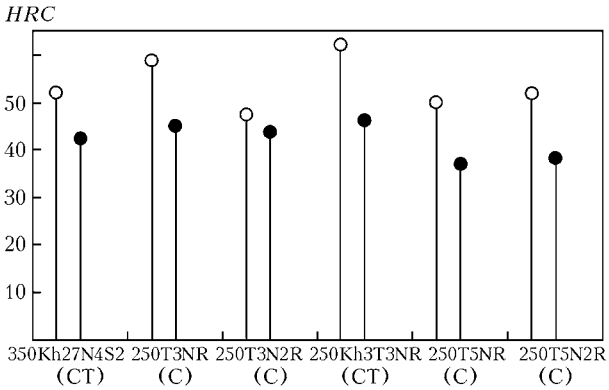

Figure 1. Hardness of deposited metal at 293 (○) and 873 (●) K: C — cracks; CT — cracks and tears in the fusion zone

Properties of deposited metal

Type of deposited metal	*Microhardness near surface of wear, MPa*	*Relative wear resistance, ε*	*Hardness HRC*	*Phase composition*	*Criterion of crack resistance H.C.S.*
30Kh10G10	10200	2.51	29	A + M	0.68
100Kh3G9T4S	4300	2.05	35–40	M + A + C	2.70
150Kh6T4M	10800	6.61	54–56	M + A + C	12.50
100Kh10G10T4S	11500	6.97	35–37	A + M + C	2.27
100Kh10G8T4S	8800	6.71	36–39	A + M + C	2.63
75Kh6G9M3T3S	9300	5.98	–	A + M + C	2.03

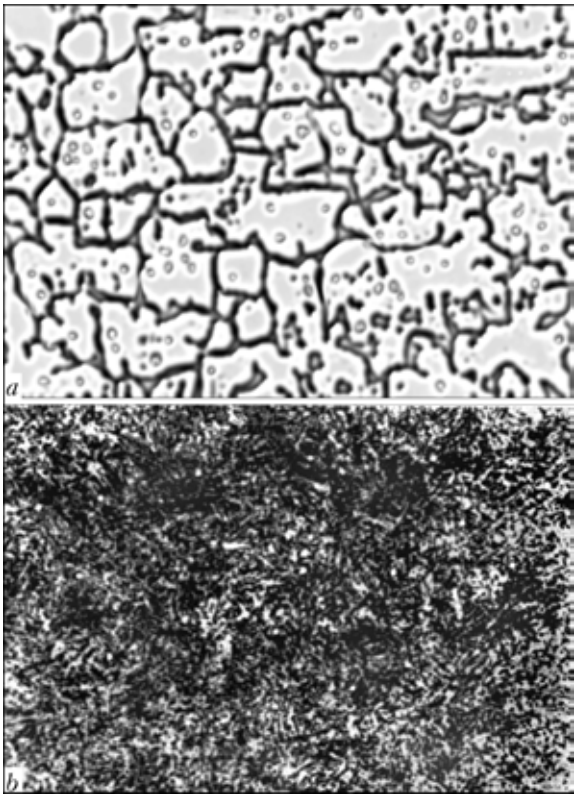

Figure 2. Microstructure of deposited metal: *a* — 100Kh10G10T4S; *b* — 100Kh3G9T4S (×600)

whereas a drawback is the susceptibility to cracking during hardfacing.

The second group is the deposited metal with a high share of a metastable austenite (100Kh10G8T4S, 75Kh6G9M3T3S). The specifics of these materials is the fact that ratio of titanium content to carbon is not less than 4 (i.e. it is such ratio at which the larger part of carbon is bound into carbides). The main share of titanium carbide is, probably, formed even in a molten metal [1]. At the further cooling the low-carbon metal is crystallized that provides the higher characteristics of technological strength as compared with materials I and II groups at values of criterion H.C.S. equal to 2.03–2.63 [7]. The high wear resistance of the deposited metal is guaranteed by the presence of a hard highly-dispersed carbide phase and high degree of strengthening of manganese metastable austenite. The phase composition is austenite, carbides and, as a rule, a small fraction of martensite (Table, Figure 2, *a*).

With increase in chromium content to 10 % (at 8–10 % Mn) the value of characteristic of relative wear resistance is increased and amounts to 6.71 and 5.98, respectively, for deposited metal 100Kh10G8T4S, 75Kh6G9M3T3S with an austenite-martensite structure. With increase in manganese content from 8 to 10 % (100Kh10G10T4S) the relative wear resistance is negligibly increased.

The metal of 100Kh3G9T4S type (third group) with a phase composition of martensite, residual austenite, titanium carbides (Figure 2, *b*) is typical of low hardness and absence of cracks. However, here, the deposited metal has a comparatively low wear resistance (ε = 1.8–2.4) that is, probably, due to a low resistance of low-carbon martensitic matrix to the abrasive wear. The deposited metal of 150Kh6T4M type has approximately the same amount of the carbide phase, but the more hard matrix, strengthened by carbon. As a result, the metal possesses the high hardness (*HRC* 54–56) and wear resistance (ε = 6.61).

The industrial tests of buckets of a rotor-type sand-slinger machine, deposited by steel 100Kh10G10T4S, showed the higher resistance of the latter as compared with that of buckets deposited by steel 10Kh13, 10Kh20N10B, 300Kh27N4S3, 320Kh22TR.

CONCLUSIONS

1. The high-manganese deposited metal strengthened by titanium carbides (at ratio of Ti / C ≥ 4) possesses sufficiently high characteristics of weldability that makes it possible to perform hardfacing without preheating.

2. The highest characteristics of abrasive wear resistance (in the given range of concentrations of alloying elements) are attained in producing austenite or austenite-martensite structure in the deposited metal.

3. Martensite (250Kh3T3NR) and martensite-austenite (150Kh6T4M) deposited metal is characterized by high wear resistance and comparatively low cost, the technological strength in this case is not high.

1. Ryabtsev, I.A., Kondratiev, I.A., Vasiliev, V.G. et al. (2002) Wear resistance of deposited metal of Fe–C–Cr–Ti–Mo alloying system. *The Paton Welding J.*, **4**, 45–48.
2. Danilchenko, B.V. (1992) Resistance of deposited metal designed for service in abrasive wear conditions. *Svarochn. Proizvodstvo*, **4**, 31–33.
3. Kalianov, V.N., Muratov, V.A., Pocheptsov, A.V. (1970) Heat resistance and wear resistance of boron–titanium deposited metal, *Ibid.*, **6**, 21–23.
4. Kalianov, V.N. (1997) Structure and characteristics of wear-resistant sparsely-alloyed deposited metal. *Ibid.*, **4**, 13–17.
5. Kalianov, V.N., Petrenko, A.N. (2004) Wear-resistant deposited metal of system C–B–Ti–Ni. In: *Visnyk KhDTUSG*. Issue 26.
6. Guk, V.A. (2000) Materials and technology for surfacing of machine parts operating under conditions of impact-abrasive wear. *The Paton Welding J.*, **8**, 11–13.
7. Kalianov, V.P., Bagrov, V.A. (1998) Weldability of deposited martensitic steels with tool steels. *Svarochn. Proizvodstvo*, **4**, 14–15.

INDEX OF ARTICLES FOR TPWJ'2004, Nos. 1–12

LIST OF AUTHORS